(2)

PSI-1006/TR-976

ROTATIONAL ENERGY TRANSFER IN METASTABLE STATES OF HETERONUCLEAR MOLECULES

Draft Final Report

S.J. Davis, K.W. Holtzclaw, and L.G. Piper

Physical Sciences Inc.
Research Park, P.O. Box 3100
Andover, MA 01810

October 1989

Unclassified

Air Force Office of Scientific Research (AFOSR)
Building 410
Bolling AFB, DC 20332-6448

UNCLASSIFIED

SECURITY CLASSIFICATION OF THIS PAGE

REPORT DOCUMENTATION PAGE

1a. REPORT SECURITY CLASSIFICATION UNCLASSIFIED	1b. RESTRICTIVE MARKINGS N/A since Unclassified
2a. SECURITY CLASSIFICATION AUTHORITY N/A since Unclassified	3. DISTRIBUTION/AVAILABILITY OF REPORT Unclassified/Unlimited
2b. DECLASSIFICATION/DOWNGRADING SCHEDULE N/A since Unclassified	
4. PERFORMING ORGANIZATION REPORT NUMBER(S) PSI-1006/TR-976	5. MONITORING ORGANIZATION REPORT NUMBER(S) AFOSR-TR- 89-1340
6a. NAME OF PERFORMING ORGANIZATION Physical Sciences Inc. / 6b. OFFICE SYMBOL (If applicable)	7a. NAME OF MONITORING ORGANIZATION Air Force Office of Scientific Research
6c. ADDRESS (City, State, and ZIP Code) Research Park, P.O. Box 3100 Andover, MA 01845	7b. ADDRESS (City, State, and ZIP Code) Building 410 Bolling AFB, DC 20332-6488
8a. NAME OF FUNDING/SPONSORING ORGANIZATION AFOSR / 8b. OFFICE SYMBOL (If applicable)	9. PROCUREMENT INSTRUMENT IDENTIFICATION NUMBER F49620-86-C-0061
8c. ADDRESS (City, State, and ZIP Code) Building 410 Bolling AFB, DC 20332-6488	10. SOURCE OF FUNDING NUMBERS PROGRAM ELEMENT NO. 61103F / PROJECT NO. 2303 / TASK NO. B1 / WORK UNIT ACCESSION NO

11. TITLE (Include Security Classification)
Rotational Energy Transfer in Metastable States of Heteronuclear Molecules

12. PERSONAL AUTHOR(S)
Davis, S.J.; Holtzclaw, K.W.; and Piper, L.G.

13a. TYPE OF REPORT	13b. TIME COVERED	14. DATE OF REPORT (Year, Month, Day)	15. PAGE COUNT
Final	FROM 860601 TO 890831	26 October 1989	102

16. SUPPLEMENTARY NOTATION

17. COSATI CODES			18. SUBJECT TERMS (Continue on reverse if necessary and identify by block number)
FIELD	GROUP	SUB-GROUP	

19. ABSTRACT (Continue on reverse if necessary and identify by block number)

The objective of this program was to measure and interpret state-to-state R-T transfer rate coefficients for selected interhalogen molecules. Spectrally resolved CW laser-induced fluorescence was the experimental method used. A CW dye laser excites pure quantum states. The resolved fluorescence of the laser-excited level and the collisionally populated J' levels are analyzed. We have determined nearly 1000 state-to-state rate coefficients for R-T transfer in IF(B). Collision partners include He, Ne, Ar, Kr, Xe, N_2, and CF_4. Rate coefficients have also been determined for several initially excited J': 13, 27, 35 and 72. We have also investigated R-T transfer during vibrationally inelastic collisions for both I_2 and IF. In addition, we have measured R-T rate coefficients in ICl(B). Finally, we have made comparisons of our R-T rate coefficients to several models that have been developed to predict R-T rate coefficient scaling as a function of ΔJ.

20. DISTRIBUTION/AVAILABILITY OF ABSTRACT ☒ UNCLASSIFIED/UNLIMITED ☐ SAME AS RPT ☐ OTIC USERS	21. ABSTRACT SECURITY CLASSIFICATION Unclassified
22a. NAME OF RESPONSIBLE INDIVIDUAL Dr. Francis J. Wodarczyk	22b. TELEPHONE (Include Area Code) 202-767-4950 / 22c. OFFICE SYMBOL NC

DD FORM 1473, 84 MAR — 83 APR edition may be used until exhausted. All other editions are obsolete.

UNCLASSIFIED

SECURITY CLASSIFICATION OF THIS PAGE

Approv...

Contents

List of Figures

List of Figures (Continued)

List of Figures (Concluded)

INTERIM PROJECT SUMMARY

1. TITLE: Rotational Energy Transfer in Metastable States of Heteronuclear Molecules

2. PRINCIPAL INVESTIGATOR: Dr. Steven J. Davis

3. INCLUSIVE DATES: 1 June 1986 - 31 August 1989

4. CONTRACT/GRANT NUMBER: F49620-86-C-0061

5. COSTS AND FY SOURCE: FY86-FY88 $386,797

6. SENIOR RESEARCH PERSONNEL: Dr. Steven J. Davis

7. JUNIOR RESEARCH PERSONNEL: Dr. Karl Holtzclaw and Mr. Don Arnold

8. PUBLICATIONS:

   1. "State-to-State Rotational Energy Transfer in IF $B^3\Pi(0^+)$ I. Collisions with He, Ne, Ar, Xe, N_2, and CF_4," S.J. Davis and K. Holtzclaw (accepted Journal of Chemical Physics).

   2. "State-to-State Rotational Energy in IF $B^3\Pi(0^+)$ II. Studies of Several Initially Populated Levels," S.J. Davis and K.W. Holtzclaw (to be submitted to Journal of Chemical Physics).

   3. "A Comparison of Rotational Energy Transfer in Homonuclear and Heteronuclear Halogen Molecules: A Case Study for $I_2(B)$ and IF(B)," S.J. Davis and K. Holtzclaw (to be submitted to Journal of Chemical Physics).

   4. "Application of Scaling Laws to R-T Transfer in IF(B)," S.J. Davis and K. Holtzclaw (manuscript in preparation).

   5. "State-to-State Rotational Energy Transfer in ICl(B)," S.J. Davis and K. Holtzclaw (manuscript in preparation).

   PRESENTATIONS:

   1. "Rotational Energy Transfer in IF," S.J. Davis and K.W. Holtzclaw, ILS-IV Atlanta Meeting (1988).

   2. "Rotational Eneragy Transfer in the $B^3\Pi(0+)$ States of ICl and IF: A Systematic Study of State-to-State Rate Coefficents." S.J. Davis and K.W. Holtzclaw.

9. ABSTRACT OF OBJECTIVES AND ACCOMPLISHMENTS:

A. Objectives

The objective of this project was to study rotational to translational (R-T) energy transfer in selected halogen molecules. In particular, we are examined R-T transfer in the $B(^3\Pi_g)$ states of IF, ICl, and I_2. We also examine R-T transfer during inelastic vibrational collisions. The experiments are conducted using a single frequency CW dye laser as the excitation source. With this laser, molecules can be prepared in a pure quantum state (v',J'). The resulting B→X fluorescence is spectrally resolved, and the rate coefficients for energy transfer are determined using a steady state kinetic analysis. In brief, the ratio of the fluorescence intensity from a satellite collisionally populated level (J_f) to that of a parent laser excited level (J_i) is directly proportional to the R-T rate, k_{if}. Knowledge of the radiative lifetime of the level J_i is required in the analysis. The lifetimes of the states being investigated have been previously determined.

The R-T rate coefficients are desired for two reasons. First, they are used to test parent theoretical scaling laws that predict the dependences of k_{if} upon J_i and upon the change in J (ΔJ) during a collision.[1,2] These are of importance because the scaling laws depend upon the intermolecular potentials. Thus, fundamental insight is gained from these measurements. Secondly, these measurements have great practical relevance. Many of the species being investigated are excellent candidates for electronic transition chemical lasers.[3,4] The degree of R-T relaxation in the excited state will in large measure determine the efficiency of the laser. In addition, knowledge of the R-T rates in

the excited B state is useful for crudely estimating R-T relaxation in the ground state.

B. Progress (Final)

Inelastic energy transfer collisions are among the most important processes that occur in molecular laser systems regardless of the excitation source. The temporal evolution of the excited state manifold will in large measure determine the operating characteristics of the laser. From a more fundamental perspective, experimentally determined cross-sections for inelastic processes serve as sensitive tests for theoretically predicted interaction potentials.[1,2]

During the past two decades there have been numerous reports describing measurements of vibration-translation (V-T) and rotation-translation (R-T) rate coefficients in excited electronic states of diatomic molecules. Molecular iodine is perhaps the most extensively studied system. The initial investigations on I_2 $B(^3\Pi_{0^+})$ were performed by Steinfeld and co-workers[3] in the mid-1960s. They applied the C-W resolved fluorescence technique and demonstrated its versatility by determining numerous V-T and R-T cross-sections for more than ten collision partners. McCaffery et al. extended the I_2 studies by examining polarization effects in the resolved fluorescence.[4,5] They also used a circularly polarized excitation laser to optically pump Zeeman sub-levels in ground state I_2. This technique is analogous to the more traditional optical pumping of atoms that has been such a valuable tool in atomic physics.

More recently, Pritchard and co-workers have used a CW dye laser to determine literally hundreds of rate coefficients for V-T and R-T transfer in Na_2,[6] Li_2[7] and I_2.[8,9] They also made comparisons of their data to several scaling

and fitting laws that have been developed to predict trends in R-T rate coefficients.

The previously reported studies of R-T transfer using resolved fluorescence techniques have been performed predominantly on homonuclear molecules. Thus, the diatomic interhalogens are relevant since they offer the opportunity to compare R-T cross sections for polar species, e.g., IF and ICl to non-polar species such as I_2. State resolved energy transfer data for the interhalogens are sparse. Although I_2 has been studied extensively, only a small data base exists for R-T transfer for other diatomic halogens and interhalogens. Indeed, in addition to I_2, state resolved R-T transfer studies have been reported only in $Br_2(B)$[10] and IF(B).[11-13] Clyne, Heaven, and Davis[10] performed a preliminary CW resolved fluorescence study on Br_2 and obtained estimates for R-T rate coefficients for Br_2 collisions with Ar. Wolf and Davis[11] reported some rate coefficients for total removal of specific J' levels in IF(B) by rare gases, but they were unable to extract detailed, state-to-state R-T rate coefficients from their data. Dorko et al.[12] have observed state-to-state R-T processes in IF(B) and have reported some R-T rate coefficients for the collision partner Kr. In a recent study Clark and Littlewood[13] used a pulsed, two photon technique to extract R-T rate coefficients from IF(B) + He collisions.

The halogens and interhalogens are particularly relevant systems to study because optically pumped lasers have been demonstrated on the B→X systems in some of these molecules: e.g., I_2,[14-17] Br_2,[18,19] and IF.[20,21] In addition, some interhalogens are attractive candidates for short-wavelength chemical lasers. Consequently, R-T transfer is important in these molecules since this

process plays a major role in laser performance. From a more fundamental perspective, however, there is a need to establish the data base for R-T transfer rate coefficients so that scaling laws can be established and tested. The premise of these scaling and fitting laws is that, for a given collision system, an entire matrix of R-T rate coefficients can be expressed in terms of only a few parameters.

In this report we describe the results of a systematic study of R-T transfer in IF, ICl, and I_2. We have used several collision partners and have determined over 1000 state-to-state cross sections. We also show comparisons of our data to predictions of several scaling laws.

B.1 Experiment

B.1.1 Method

The technique of CW resolved fluorescence is simple, but can be quite susceptible to systematic errors. The fundamental concept is that, upon population of a single excited quantum state, spontaneous emission can be observed from both the initially populated (parent) level and other adjacent (satellite) levels that are populated by collisional energy transfer. In the absence of any collisions during the radiative lifetime of the relevant excited state, emission is observed exclusively from the parent level. On the other hand, if energy transfer collisions take place, then emission is observed from both the parent and satellite levels. As we show later, concomitant measurements of both the parent and satellite line intensities can be used to determine the rate coefficients for R-T transfer if the lifetime of the excited satellite state is known. Due to symmetry restrictions, the Q branch is absent

in the $B^3\Pi(0^+) \rightarrow X^1\Sigma^+$ system of the interhalogens, and the spectrum consists of only simple P & R doublets; overlaps of spectral features are thus minimal.

B.1.2 Apparatus

A block diagram of the apparatus is shown in Figure 1. The experiment consisted of three major components: a) the laser source, b) the reaction cell, and c) the detection system. For clarity we describe each of these components below.

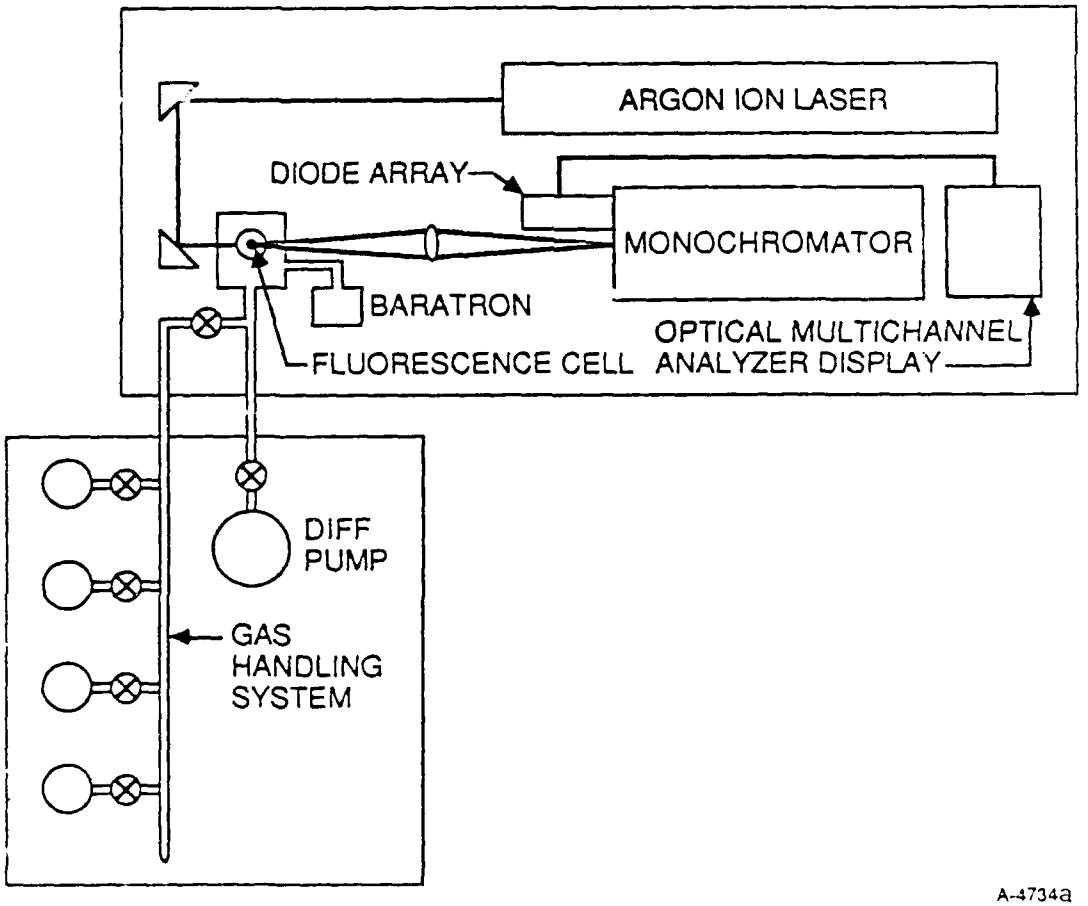

Figure 1.

Block Diagram of Experimental Arrangement

B.1.3 Laser Sources

We employed spectrally resolved CW laser-induced-fluorescence (LIF) as the primary experimental method. Excitation of single quantum states (v', J') of the molecules studied was facilitated using a Coherent Radiation CR 699-05 ring dye laser. This device provided powers of several hundred mW with subdoppler linewidths. Although our laser was only passively stabilized, we were able to remain at absorption line centers for several minutes which was adequate for the required data collection. For most experiments Exciton LD-590 dye was used. However, a series of runs on IF B(v'=6, J'=72) was performed using the 476.5 nm line of the Ar^+ ion laser that usually was used to pump the dye laser. This Ar^+ line is resonant with the R(71) line of the IF(6,0) band. The Ar^+ laser was run in a single mode configuration using a temperature stabilized intracavity etalon.

The wavelength of the dye laser was determined with a Burleigh WD-20 wavemeter. A Tropel Model 240-03 spectrum analyzer was used to confirm that the ring dye laser was operating in a single longitudinal mode.

B.1.4 Reactant Preparation

Iodine monofluoride is an unstable molecule and must be chemically produced in the gas phase. Since it rapidly disproportionates on cell walls, the IF source must be close to the volume in which observations are made. Iodine monofluoride is most efficiently produced by reacting F atoms with an iodine containing compound such as I_2 or CF_3I. Fluorine atoms were produced by passing CF_4 through an Evenson microwave cavity operating at 2.45 GHz and at a power of 60W. The CF_4 discharge flow tube was constructed from 14 mm o.d. alumina, and the CF_4 pressure in the flowtube was maintained at approximately

100 mTorr. The pressure in the observation region was required to be at least an order of magnitude less so that the experiment could be performed under essentially single collision conditions. This was accomplished by inserting a Teflon plug in the end of the discharge tube. The plug had a one mm diameter hole, and this caused a pressure drop of approximately an order of magnitude. The typical operating pressure of CF_4 in the reaction cell was 8 mTorr.

Molecular iodine was introduced through a small ring injector (2.5 cm diameter) that was placed 0.5 cm beyond the end of the CF_4 discharge tube. This configuration allowed the fluorine atoms and I_2 to mix and react for 2 cm prior to the observation region. The room temperature I_2 was contained in a small 300 ml flask that was connected to the ring injector. This source provided an I_2 pressure of approximately 1.0 mTorr in the reaction cell.

The reaction of I_2 + F is fast, $k = 4.1 \times 10^{-10}$ cm^3 molecule^{-1} s^{-1},[23] and produces an inverted vibrational distribution[24] of ground state IF with $v'' \leq 19$. We observed no visible chemiluminescence that could have caused spectral interferences. The IF(X) concentration in the present experiment is unknown but an upper limit is defined by the I_2 concentration to be 3.2×10^{13} molecules cm^{-3}. The hard sphere rate coefficient for IF+IF collisions is 1.80×10^{-10} cm^3 molecule^{-1} s^{-1}, and the IF+IF collision rate at [IF] = 1 mTorr is 5.8×10^3 s^{-1}. The radiative lifetime of IF(B, v'=6) is 8.2 μs[25] and is independent of J'. This implies that the average time between IF+IF collisions is twenty IF(B) lifetimes. Consequently, IF+IF collisions were negligible under our conditions.

For I_2 and ICl studies, I_2 and ICl vapors were introduced directly into the reaction/fluorescence cell since they are stable compounds.

The bath gas collision partner was introduced into the reaction cell through a 6 mm diameter tube. The pressure in the reaction cell was measured with a 0-1 Torr model 220 Baratron capacitance manometer.

B.1.5 Fluorescence Detection System

The laser beam was introduced through a sidearm that contained a series of light baffles, and it exited the cell through a similar sidearm. The laser beam was approximately collimated (diameter = 2 mm) in the chamber by means of a single lens. The laser induced fluorescence (LIF) was collected by a 30 mm diameter f/0.7 aspheric lens situated approximately 2.5 cm from the beam interaction region. The fluorescence was dispersed with a Spex 1.26 meter monochromator. Previously reported R-T transfer studies using LIF have been performed by mechanically scanning a monochromator over the bands of interest. An unavoidable difficulty with this arrangement is that power variations or frequency drifts in the laser during the scan cause drastic variations in the signal. One must then normalize and correct the fluorescence intensities to account for these variations. Since a scan often requires 10 to 20 min to record, the corrections can be significant and add to the systematic uncertainty of the overall result.

In order to minimize these problems we employed a Princeton Research Inc. Model 110 optical multichannel analyzer (OMA). The detector head consists of 1024 diode elements, each 25 μm wide. The spectral resolution for all experiments was 0.80Å which gave 5 pixels per resolution interval, an adequate compromise between sensitivity and resolution. The OMA detector head is an intensified reticon array with an extended S-20 response and a quantum efficiency of approximately 0.2. The readout time of the diode array is

16.2 ms and was the rate limiting process for acquisition of a single spectrum. Typically we exposed the detector head to the dispersed LIF for 15s and stored the resulting signal in the OMA memory. This process was repeated ten times with each record being averaged with the previously recorded runs. This technique produced a composite spectrum which required only several minutes to record yet represented the average of several thousand scans. The individual spectra were stored on floppy disk for subsequent analysis. A major advantage of using the OMA is that a single scan is obtained nearly instantaneously and consequently laser intensity drift is an insignificant source of error.

B.2 Kinetic Analysis

B.2.1 Method

The R-T rate coefficients were determined using a steady state analysis. Under single collision conditions, the steady state population of any final level J_f, formed by R-T transfer from the laser excited level J_i is given by Eq. (1)

$$\frac{d[N_f]}{dt} = [N_i][M]\, k_R(i \rightarrow f) - [N_f]/\tau_r = 0 \quad . \tag{1}$$

Rearrangement of Eq. (1) yields Eq. (2).

$$[N_f]/[N_i] = [M] k_R(i \rightarrow f)\, \tau_r \quad . \tag{2}$$

In Eqs. (1) and (2)

$[N_i]$ = population of laser pumped level

$[M]$ = bath gas concentration

$k_R(i \rightarrow f)$ = rate coefficient for transfer from J_i to J_f

and τ_r = radiative lifetime of J_f.

Consequently, a plot of $[N_f]/[N_i]$ versus $([M]\ \tau_r)$ should yield $k(i \rightarrow f)$. However, if the number density of M is too high, secondary collisions can occur and Eq. (2) is no longer an adequate description. If the bath gas pressure is high enough that two or more R-T events occur during the period τ, then the ratio $[J_f]/[J_i]$ no longer depends linearly upon the pressure. For example, in the extreme case of complete rotational thermalization, this ratio will be independent of pressure. Departure from linearity in the plots of $[J_f]/[J_i]$ versus $[M]\tau$ indicates that multiple collisions are occurring. (We noted small departures from linearity at pressures greater than 40 mTorr.) The treatment of multiple collisions can take on varying levels of complexity and indeed can become computationally unwieldy. Ideally one would always work at pressures sufficiently low that the probability of two or more collisions during one radiative lifetime is negligible. Unfortunately, these conditions are not always compatible with an adequate signal strength, and the possibility of multiple collisions must be considered. For IF(B), a bath gas pressure of approximately 25 mTorr would cause one collision per lifetime assuming a gas kinetic collision cross section. We obtained most of our data at pressures lower than this. Nevertheless, we explored the effects of multiple collisions.

Secondary collisions have the effect of shortening the lifetime of the final state, J_f. The first order correction is accomplished by accounting for non-R-T processes such as collisional quenching of J_f, collisional predissociation of J_f, and V-T removal from v_i. Consideration of these effects leads to Eq. (3)

$$[N_f]/[N_i] = \frac{k_R(i \rightarrow f)[M]\ \tau_r}{1 + (k_Q[M] + k_p[M] + k_v[M])\tau_r} \quad , \tag{3}$$

where k_Q, k_p, and k_v are the respective rate coefficients for electronic quenching, predissociation, and V-T transfer. Note that all removal processes refer to the final rotational level, J_f. From Eq. (3) we observe that a plot of $[N_f]/[N_i]$ versus [M] can be used to determine k_R if τ_r, k_Q, k_p, and k_v are known.

Electronic quenching of IF(B) by most of the bath gases used in this study, viz.: He, Ne, Ar, Kr, Xe, and N_2 has been previously shown to be uniformly inefficient and this process is negligible under our conditions.[26] The correspondng V-T rate coefficients have also been determined previously,[11] and the appropriate values are used in Eq. (3). However, since the V-T rate coefficients are all $\lesssim 10^{-11}$ cm^3 molecule^{-1} s^{-1}, and since bath gas pressures were always $\leq$ 25 mT, the first order V-T rate was always less than 10 percent of the radiative rate.

The quenching rate coefficient for IF(B) by I_2 was estimated by Wolf and Davis[26] to be on the order of 3.9×10^{-10} cm^3 molecule^{-1} s^{-1}. This was later confirmed by Berman and Whitefield[27] who determined a value of $(3.5 \pm 0.3) \times 10^{-10}$ cm^3 molecule^{-1} s^{-1}. Since the I_2 pressure was less than 1 mTorr, quenching of IF(B) was essentially negligible. Although there have been no reported measurements of IF(B) electronic quenching by CF_4, we expect it to be weak since the molecule CF_4 is inert and non-polar. The quenching rate coefficients for such partners are small,[26] $\sim 10^{-14}$ cm^3 molecule^{-1} s^{-1} for He, Ne, Ar, Kr, Xe, N_2, and SF_6. We expect CF_4 to exhibit similar behavior. In an effort to confirm this we observed total, spectrally unresolved LIF as CF_4 was added to the reaction chamber. No diminution of the fluorescence intensity was observed over the pressure regime 0 to 40 mTorr. We conclude that the quenching of IF(B) by CF_4 is negligible under our conditions.

Until recently,[28] collisional predissociation in IF(B, v=6) had never been observed. Indeed, in detailed LIF work, Clyne and McDermid concluded that the manifolds of $v'<8$ are all essentially stable.[25] Predissociation first occurs in $v'=8$, $J'=52$. Although Clyne and McDermid only measured lifetimes for $J' \leq 57$ in $v'=6$, the very significant rotational barrier should insure stability for J' considerably greater than 57 in $v'=6$. For example in $v'=8$, predissociation is first observed at $J'=52$ which is 230 cm^{-1} greater than the IF dissociation energy. Predissociation is also observed for ($v'=9$, $J'=7$).[25] A linear extrapolation of these two predissociation energies versus $J(J+1)$ implies that the rotational barrier for $J'=85$ is at least 600 cm^{-1} greater than the IF dissociation energy of 22333 cm^{-1}. Thus, predissociation in $v'=6$ is expected for energies greater than approximately 22933 cm^{-1}. However the energy of $v'=6$, $J'=85$ is only 22732 cm^{-1}. Consequently all $v'=6$, $J' \leq 85$ are expected to be stable, and we observed no anomalous intensity distribution from any of these levels. Indeed, very recent work by Girard et al.[28] has shown that all $J'<120$ are stable in $v'=6$. For the data reduction we used an average radiative lifetime of $\tau_o = 8.2$ μs for all $J \leq 85$ (Ref. 25).

The next level of approximation allows for R-T removal from J_f to all other rotational levels within v_i. This treatment, first described by Steinfeld and Klemperer[3] in their pioneering I_2 studies, yields Eq. (4)

$$[N_f]/[N_i] = \frac{k_R(i \rightarrow f)\,[M]\,\tau_r}{1 + \underbrace{\left(k_R^T[M] + k_v[M] + k_p[M] + k_Q[M]\right)\tau_r}_{\alpha}} , \qquad (4)$$

where

$k_R^T \equiv$ total rate coefficient for R-T transfer from J_f to all other J within v_i.

This correction does not allow for the potentially important channel of repopulation of J_f via a secondary collision from intermediate rotational levels. Bergmann and Demtröder accounted for these secondary collisions in their analysis of Na_2 data.[29] Using a similar approach we find that if we call these intermediate levels , then the term α becomes

$$\alpha = \left(k_R^T[M] - \sum k_R(\ell \rightarrow f) \left\{ \frac{[N_\ell]}{[N_f]} [M] \right\} + k_v[M] + k_Q[M] \right) \tau_r \quad . \qquad (5)$$

where $\ell \neq i$.

This additional term has the effect of counteracting the removal of J_f via the $k_R^T[M]$ term. In practice, multiple collisions are treated using Eq. (6) in an iterative fashion

$$[N_f]/[N_i](1+\alpha) = k_R(i \rightarrow f)\ [M]\ \tau_r \quad . \qquad (6)$$

First, one examines plots of $[N_f]/[N_i]$ versus $[M]$ at the lowest attainable $[M]$ and extrapolates a linear slope. If this is done for each J_f, then a first order set of $k_R(i \rightarrow f)$ can be obtained. Using these $k_R(i \rightarrow f)$, one calculates α and modifies $[N_f]/[N_i]$. New $k_R(i \rightarrow f)$ are obtained and compared to the original set. The process is repeated until the $k_R(i \rightarrow f)$ converge. Several groups have used this approach when $|\Delta J| \lesssim 15$. For example this treatment was applied to Na_2,[29] and OH.[30] Even though our Stern-Volmer plots displayed little discernable curvature, we constructed a code to treat the corrections, through one iteration, using Eq. (6). After one iteration, this treatment resulted in large corrections (> 50%) being indicated for some of the $k(72 \rightarrow f)$ produced with the single collision analysis. It was clear that many iterations would have to

be performed in order to arrive at a converged set of rate constants. We concluded that in $I\Gamma(B)$ where $|\Delta J| \lesssim 60$, the iterative treatment introduces large uncertainties. A large portion of these uncertainties arises from the need to determine $[N_i]/[N_f]$ for each iteration. This approach appeared to be very laborious and impractical. Rather, we performed several tests to examine empirically the potential problem of multiple collisions. The first test is simply the observation that, for all bath gases, plots of $[N_f]/[N_i]$ versus $[M]$ were linear to within approximately $\pm$ 10 percent for pressures up to 20 mTorr for all gases studied.

For the case of J_i=72 we also carefully examined the populations of all $J_f \leq 19$ as a function of $[M]$. We chose this region since it represented an exchange of rotational energy of nearly 5 kT (at 300 K) and the effects of two consecutive collisions would be most prominent for these large ΔJ. Multiple collisions would be manifest in these plots of $[\sum_{0}^{19} J_f]/[J_i]$ versus $[M]$ as a quadratic dependence on $[M]$. In all cases we observed a linear dependence upon $[M]$ for pressures < 20 mTorr. At higher pressures a non-linear behavior was observed. This is illustrated for Ar in Figure 2. From similar plots we empirically determined pressures below which the dependence was linear for the other collision partners. All analyses were completed using only those data with $[M]$ below these "critical" pressures.

We also performed a third test to determine whether our (essentially) single collision model was adequate. Using the $k_R(i \rightarrow f)$ determined from the treatment described above, we predicted resolved LIF spectra as a function of $[M]$ using the single collision model. In Figure 3 we compare the predicted spectrum to data using He at the relatively high pressure of 34 mTorr. The

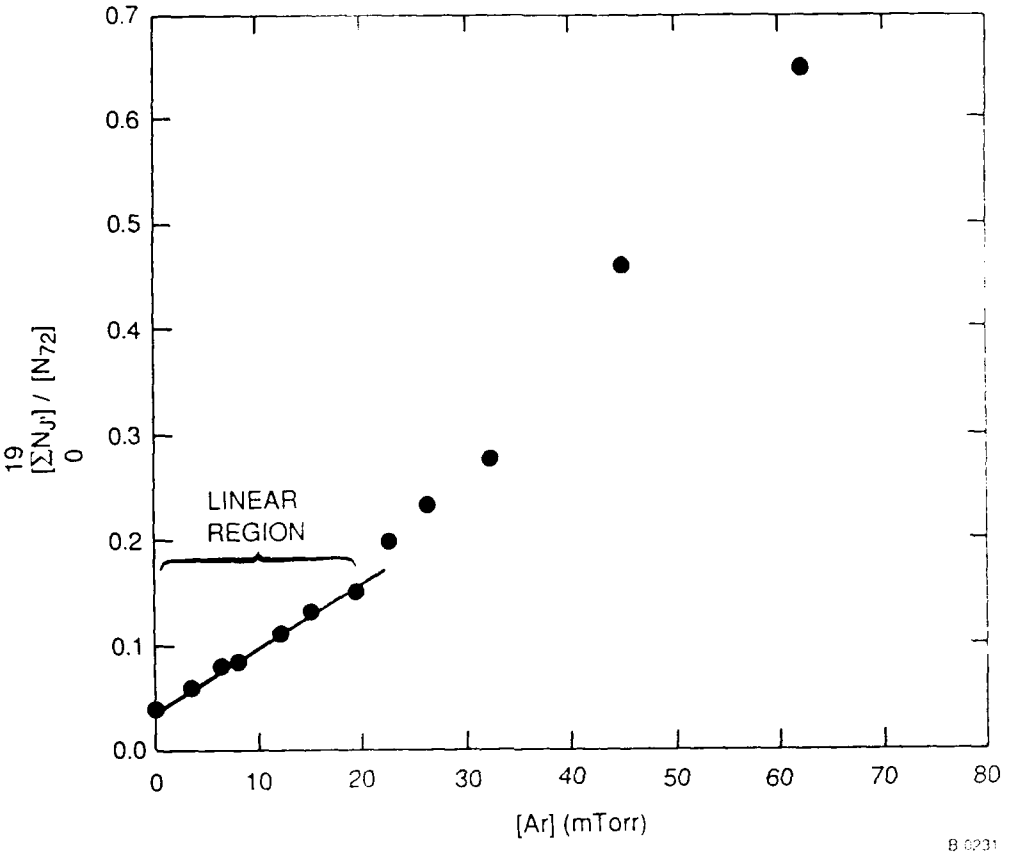

Figure 2.

Stern-Volmer Plot of $[\sum_{0}^{19} N_J]/[N_{J=72}]$ versus [Ar]. Note linear behavior for pressure less than 20 mTorr.

agreement is excellent, supporting our contention that multiple collision effects are insignificant at these low pressures. It appears that if multiple collisions are taking place, the depopulation of J_f is balanced by repopulation of the level from nearby levels. We cannot discern the difference between these two cases. However, either case is adequately described by our analysis.

B.2.2 Population Determinations

The intensity $I^{v',v''}_{J',J''}$ of a rovibronic emission line is related to the population in the upper state $N^{v'}_{J'}$ through Eq. (7)

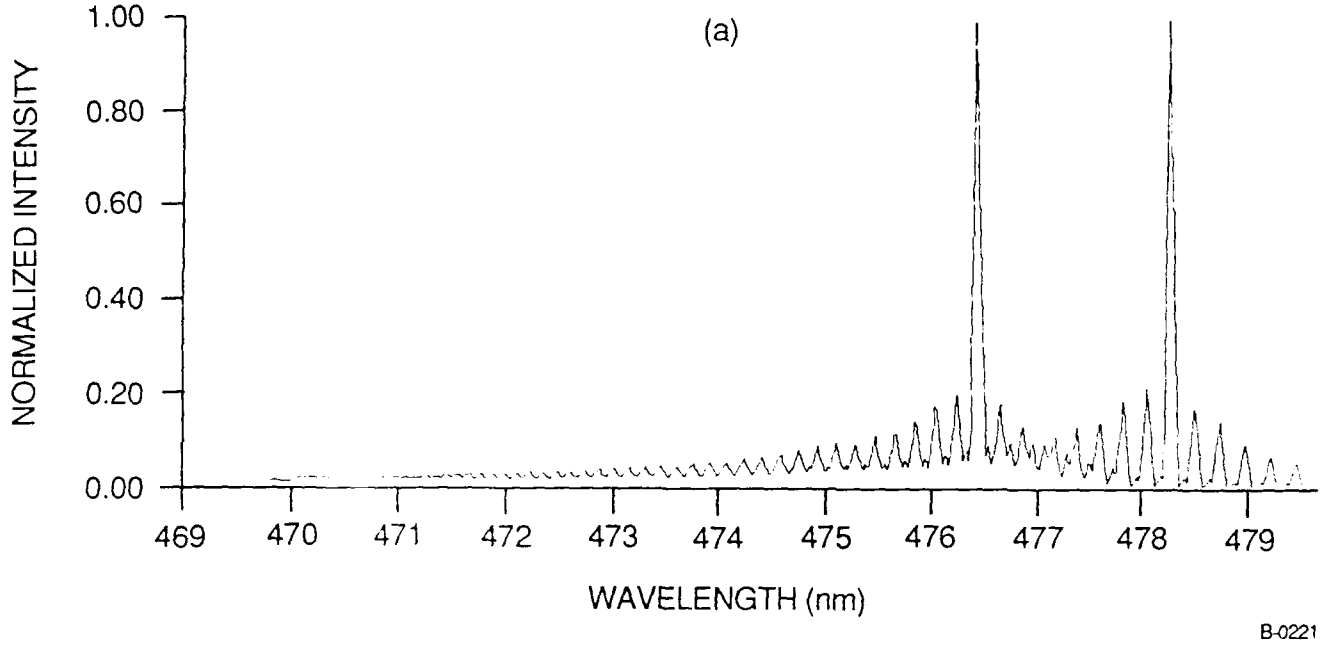

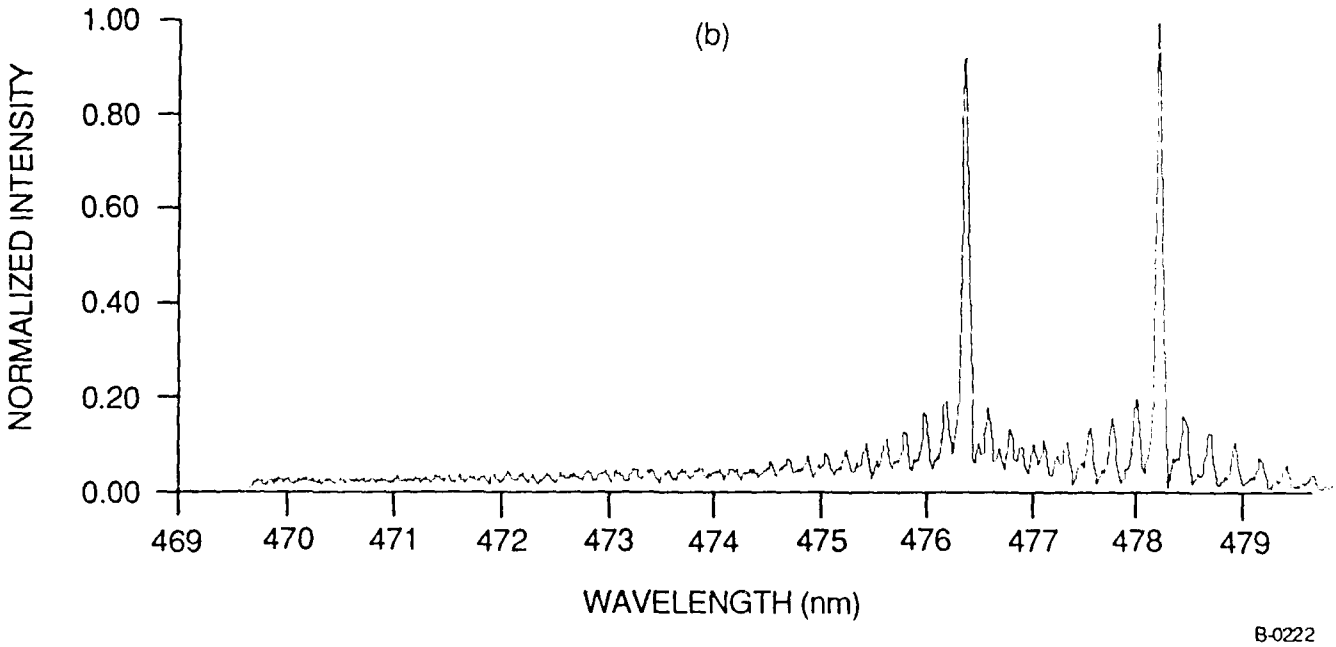

Figure 3.

a) Synthetic Spectrum Produced by Assuming Single Collision Model and Measured Rate Coefficients for He. Calculation run at [He] = 34 mTorr. b) Resolved LIF data for He at 34 mTorr.

$$I^{v',v''}_{J',J''} = N^{v'}_{J'}\ \nu^3\ |R_e|^2 q_{v',v''}\ \frac{S_{J',J''}}{2J+1} \quad , \tag{7}$$

where ν is the frequency of the transition,

$|R_e|^2$ is the electronic transition moment,

$q_{v',v''}$ is the Franck Condon factor,

and $S_{J',J''}$ is the rotational line strength.

The determination of $N^{v'}_{J'}$ from an intensity measurement is very difficult because absolute photometric techniques are required, however, we need only the ratio $[N_f]/[N_i]$ to determine $k_R(i \rightarrow f)$. (Note that the index denoting the initial vibrational level will be suppressed because $v_i = v_f$ in this study.) Consequently,

$$\frac{[N_f]}{[N_i]} = \frac{I_{J_f}\ (2J_f+1)\left(S_{J'_i,J''_i}\right)\ \nu_i^3}{I_{J_i}\ (2J_i+1)\left(S_{J'_f,J''_f}\right)\ \nu_f^3} \quad . \tag{8}$$

In principle, either peak intensities or integrated intensities can be used to determine $[N_J]$ However, if one employs peak intensity measurements to determine N_J, then complete resolution of each rotational feature is required to insure that contributions from adjacent levels are negligible. This presents a difficulty in IF(B→X) bands because there are many near coincidences between P(J) and R(J+n), where n depends upon the particular v',v" band being observed. For example, in the (6,10) band, P(J) and R(J+9) are nearly coincident while in (3,11) the overlap occurs for P(J) and R(J+14). One can minimize this problem through judicious choice of vibrational band, but there is an additional problem that is unavoidable. Near the bandhead spectral resolution is lost since the emission lines are very closely spaced. Where

resolution of features is incomplete, the better approach is to use a spectral fitting routine. We have used this technique as described below.

The fitting of the experimental spectra to determine rotational level populations was carried out by first creating very high resolution synthetic spectrum for each of the individual rotational levels contained in the experimental spectrum. The line positions were calculated using the Dunham expansion coefficients of Prikl and Wanner.[31] A triangular slit function was then convoluted with each spectrum giving "basis set" spectra with the appropriate resolution and with intensity corresponding to unit population. These spectra were then used in a linear least squares fitting procedure in which the populations associated with each rotational level were varied to produce a point by point best fit to the data. Prior to fitting, a constant background signal was subtracted from each experimental spectrum and then a correction for relative instrument spectral response was made. Using the resulting rotational level populations, N_J, ratios of $N_{satellite}/N_{parent}$ were calculated.

In order to determine accurately the population ratios from recorded spectra, one must know the response function of the entire detection system which includes the lens, monochromator, and diode array. Typically one would use a standard irradiance lamp. However, our 100W lamp was so intense that neutral density filters would have been required to prevent saturation of the OMA detector. These filters would not have been used during actual data acquisition and the calibration of these filters would have introduced additional uncertainties. Consequently, we selected the NO/O afterglow as our reference source.[32] The chemiluminescence from this reaction, in the 4700 to

4800Å region, is well characterized and no filters were required. This spectrum was recorded using the same monochromator slit widths as used in the actual R-T experiments. The response function obtained using this technique was very uniform, and only a 20 percent variation over the entire range of the IF (6,0) band was observed.

The possibility that laser saturation could affect the results was checked by monitoring $[N_f]/[N_i]$ as a function of laser power. No changes were observed for a variation in the laser power of over an order of magnitude. We note that this is expected from Eq. (2) which predicts that $[N_f]/[N_i]$ depends only upon the lifetime of J_f which should not be a function of laser saturation of J_i.

Analogous spectral fitting analyses were used to determine $[N_f]/[N_i]$ in the I_2 and ICl studies. Since the radiative lifetime ICl(B)[34-36] is considerably shorter than that for IF(B) we could work at considerably higher bath gas measures.

C. Results

C.1 IF($v'=6$, $J'=72$) Data Reduction

We succeeded in recording spectrally resolved fluorescence from $0 < J_f < 87$ subsequent to laser excitation of $J'=72$ using the collision partners He, Ne, Ar, Kr, Xe, N_2 and, CF_4. We recorded and averaged 4000 individual spectra for each buffer gas pressure, and typically 10 to 12 pressures were employed for each bath gas.

Three resolved LIF spectra are shown in Figure 4. These data clearly demonstrate the R-T transfer that occurs upon the addition of helium. In

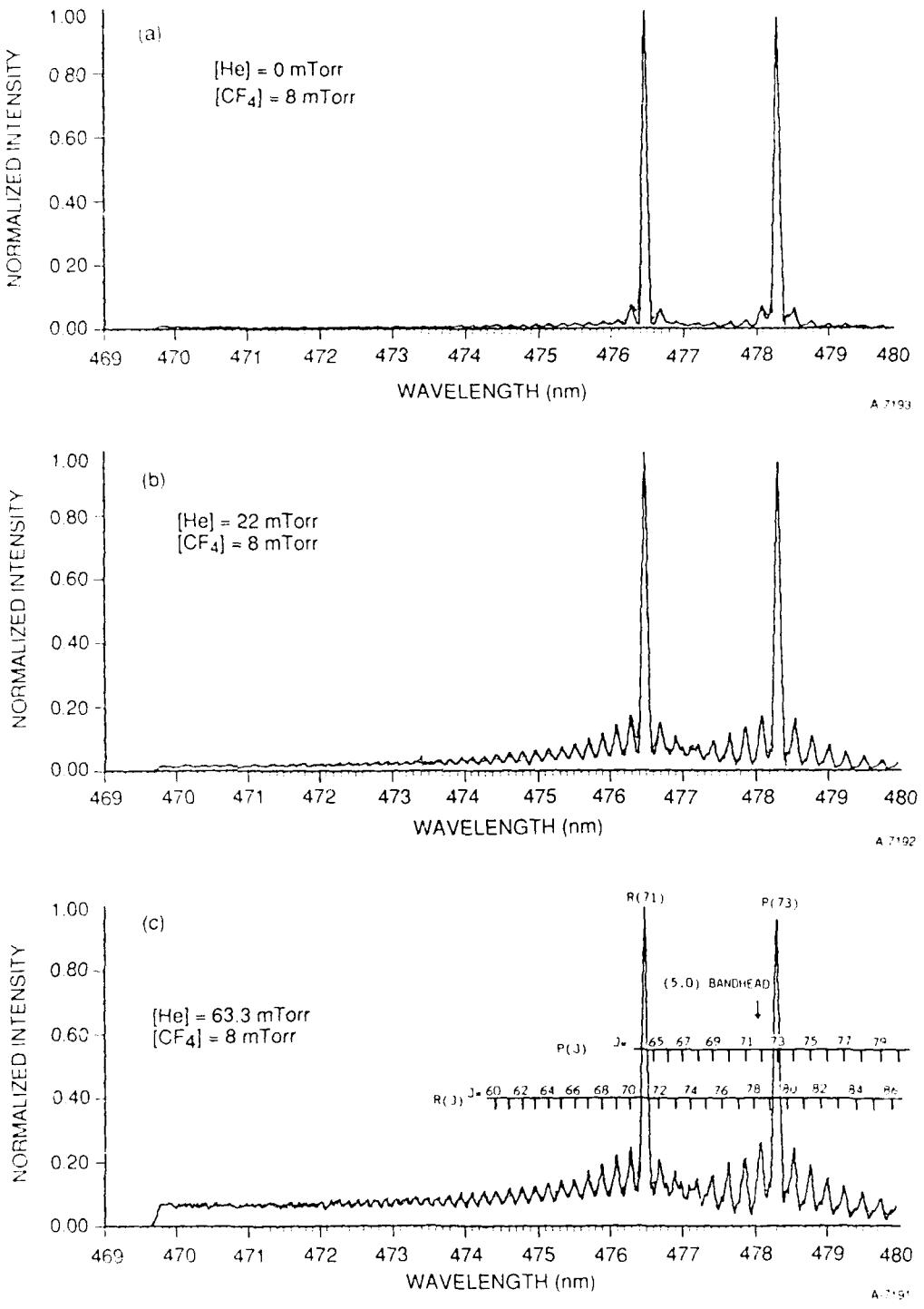

Figure 4.

Resolved LIF for Three Different He Bath Gas Pressures: a) [He] = 0.0 mTorr, b) [He] = 22 mTorr, c) [He] = 63.3 mTorr. For all data shown, $[CF_4]$ = 8.0 mTorr. Light lines are data and dark lines are the spectral fits.

Figure 4 the light lines represent the experimental data and the bold-faced lines are the spectral fits from which the population ratios are determined. The data in Figure 4a, obtained in the absence of helium, show the strong parent P-R doublet and a few weak satellite features caused by collisions of IF(B) with CF_4. Figures 4b and 4c show the results of adding helium. While the (6,0) band is far from being rotationally thermalized, extensive rotational relaxation has occurred.

We observe from Figure 4 that reproduction of the individual P and R lines in the (6,0) band is excellent even near the bandhead. The position of the (5,0) bandhead is also shown in Figure 4. With the spectral fitting code, we can also determine any population that is transferred to $v'=5$ via V-T collisions. In a future paper we will discuss ΔJ processes during a vibrationally inelastic collision.

The spectral fitting program provides the population ratio $[N_f]/[N_{72}]$ for each J_f as discussed previously. To determine individual $k_R(72 \rightarrow f)$, a Stern-Volmer plot must be constructed for each J_f. In practice this is accomplished by creating data files of $[N_f]/[N_{72}]$ and [M] from the results of the spectral fitting routine. These data arrays are then input into a kinetic code which performs the required Stern-Volmer analysis.

The total transfer rate coefficient $\sum_{J'=0}^{87} k_R(72 \rightarrow f)$ is also obtained from the analysis. Truncation at $J'=87$ is done since that is the highest J' observed in our resolved spectra of the (6,0) band. Due to the 120Å bandwidth, determined by the size of the diode array, observation of higher J' would not allow viewing of the bandhead. We chose to follow the $\Delta J'<0$ processes all the

way to the (6,0) bandhead. We have also performed experiments observing J'>87 and the populations become negligibly small.

Typical Stern-Volmer plots for $\Delta J = -12$ and $\Delta J = -22$ are shown in Figures 5 and 6 for helium bath gas. The solid lines represent a non-weighted linear least squares fit to the data. The linearity of the data provides strong evidence that multiple collisions are negligible. In Figure 7 we show a Stern-Volmer plot from which the total R-T transfer rate coefficient is determined. Again, the linearity of the data is very good which seems to confirm that, under our experimental conditions, only single collision events need to be considered.

We completed similar studies using Ne, Ar, Kr, Xe, N_2, and CF_4 bath gases. For illustration, in Figures 8(a) through 8(d) we show resolved fluorescence spectra for He, Ne, Ar, and Xe all at approximately the same pressure (~25 mTorr). It is obvious that collisions with the heavier rare gas atoms Ar and Xe promote larger rotational quantum changes than either Ne or He.

C.2 Cross Section for R-T Transfer

The R-T cross section is a more fundamental parameter than the rate coefficient. While we cannot determine velocity dependent cross-sections from our data, we can calculate effective hard sphere cross sections $\sigma(i \to f)$ using the conventional definition given by Eq. (9)

$$\sigma_R(i \to f) = \frac{k_R(i \to f)}{v} \quad . \tag{9}$$

In Eq. (9) v is the center of mass RMS thermal velocity of the IF+M system. In Table 1 we present the total R-T cross sections ($\sum_f \sigma(i \to f)$) for He, Ne, Ar, Kr, Xe, N_2, and CF_4. We also list the ratio of the total R-T cross section (σ_R) to the effective hard sphere cross section (σ_g) obtained from Lennard-Jones We

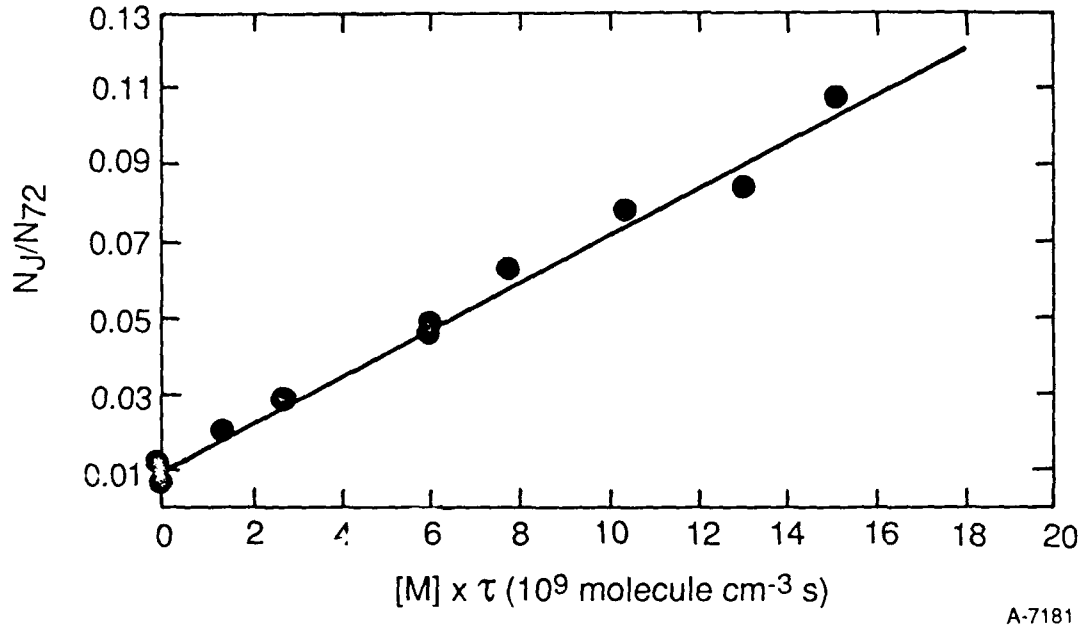

Figure 5.

Stern Volmer Plot for ΔJ = -12 per Collision Using He Bath Gas

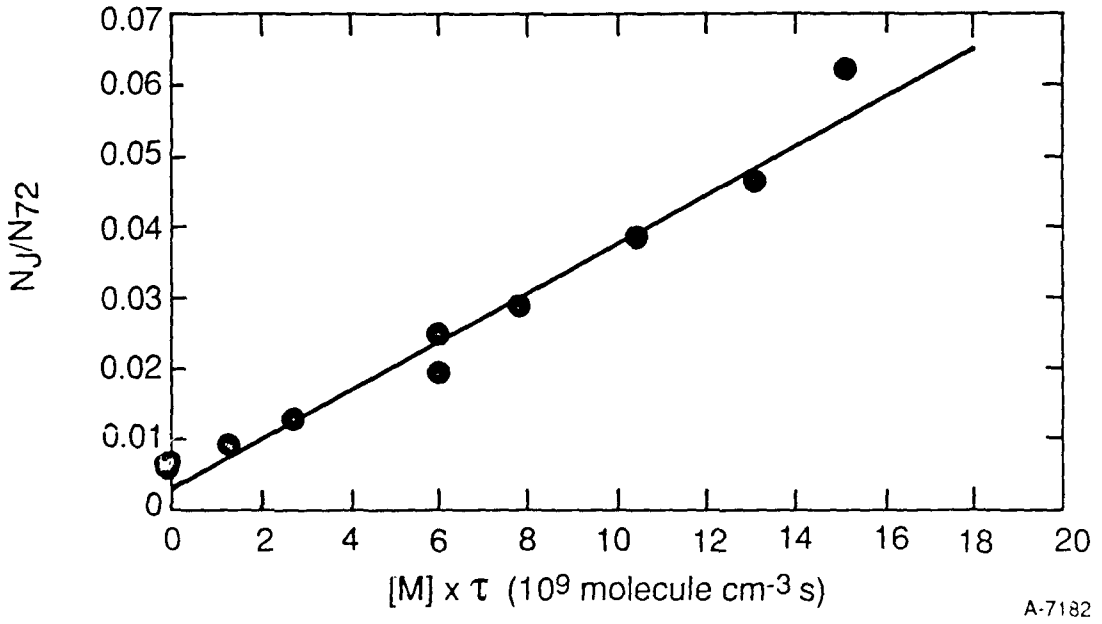

Figure 6.

Stern Volmer Plot for ΔJ = -22 per Collision Using He Bath Gas

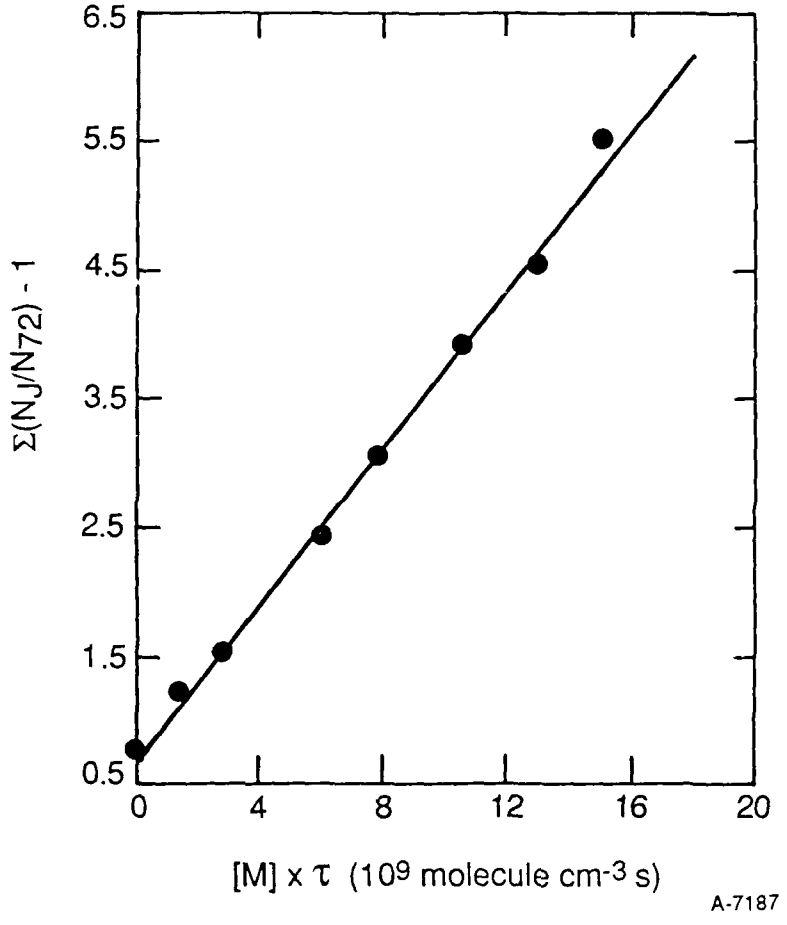

Figure 7.

Stern Volmer Plot for Total Rotational Energy Transfer; $-72 < \Delta J < +15$ Events are Included. Collision partner was helium.

consider a classical model[1,3] to aid in the interpretation of the results. The average amount of angular momentum, L, available for exchange in a collision is

$$\underline{L} = \underline{r} \times \underline{P} \quad . \tag{10}$$

In scalar form this equation can be written as

$$L = \mu v b = \left(\frac{8kT}{\pi}\right)^{1/2} \mu^{1/2} \, b \tag{11}$$

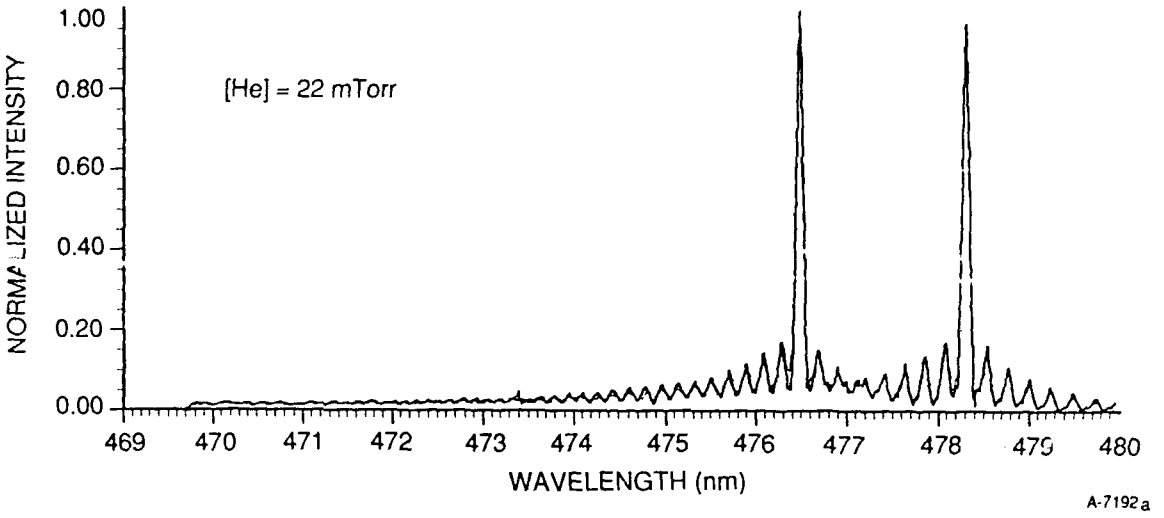

(a)

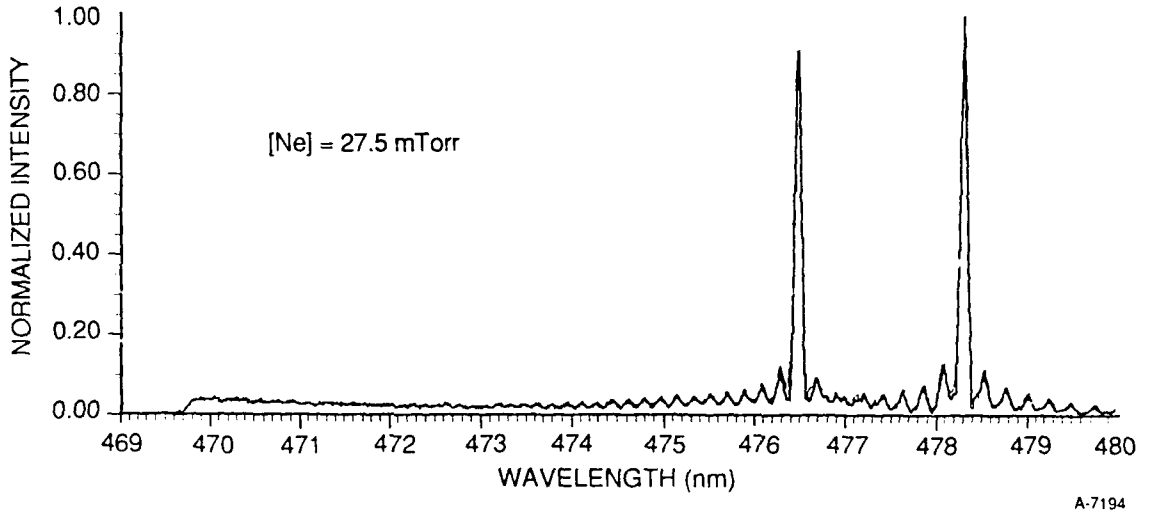

(b)

Figure 8.

Resolved LIF Spectra and Spectral Fit Using Several Rare Gas Collision Partners at Comparable Pressures

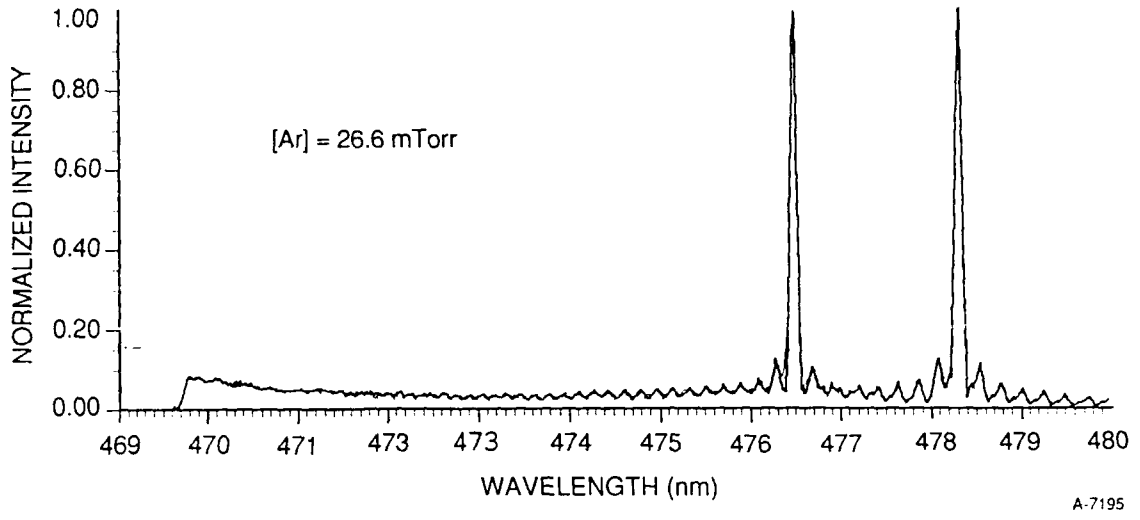

(c)

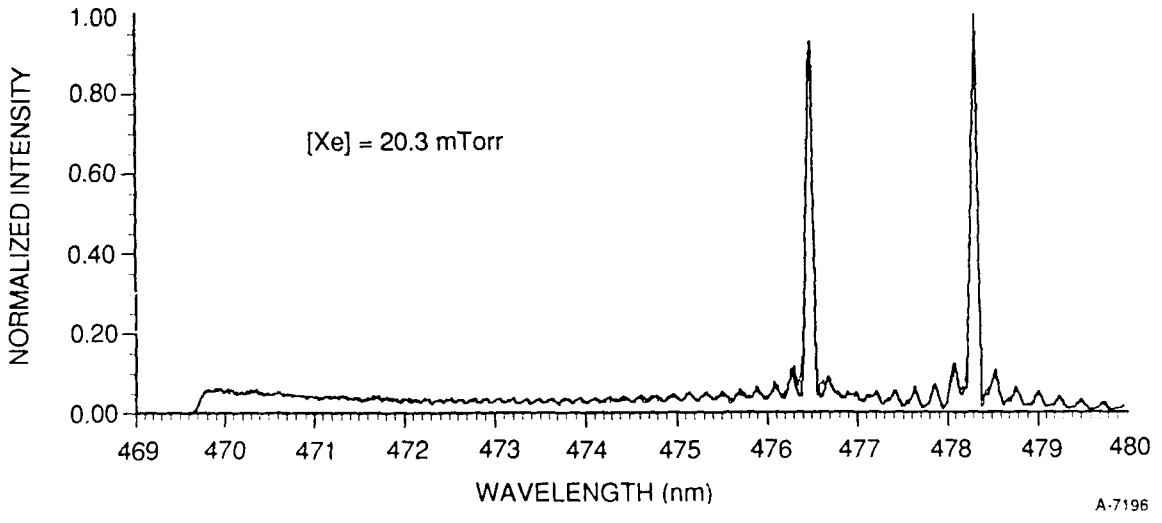

(d)

Figure 8.

Resolved LIF Spectra and Spectral Fit Using Several Rare Gas Collision Partners at Comparable Pressures (Concluded)

Table 1.

Rate Coefficients and Velocity Independent Cross Sections for Total R-T Removal From J_i=72

Collision Partner	Rate Coefficient 10^{-10} cm^3 mol^{-1} s^{-1}	Cross Section (10^{-16} cm^2)
Helium	2.94	23.1
Neon	2.29	38.3
Argon	2.16	48.1
Krypton	1.92	55.7
Xenon	2.15	71.1
N_2	3.69	71.1
CF_4	2.42	60.7

where we have used the rms thermal velocity $v = \left(\frac{8kT}{\pi\mu}\right)^{1/2}$. In Eq. (11) μ is the reduced mass and b is the impact parameter. Figure 9 is a plot of σ_R/σ_g versus $\mu^{1/2}b$ where b is taken to be the sum of the particle radii.

The data in Figure 9 show that the efficiency of the R-T process does increase as the mass of the collision partner increases. For example the ratio of $(\sigma_R/\sigma_g)_{Xe} \Big/ (\sigma_R/\sigma_g)_{He}$ is approximately 2·3. The analogous ratio[3] for I_2(B) (v_i'=25, J_i'=34) is 2·5. Indeed, the relative efficiencies for R-T transfer out of IF(B, v'=6, J'=72) are very similar to those out of I_2(B, v'=25, J'=34) when the collision partner is a rare gas atom. This is an intriguing result since IF is polar and I_2 is not. At the present time we cannot conclude that the observed increase in the efficiency of the R-T process as a function of reduced mass is attributable only to the mass of the collision partner since the heavier particles also have larger polarizabilities. For example, in an earlier study, Wolf and Davis[11] used a classical model and showed that (σ_R/σ_g) for R-T transfer out of IF(B, v'=3, J'=22) scaled as $(\alpha\mu^{1/2})^{1/3}$, where α is the polarizability of the collision partner.

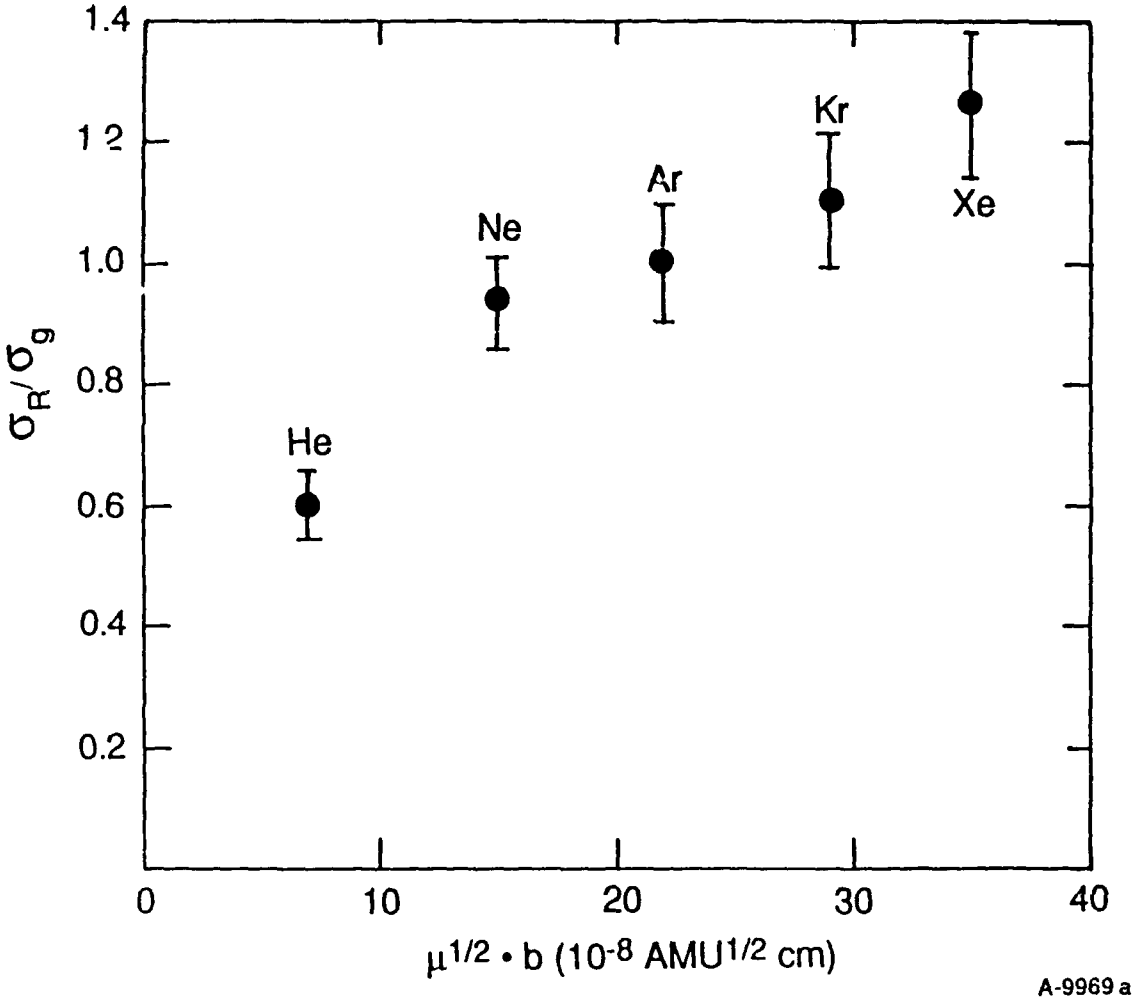

Figure 9.

Plot of σ_R/σ_g versus the Product of $b \cdot \mu^{1/2}$ of the Collision System for $J_i = 72$

Since IF(B) possesses a permanent dipole moment, energy transfer and quenching studies may lead to a more thorough understanding of the importance of the polarity of the collision partners. Previous studies of these processes in $I_2(B)$ have shown that the efficiency of R-T transfer seems to increase with the polarity of the collision partner. For example, Steinfeld and Klemperer[3] found that the polar species SO_2 and CH_3Cl were considerably more efficient R-T

partners than non-polar species of comparable mass and they suggested that the permanent dipoles were active in the R-T process. However, they also found that the non-polar CO_2 molecule was also an efficient R-T partner. At the present time we are not able to make a definitive conclusion with respect to the role of polarity in R-T collisions involving heteronuclear halogens since we have only used one collision partner (ICL on itself) possessing a permanent dipole. The ICL-ICL results do tentatively support this notion since, for example, the total rate coefficient for R-T transfer is roughly twice as large as that for the inert gases helium on argon when $J_i = 55$ is probed. (These results are described in greater detail in a subsequent section.) It seems likely that the long range forces associated with two interacting dipoles could play a major role in the R-T transfer process. In future experiments we plan to examine rotational energy transfer in IF(B) using polar species such as HF and H_2O.

It is also instructive to examine the state-resolved cross sections for R-T transfer, and these are shown in Figure 10(a)-(d). From these data we see that distributions of the cross sections as functions of ΔJ become broader as the mass of the collision partner increases. It is clear that, with greater collision-partner mass, the cross sections for large ΔJ transfer increase substantially. While the cross sections for small ΔJ are within a factor of two for all four collision partners in this figure, those for the largest ΔJ increase dramatically with greater collision-partner mass. This behavior was first observed in $I_2(B)$ by Steinfeld and Klemperer[3] and was interpreted by them using the classical model described above. They argued that the heavier masses bring more angular momentum to the collision and that this angular momentum

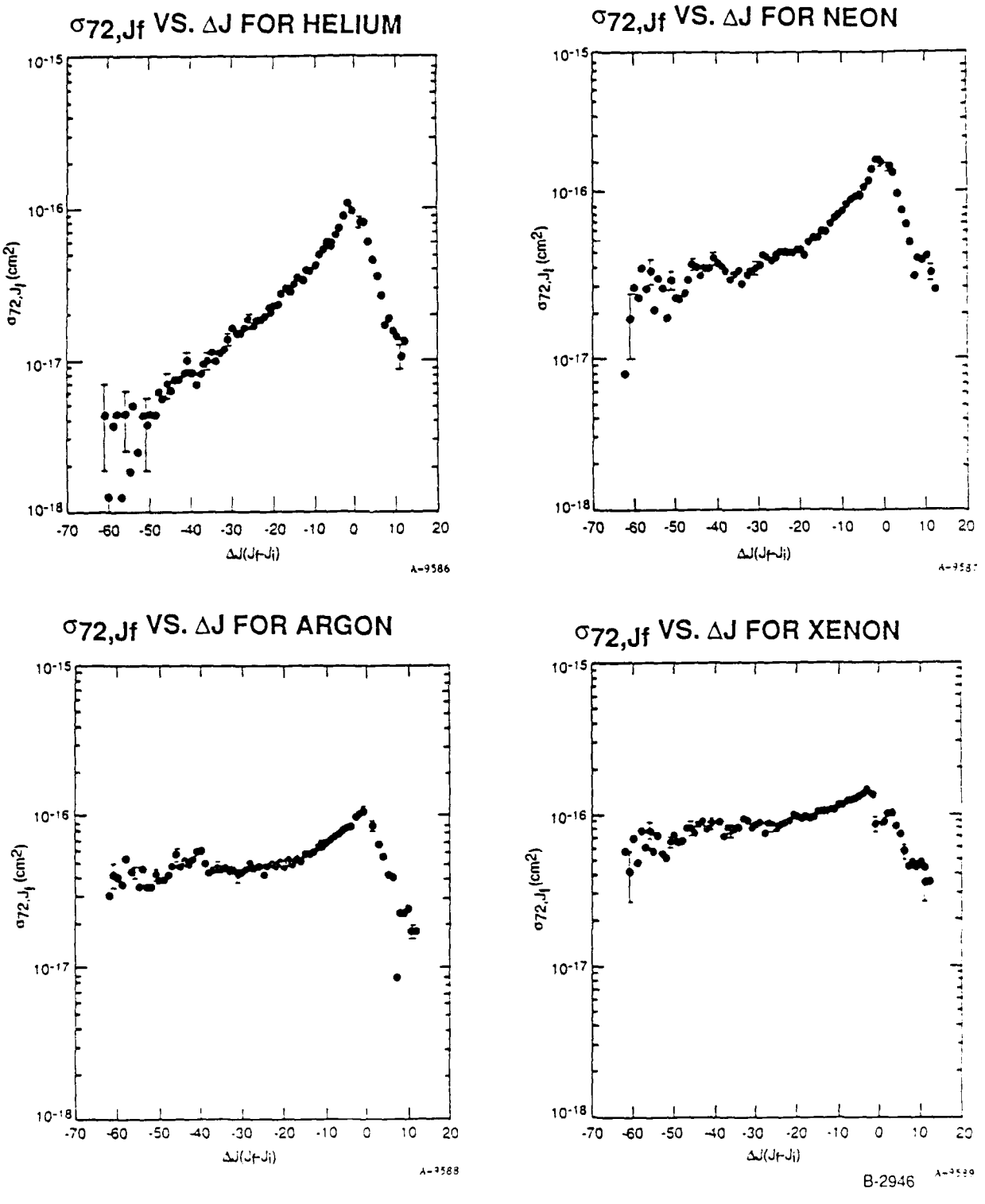

Figure 10.

State-to-State Cross Sections for Several Collision Partners;
a) He, b) Ne, c) Ar, and d) Xe

couples into rotation of the I_2 molecule. We observe a similar behavior in IF(B) as evidenced both in the spectra shown in Figure 8 and in the cross sections displayed in Figure 10. Thus, the increase in the total cross section as a function of the collision partner mass is due to larger ΔJ processes being more probable for the heavier particles. Pritchard and co-workers[9] have recently reported a similar trend for several initially populated J' in I_2(B, v=11). They used only two noble gases He and Xe, but the distributions for Xe were broader than those for He for each initially excited J'. The classical model seems to give a satisfactory qualitative picture for the general shape of the state to state cross section distributions for both I_2 and IF.

Similar plots for Kr, N_2, and CF_4 are shown in Figure 11. The CF_4 data illustrated in Figure 11 shows that a polyatomic collision partner behaves very differently from an atomic partner. The individual R-T cross sections are nearly uniform over a large range of ΔJ. This implies that the internal degrees of freedom in CF_4 may be efficient acceptors of the rotational energy in IF. We are presently investigating other molecular collision partners.

C.3 R-T Transfer with J_i=13, 27 and 35

A typical resolved LIF spectrum for J_i=35 with the collision partner helium is shown in Figure 12. Several interesting features are evident. First, extensive R-T transfer occurs for both $\pm\Delta J$. Secondly, considerable vibrational to translational (V-T) transfer is observed. Finally, the satellite vibrational band (5,0) appears to be much more rotationally thermalized than the parent (6,0) band.

In Figures 13 and 14 we compare resolved LIF spectra for J_i=13 using He and Xe as collision partners at nearly the same pressure. Two conclusions can

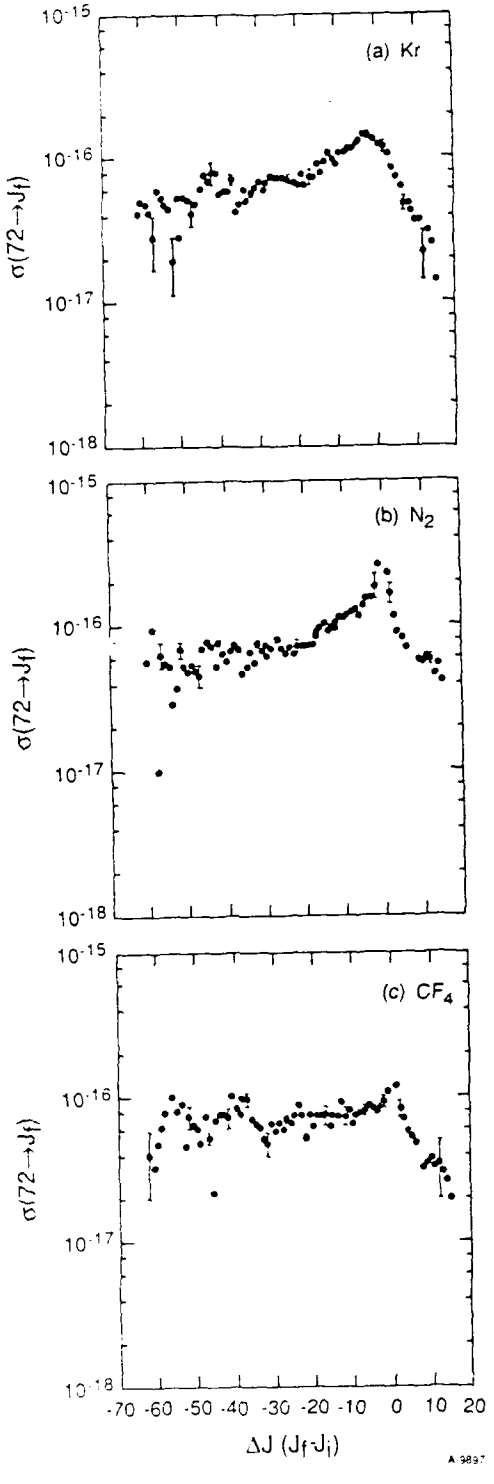

Figure 11.

State-to State Cross Sections for Kr, N_2, and CF_4

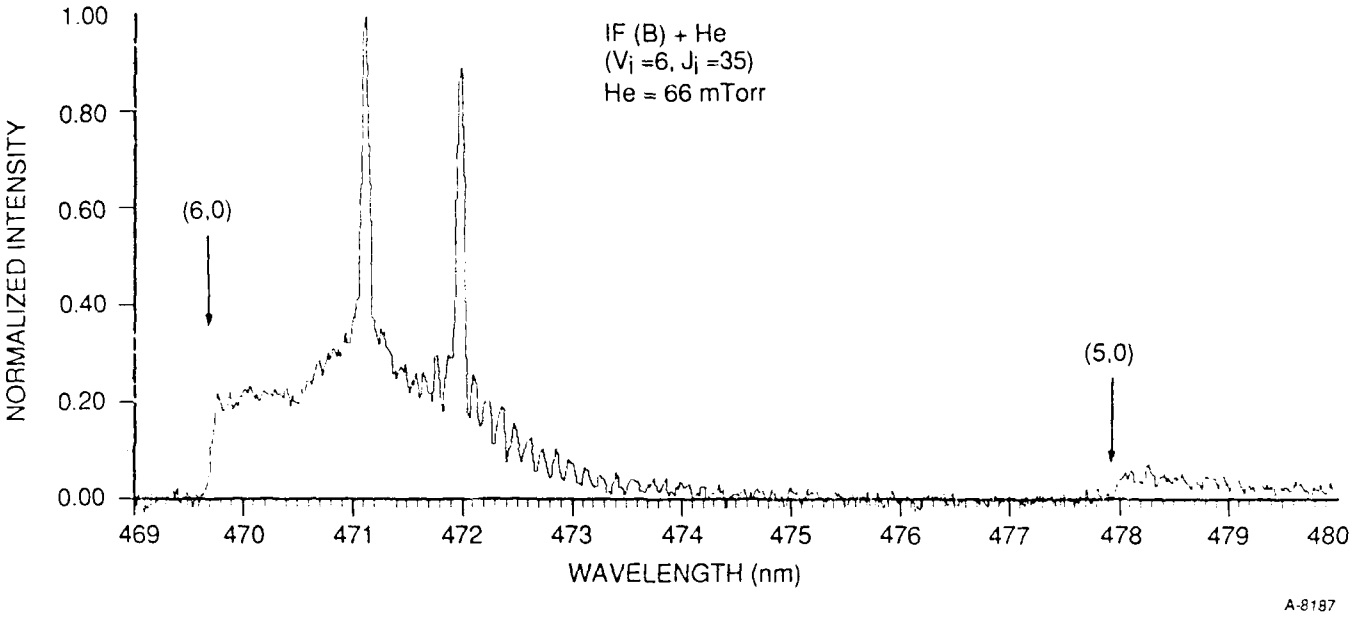

Figure 12.

Resolved LIF spectrum of IF Subsequent to Excitation of J=35 in v'=6. Helium pressure was 66 mTorr.

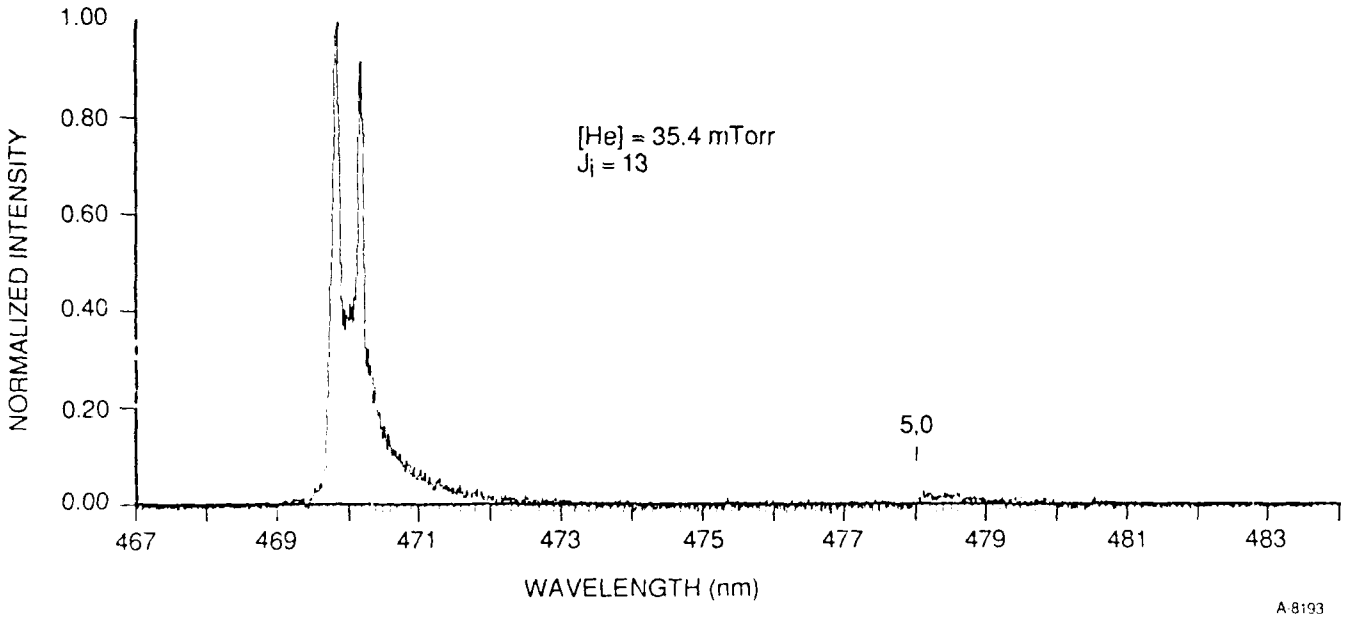

Figure 13.

Resolved LIF Spectrum of IF Subsequent to Excitation of J=13 in v'=6. Helium pressure was 35.4 mTorr.

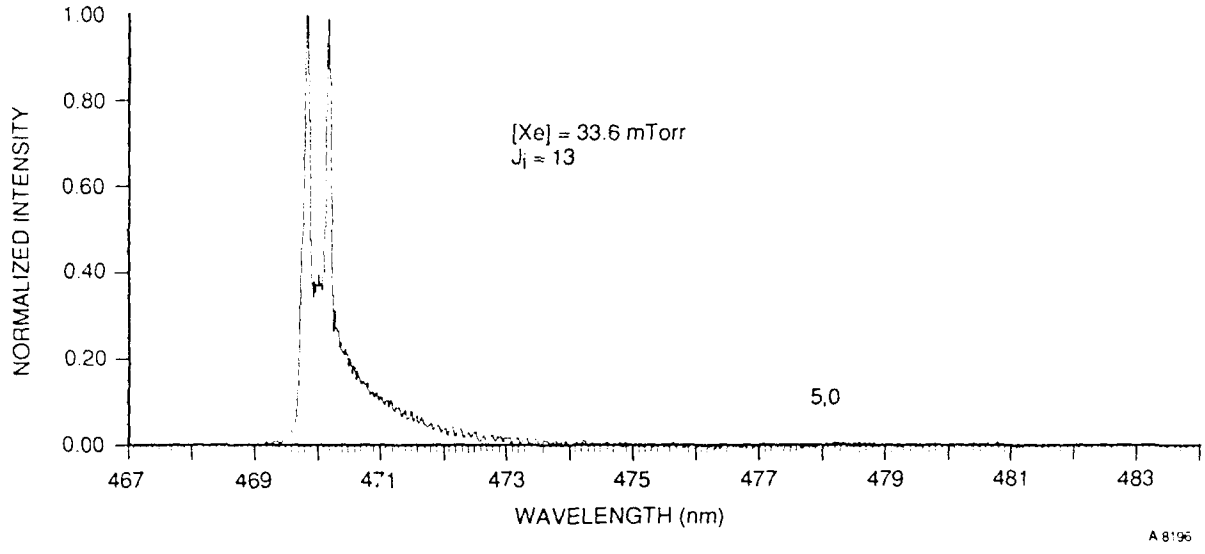

Figure 14.

Resolved LIF Spectrum of IF Subsequent to Excitation of J=13 in v'=6. Xenon pressure was 33.6 mTorr.

be drawn from these data. Collisions causing large ΔJ are more probable for Xe than for He. In contrast, V-T transfer is more evident for He than for Xe. Indeed Figures 13 and 14 are beautiful qualitative illustrations of the different dependences of R-T and V-T transfer upon the mass of the collision partner.

A typical Stern-Volmer plot for J_f=18 and J_i=13 using helium as the collision partner is shown in Figure 15. The plot is linear and the slope yields $k(13 \rightarrow 18) = 1.01 \times 10^{-11}$ cm^3 molecule^{-1} s^{-1}. The [He]=0 intercept represents the residual R-T transfer into J=18 caused by the ~8 mTorr background of CF_4. A series of Stern-Volmer plots analogous to that shown in

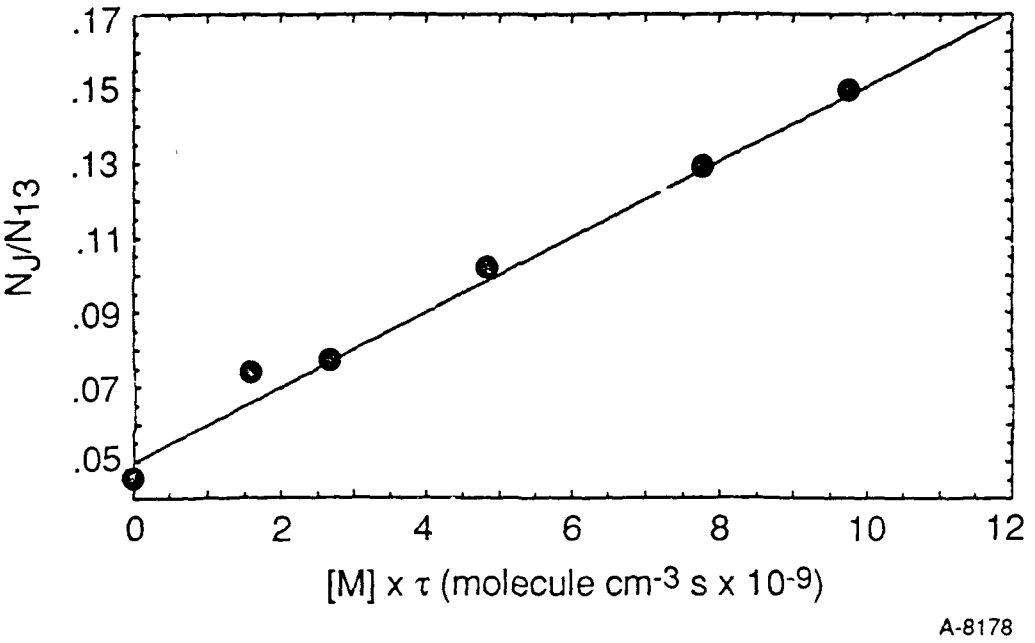

Figure 15.

Stern-Volmer Plot for Determining k(13→18) Using Helium Bath Gas. The highest pressure point is approximately 30 mTorr.

of $\sum_{J_f}([J_f]/[J_i]) - 1$ were constructed to produce values for the total R-T rate coefficient from specific J_i. A typical plot for J_i=13 using He is shown in Figure 16.

A convenient way to present the measured rate coefficients is to construct plots of ln $k(J_i \rightarrow J_f)$ versus ln ΔJ. We show a few typical plots in Figures 17 through 22.

Figure 17 shows data for J_i=13 using helium. The two data sets shown were obtained over a month apart and indicate the excellent reproducibility of the experimental results. The error bars represent one standard deviation in the slope of the respective Stern-Volmer plot. In general the overlap of the two runs shown is within this uncertainty which indicates no significant systematic

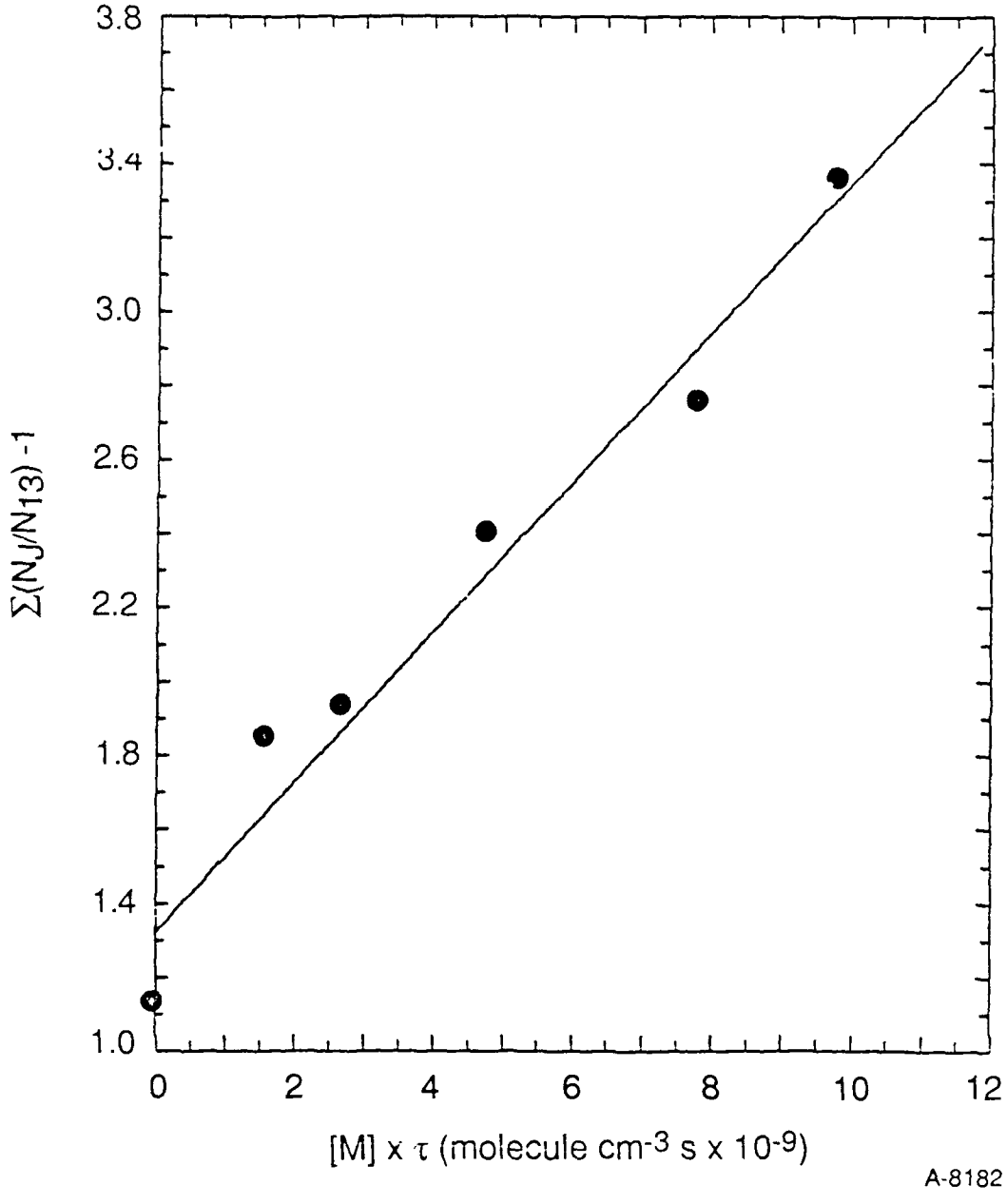

Figure 16.

Stern-Volmer Plot for Determining Total R-T Rate Coefficient from J_i=13 Using Helium Bath Gas

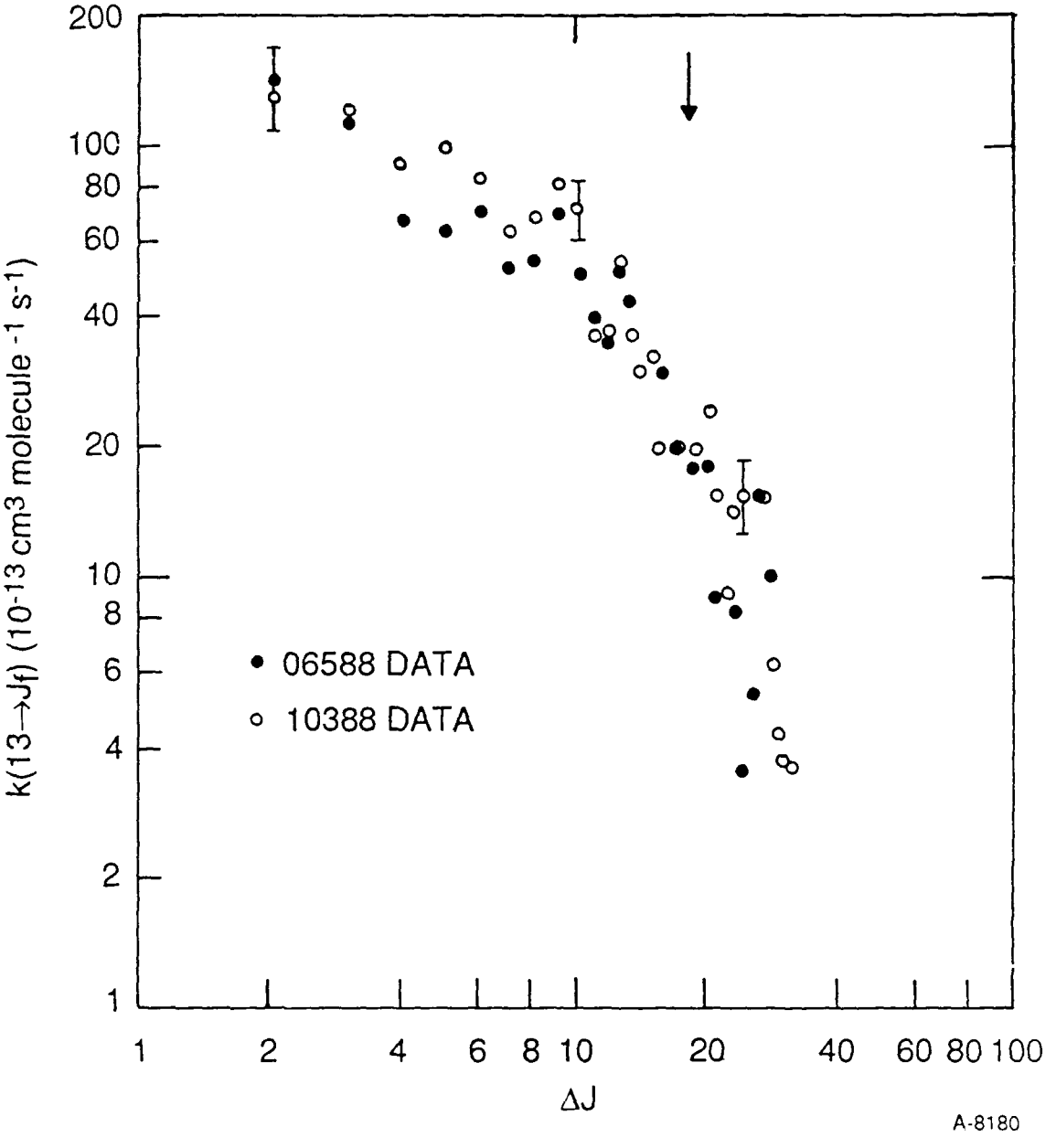

Figure 17.

Plots of $k(13 \rightarrow J_f)$ versus ΔJ. Two data sets using helium bath gas are shown. Arrow indicates an energy change of 1 kT.

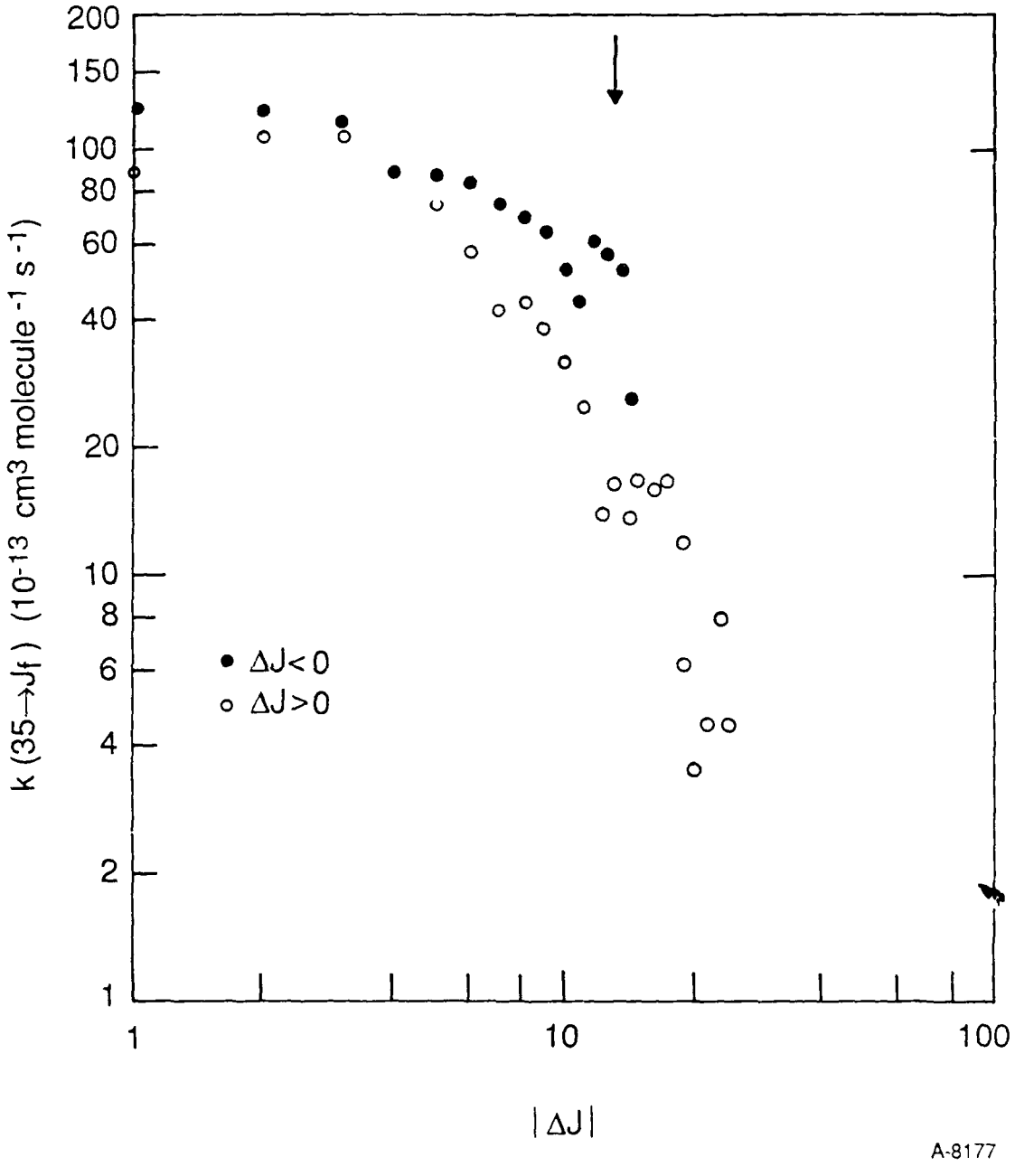

Figure 18.

Plots of $k(35 \rightarrow J_f)$ versus ΔJ Using Helium Bath Gas.
Arrow indicates energy exchange of 1 kT.

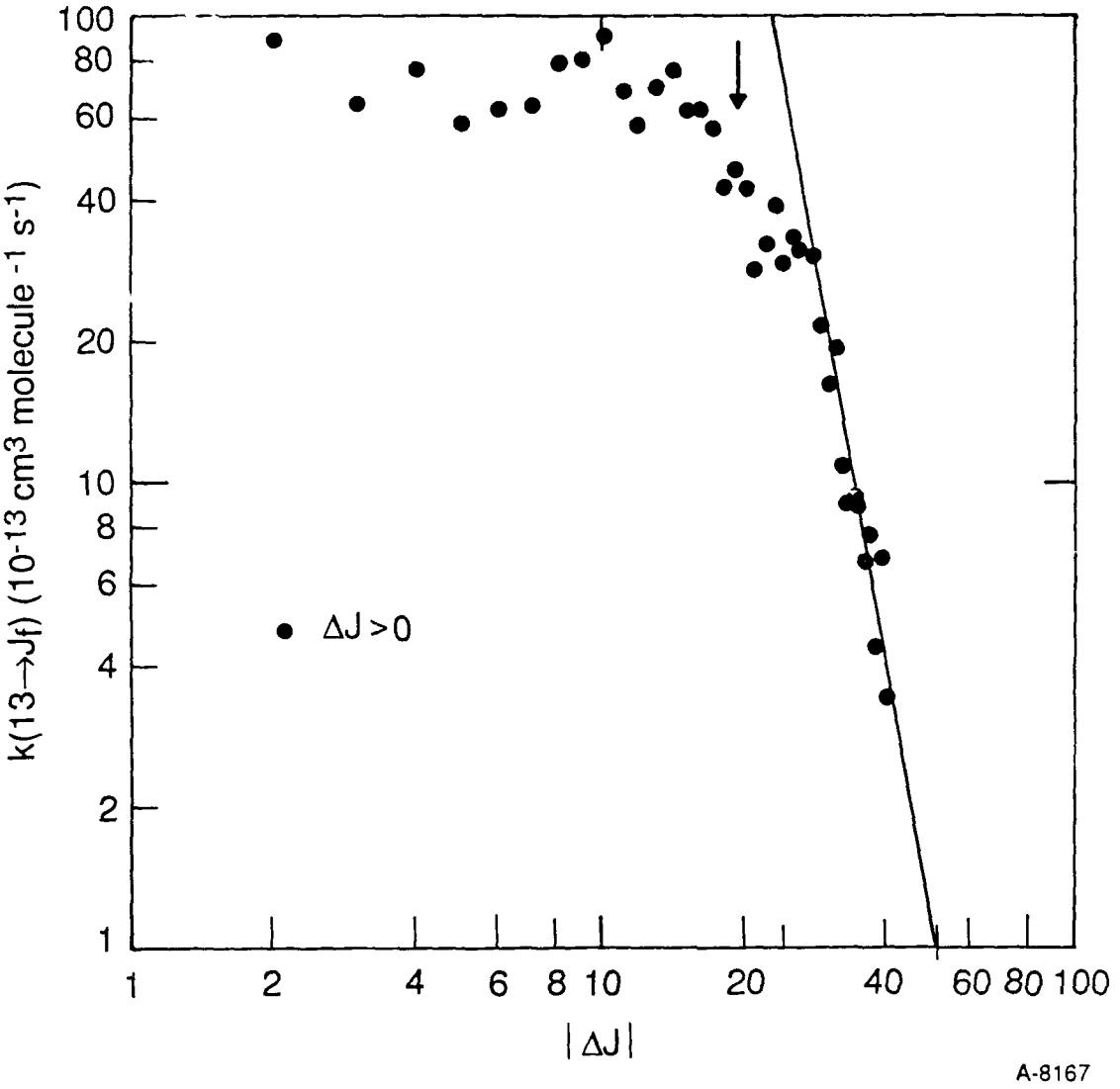

Figure 19.

Plot of $k(13 \rightarrow J_f)$ versus ΔJ Using Argon Bath Gas.
Arrow indicates energy exchange of 1 kT.

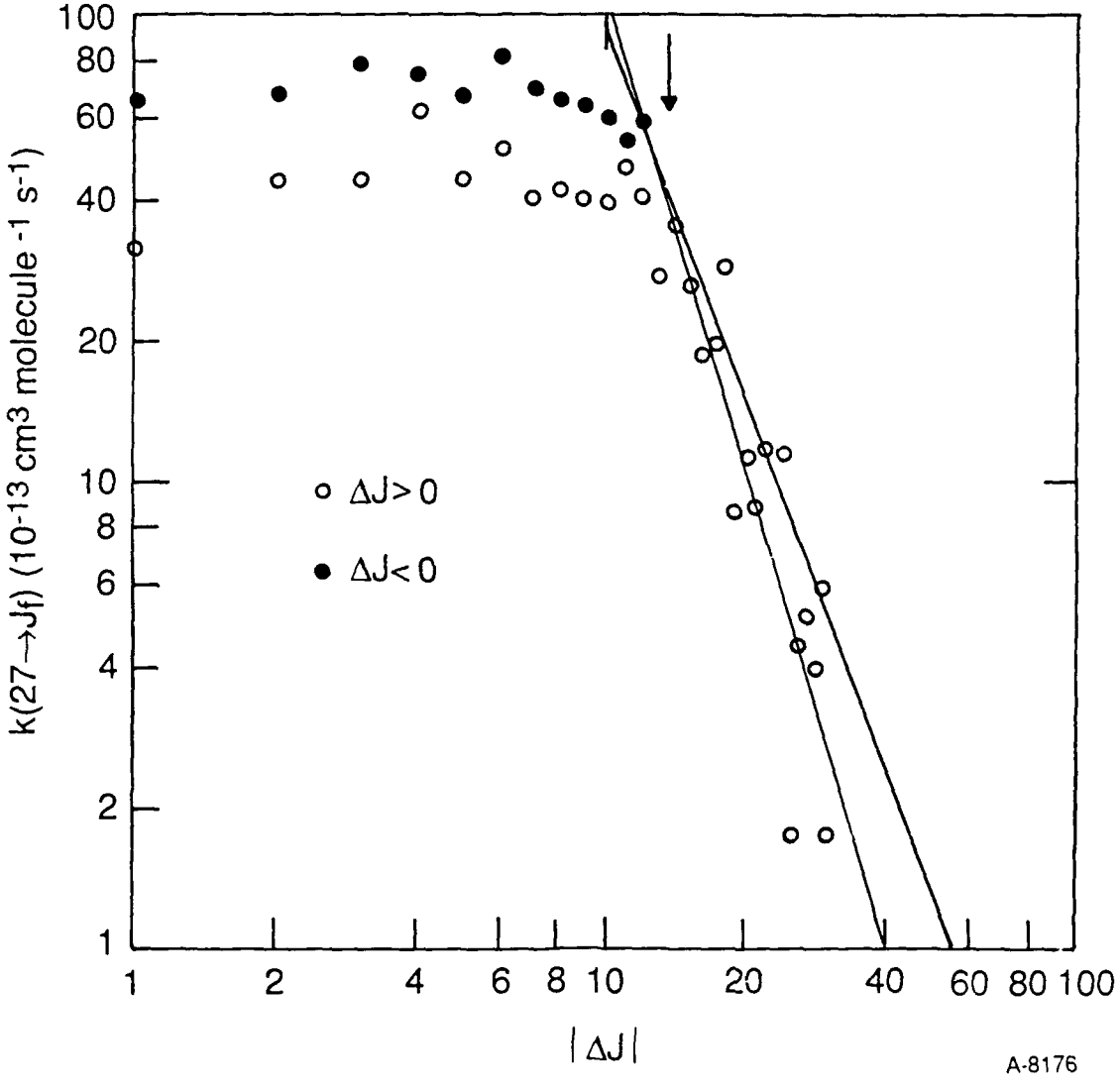

Figure 20.

Plots of $k(27 \rightarrow J_f)$ versus ΔJ Using Argon Bath Gas.
Arrow indicates energy exchange of 1 kT.

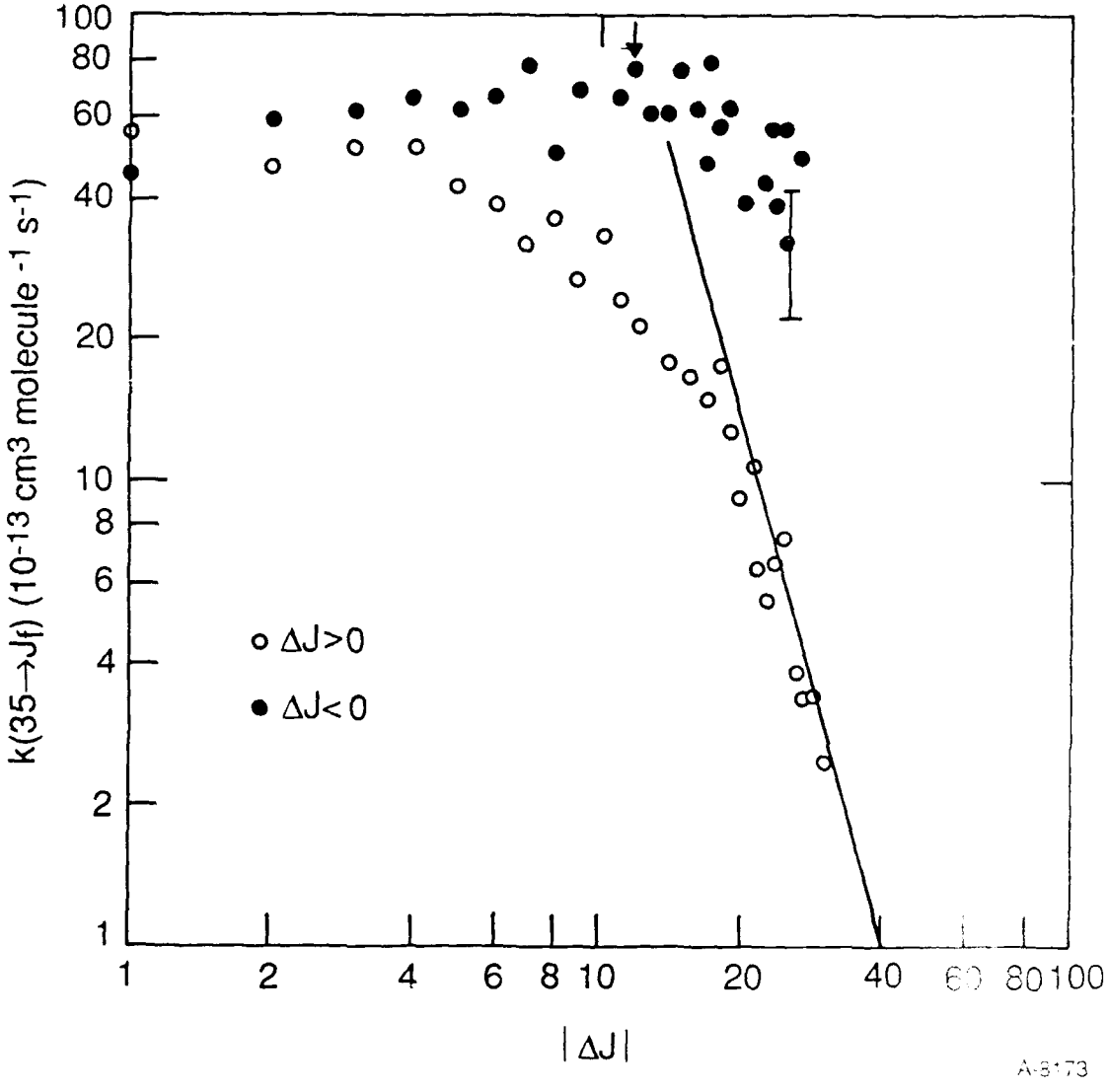

Figure 21.

Plots of $k(35 \rightarrow J_f)$ versus ΔJ Using Argon Bath Gas. Arrow indicates energy exchange of 1 kT.

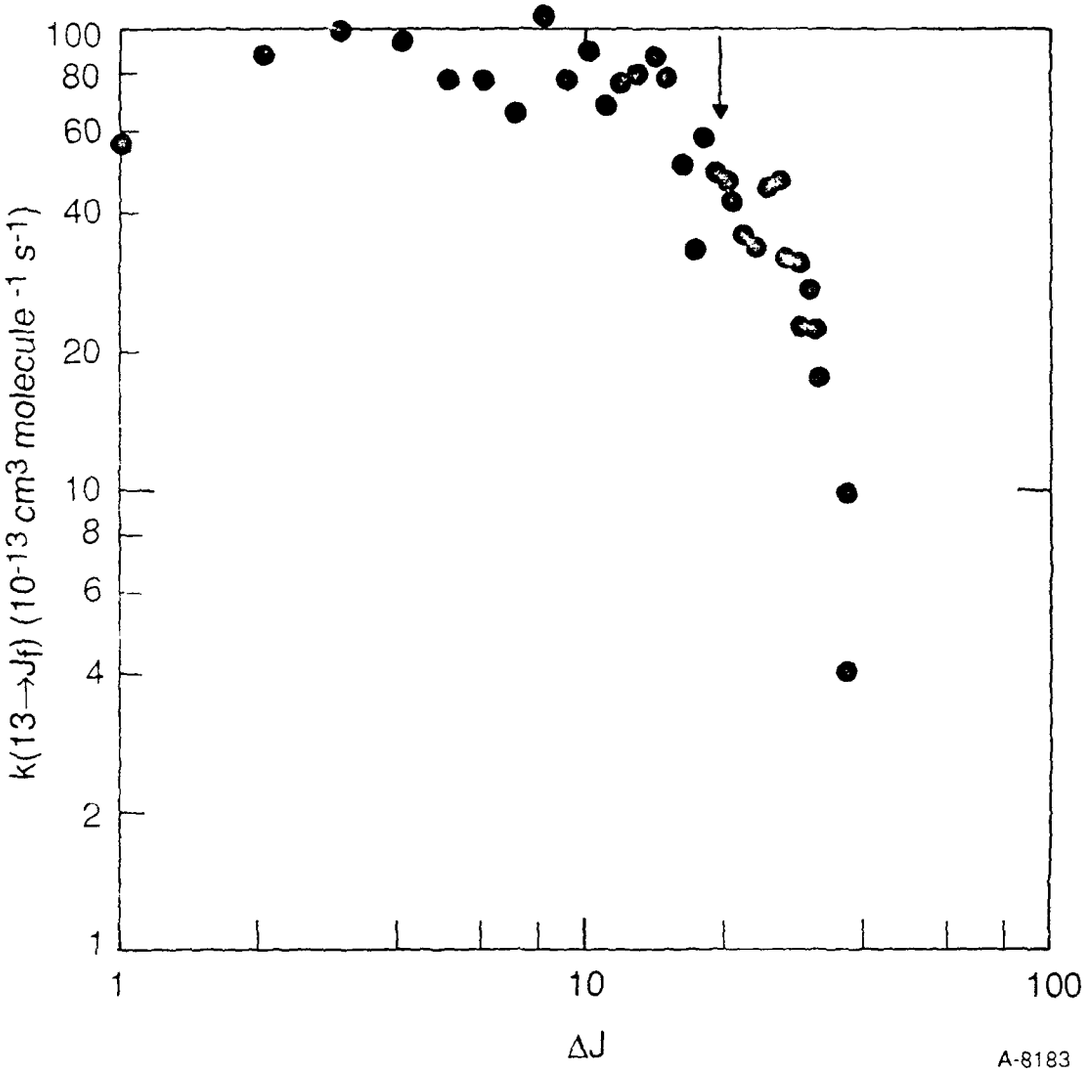

Figure 22.

Plot of $k(13 \rightarrow J_f)$ versus ΔJ Using Xenon Bath Gas. Only $\Delta J > 0$ collisions are shown. Arrow indicates energy exchange of 1 kT.

errors. Figure 18 shows a similar plot for J_i=35. Here the two data sets are for $\Delta J < 0$ and $\Delta J > 0$ processes. Similar plots using Ar and Xe are shown in Figures 10 through 13.

Some interesting and important features can be discerned from these plots. Firstly, the fall-off of $k(J_i \rightarrow J_f)$ with increasing ΔJ is greater for He than for either Ar or Xe. As an example the J_i=13 rate coefficients for $\Delta J > 0$ processes with Ar and Xe are nearly constant for $\Delta J > +20$ whereas those for He are essentially a monotonically decreasing function of ΔJ. It is perhaps significant that from J_i=13 a $\Delta J = +20$ transfer implies that the collision partner must supply approximately 1 kT (at 300 K) of energy. Thus upward transfer of $\Delta J > 20$ is probably energetically limited and a fall-off is not surprising for large ΔJ. However, for helium the diminution of $k(13 \rightarrow J_f)$ occurs for ΔJ much smaller than 20. This is indicative of some dynamical, angular momentum constraint.

C.4 R-T Transfer IF During an Inelastic V-T Collision

We also examined R-T transfer during a V-T collision. For these runs only helium was used since it yielded the largest vibrational satellite bands (5,0) subsequent to excitation of (v'=6). From data such as shown in Figure 12, we note that the signal level for (5,0) is much smaller than for the parent (6,0) band. Consequently the signal-to-noise ratio was considerably degraded for the (5,0) band.

For these experiments two J_i were selected for study: J_i=6 and 41. Two representative spectra are shown in Figures 23 and 24 for J_i=6 and 41 respectively, each taken with 80 mTorr of added He. The rather high He pressure

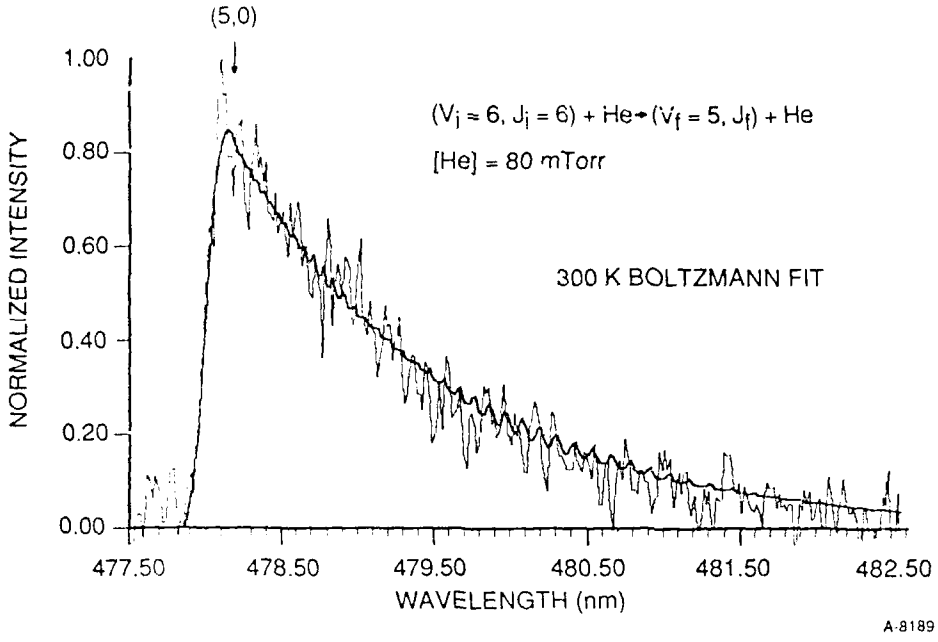

Figure 23.

Resolved LIF Spectrum of IF (5,0) Band Subsequent to Laser Excitation of (J'=6, v'=6). Bath gas was helium at 80 mTorr. Dark line is spectral fit assuming a 300 K Boltzmann rotational distribution.

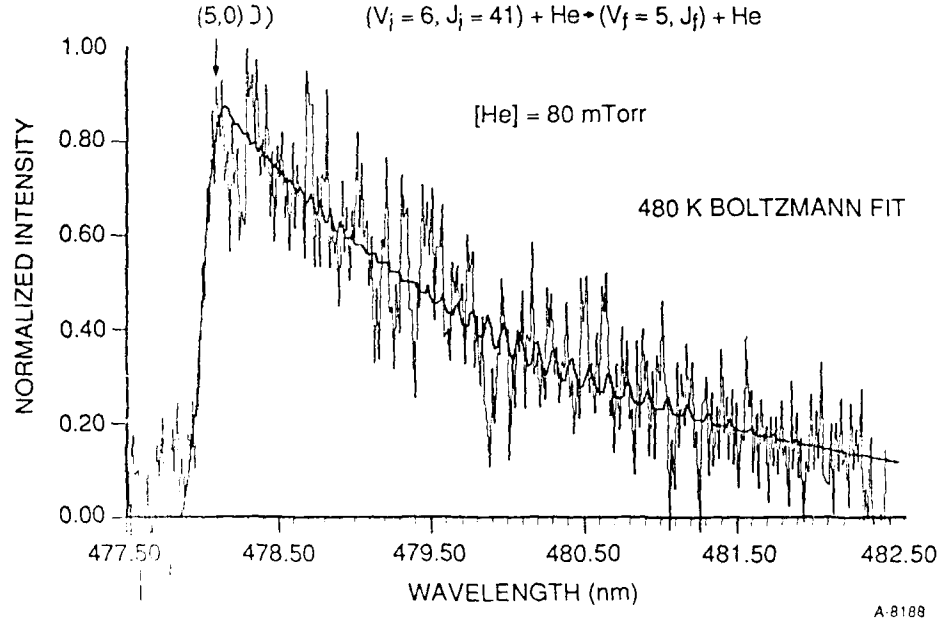

Figure 24.

Resolved LIF Spectrum of IF(5,0) Band Subsequent to Laser Excitation of (J'=41, v'=6). Bath gas was helium at 80 mTorr. Dark line is spectral fit assuming a 480 K Boltzmann rotational distribution.

required so that the (5,0) band could be observed. (Even at this pressure the parent (6,0) band is very non-thermal as shown in Figures 25 and 26.) The satellite (5,0) band appears quite relaxed and indeed we found good agreement between the data and a fit to a Boltzmann distribution in each case. The dark lines indicate the fits to a Boltzmann rotational distribution. We note that excitation of J_i=6 yields a much cooler distribution in v=5 than does excitation of J_i=41.

In Figure 27 we plot the distribution of N_J versus J for the two fits. Also shown are the positions of the two J_i. Since J_{MAX}=21 at 300 K, J_i=6 and 41 present two distinct cases. The v=5 distribution for J_i=6 in v=6 is essentially thermal while that for excitation of J_i=41 is not. Although there is some apparent retention of J_i during a V-T encounter, the degree of rotational redistribution is dramatic. Perhaps a V-R-T process is operative.

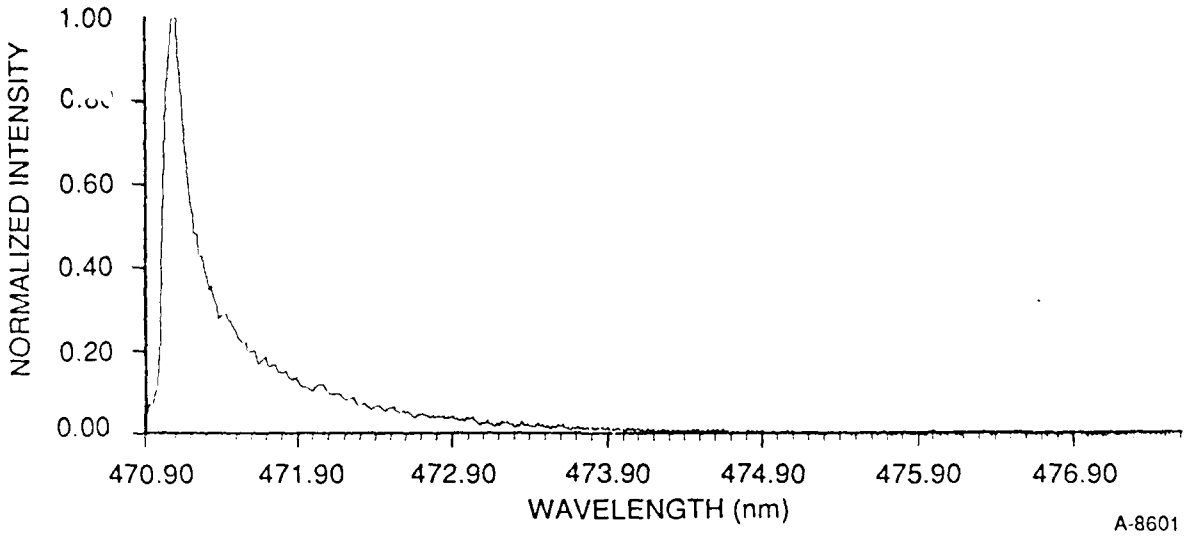

Figure 25.

Resolved LIF Spectrum of (6,0) Band Subsequent to Laser Excitation of (J'=6, v'=6). Conditions are identical to those in Figure 23.

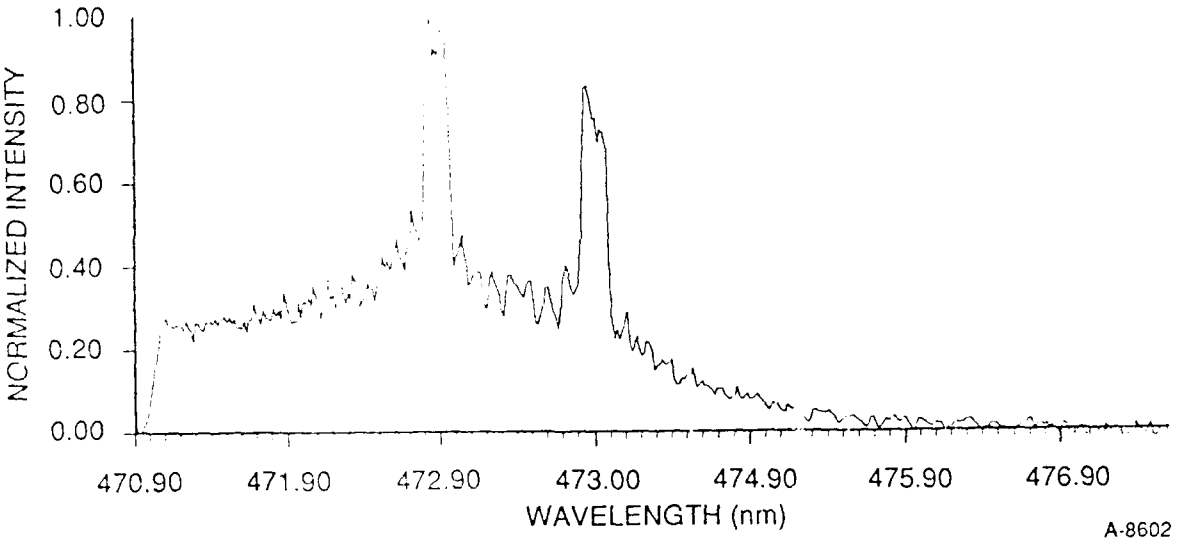

Figure 26.

Resolved LIF Spectrum of (6,0) Band Subsequent to Laser Excitation of (J'=41, v'=6). Conditions are identical to those in Figure 24.

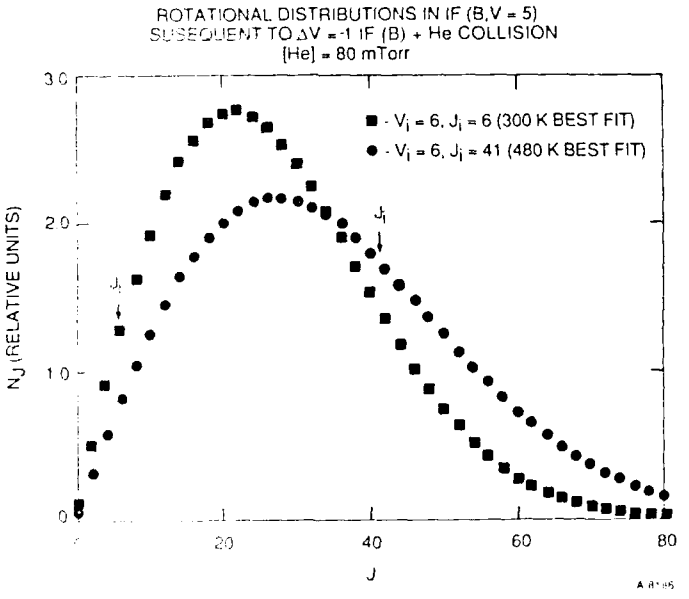

Figure 27.

Rotational Distribution in IF(B, v=5) Subsequent to a $\Delta v=-1$ Collision with Helium at 80 mTorr. The distributions are extracted from the fits shown in Figures 23 and 24 and are normalized to the same area.

For comparison we completed a similar experiment with I_2 by exciting two J_i in I_2(B, v=15) in the presence of helium. We monitored resolved fluorescence from v=14. Two spectra and the corresponding spectral fits (non-Boltzmann) are shown for J_i=20 and 53 in Figures 28 and 29 respectively. Also shown are the positions of the (14,6) band heads. It is clear that these two spectra represent dramatically different rotational distributions. The relative distribution determined by the spectral fits are presented in Figures 30 and 31. We note that the population v=14 peaks at the same J level excited in v=15. The retention of J_i throughout a V-T collision is dramatic.

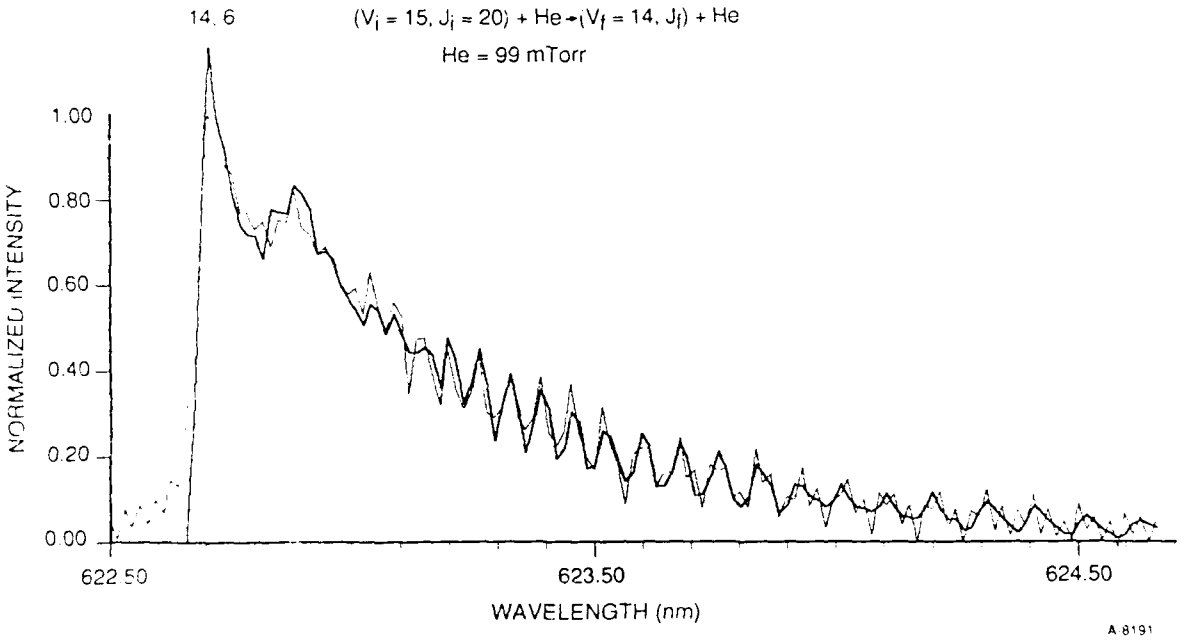

Figure 28.

Vibrational Satellite Band (14,6) in I_2 Subsequent to $\Delta v=-1$ Collision with Helium at 99 mTorr. Initial band excited was v'=15, J'=20. Dark line is spectral fit to the data.

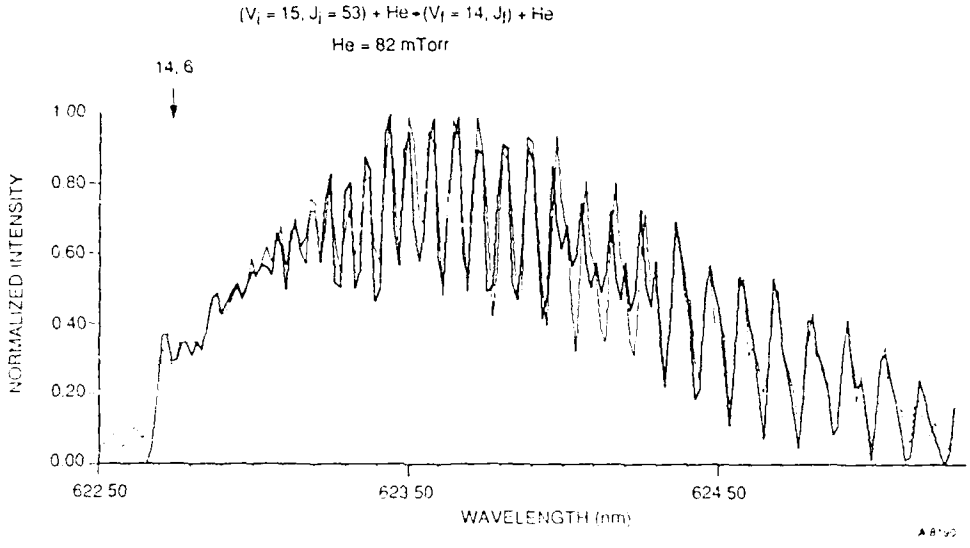

Figure 29.

Vibrational Satellite Band (14,6) in I_2 Subsequent to $\Delta v=-1$ Collision with Helium at 99 mTorr. Initial and excited was $v'=15$, $J'=53$. Dark line is spectral fit to the data.

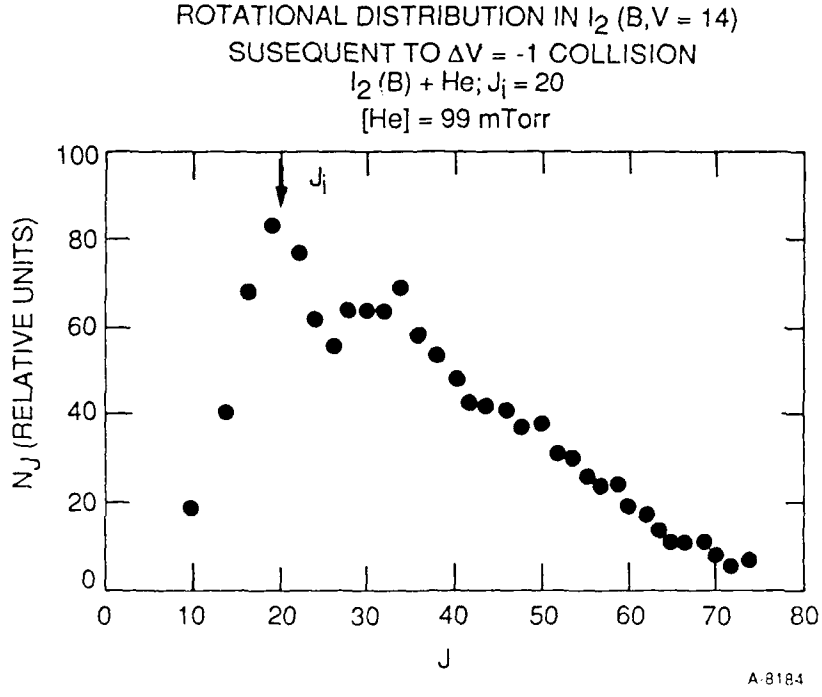

Figure 30.

Rotational Distribution Obtained from Spectral Fit to Data in Figure 28

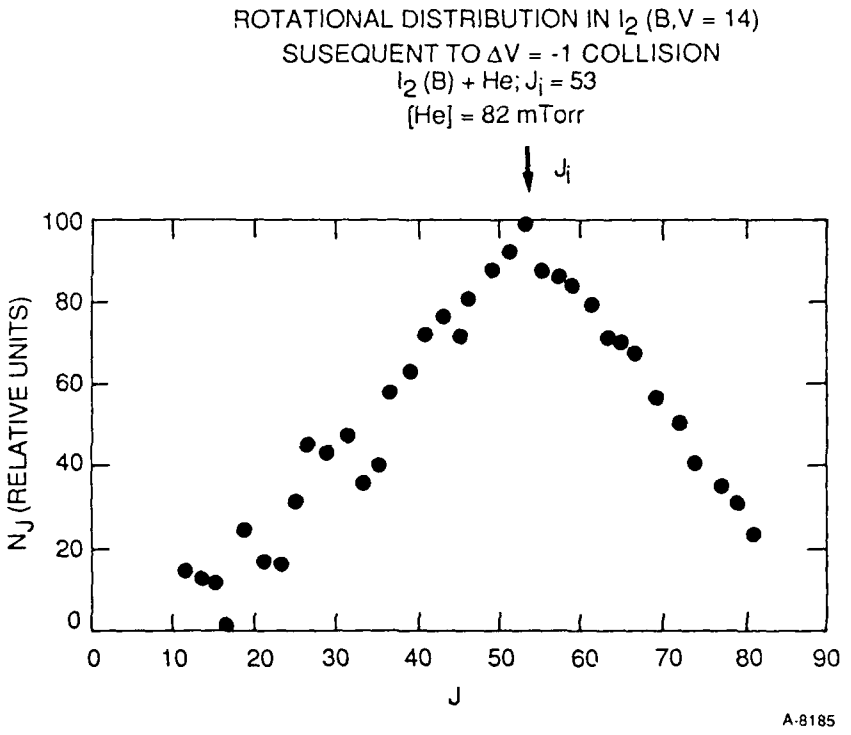

Figure 31.

Rotational Distribution Obtained from Spectral Fit to Data in Figure 29

The examples presented above illustrate the potential of the experiment to probe microscopic details of rotational redistribution during both vibrationally elastic and inelastic collisions. Although Refs. 2 and 9 also showed that in I_2 there is preservation of J_i during events in which v is not preserved, our results are the first direct comparisons of this process for both homonuclear and heteronuclear molecules. These results also furnish the first convincing evidence of rotational selectivity during a V-T encounter in an interhalogen molecule.

In an attempt to probe, in greater detail, R-T transfer during a VT encounter we completed a series of runs using the Ar^+ 476.5 nm line to pump IF

B(v'=6, J'=72). Note that J'=72 is far from the Boltzmann maximum at T=300 K. For these runs we used helium bath gas and simultaneously monitored both the (6,0) and (5,0) bands. Representative data and the corresponding spectral fit are shown in Figure 32. As indicated from Figure 32 there was considerable overlap of some (6,0) and (5,0) lines. We used He pressures in the range of 20 to 80 mTorr and completed a Stern-Volmer analysis as described earlier. The results of this data reduction are shown in Figure 33. The detailed state-to-state rate coefficients show an interesting bi-modal distribution. The lower J_f levels are very suggestive of a Boltzmann distribution. Indeed, when we constrained the populations in these levels to be described by a Boltzmann distribution the spectral fits to the data were excellent. (The rate coefficients shown in Figure 33 were obtained using no a-priori constraints in

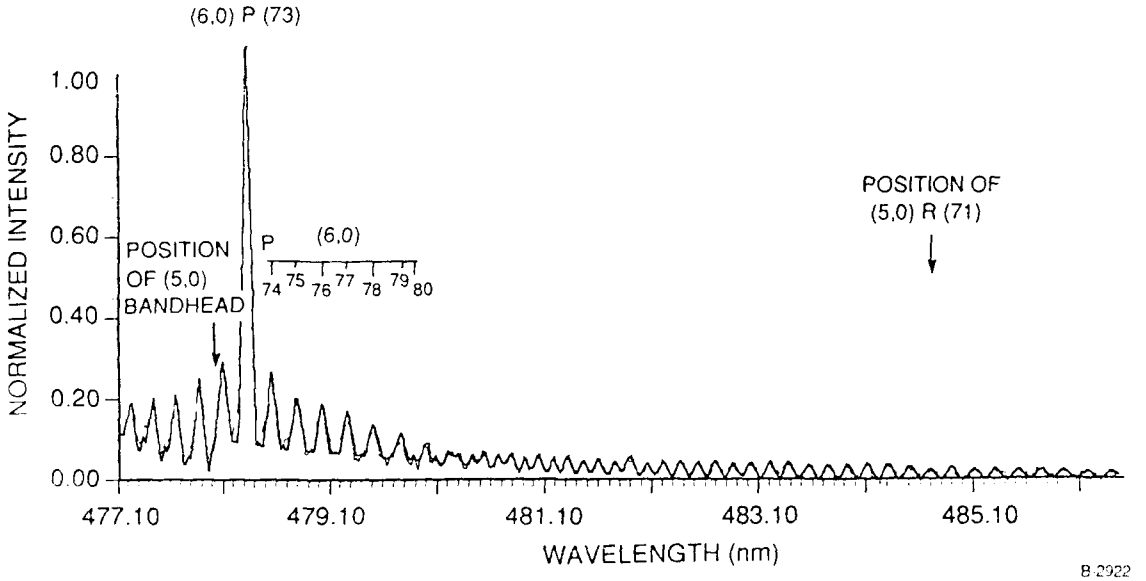

Figure 32.

Positions of (6,0) and (5,0) Bands. Pump level was J'=72, v'=6. Positions of (5,0) bandhead and R(71) lines are shown. Note little preservation of originally pumped J' remains in v'=5

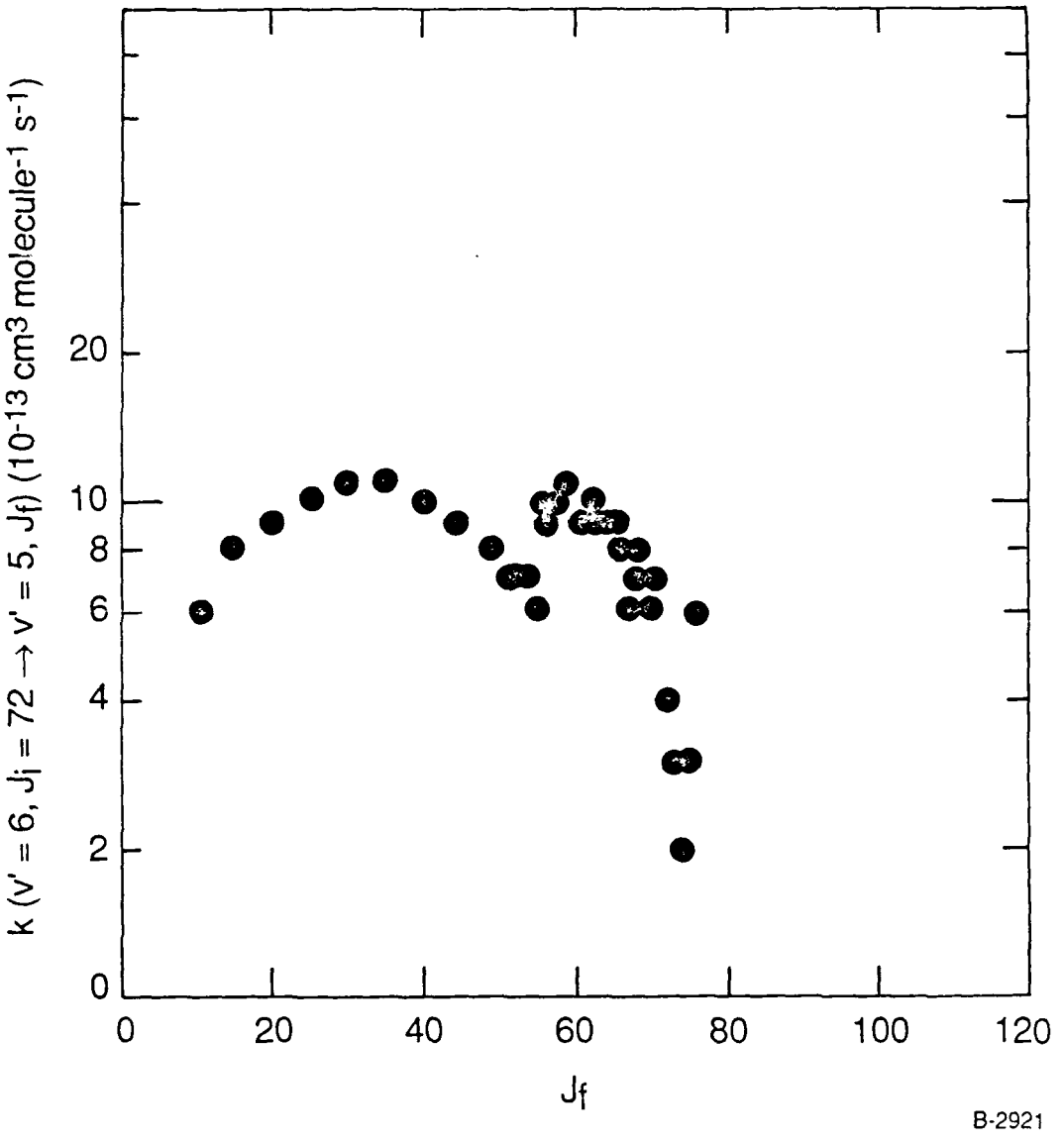

Figure 33.

R-T Rate Coefficient for IF(B) (v'_i-6, J_i=72 → v_f=5,J_f) Collisions. Collision partner was helium

the fitting routine.) There is also a clear peak in the rate coefficients near J'=60. Our present interpretation of these distributions is as follows. The peak at high J' in v'5 is consistent with some preservation of the initially populated J' in the parent v'=6 level subsequent to a V-T encounter. For some runs, we had to use He pressures sufficiently high that multi-collision effects may be operative. Thus the distribution in v'=5 also shows a thermal component. At this time we cannot quantitatively conclude how much of the apparent thermal component is due to multi-collision effects. However, even at He pressures low enough that multi-collision effects are negligible we still observed a much broader distribution of k(i→f) in v'=5 then we saw in the parent v'=6 band. The data shown in Figure 33 are the first detailed state-to-state R-T rate coefficients for an inelastic V-T process.

C.5 R-T Transfer in ICl(B)

Typical resolved LIF spectra for ICl(B→X) using He and Ar bath gases are shown in Figures 34(a) and 34(b), respectively. These data are for the initially populated level (v',J') = (1,55). We note that analogous to all the IF results the heavier collision partner is more efficient in causing larger ΔJ changes. Plots of the RET cross sections σ(i→f) for Ar and He are shown in Figures 35 through 40 for several J_i.

An analogous plot for ICl as its own collision partner is presented in Figure 41. When compared to Figures 34(a) and 34(b) we note that ICl + ICl collisions seem to give a much more peaked distribution for small ΔJ. Perhaps this is evidence for an active role by the permanent dipole moment of ICl during a ΔJ collision. We plan to test polar collision partners much more thoroughly in future studies.

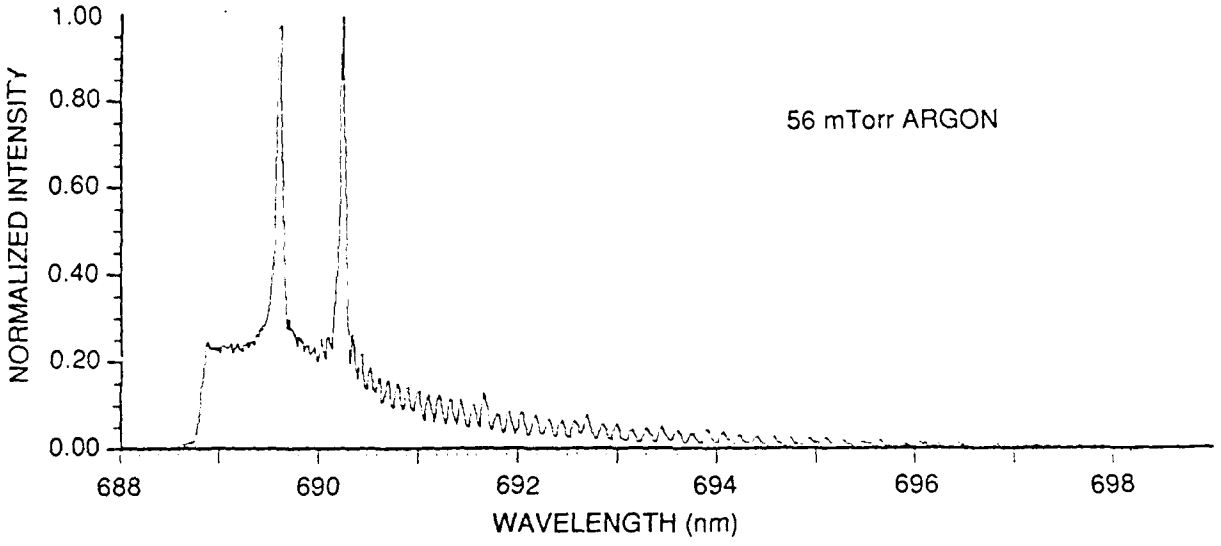

(a)

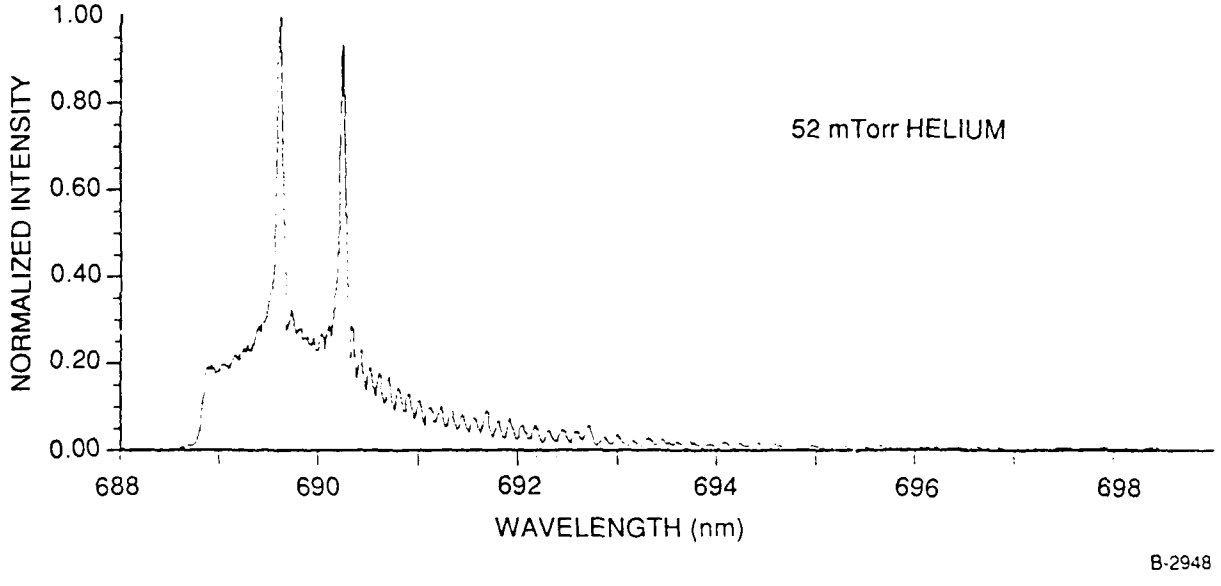

(b)

Figure 34.

Resolved LIF from ICl(1-8) Band. (a) Ar bath gas; (b) He bath gas; J_i=34 in each case

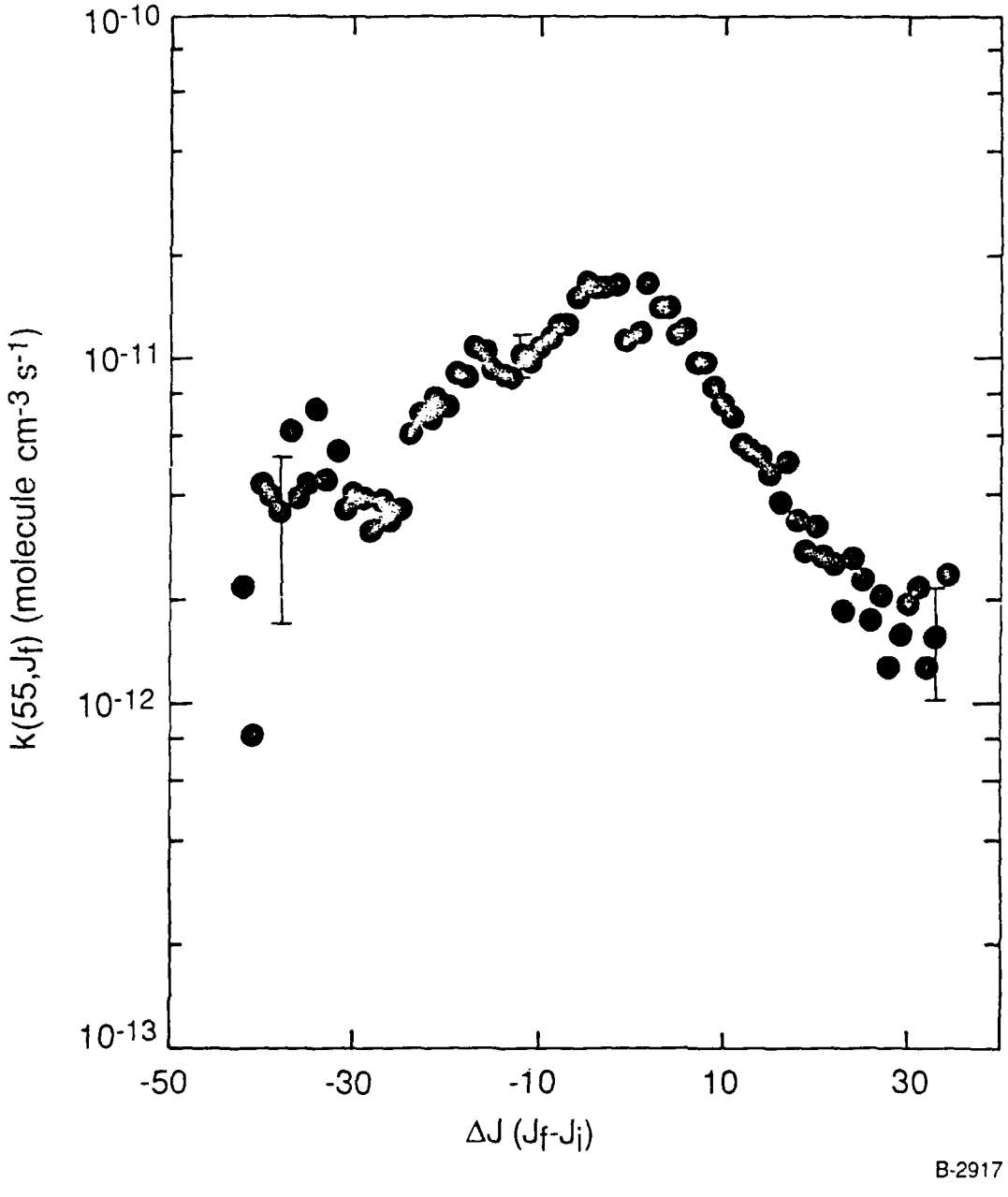

Figure 35.

R-T Rate Coefficients for ICl(B) Collisions with Helium (v_i=1, J_i=55)

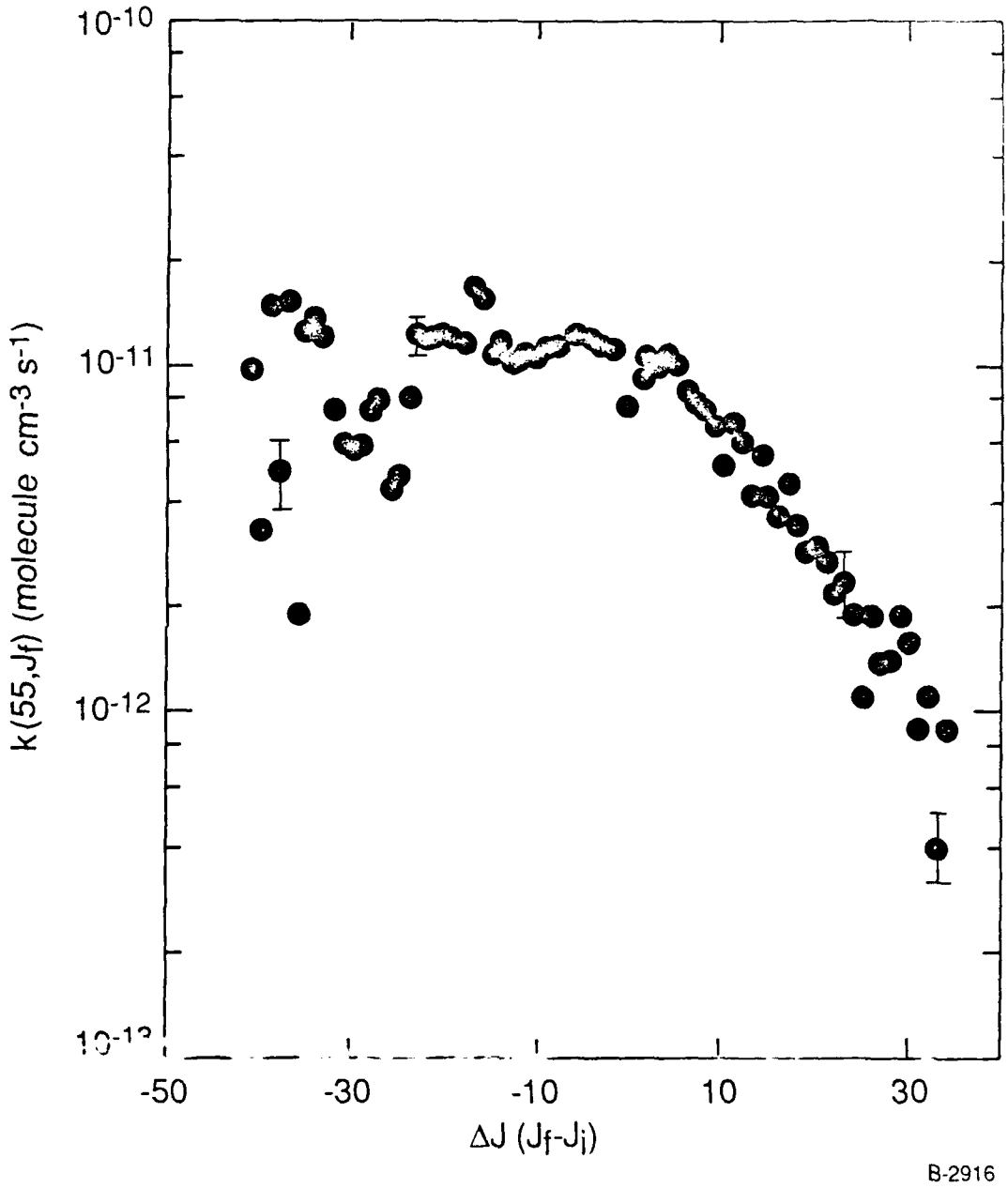

Figure 36.

R-T Rate Coefficients for ICl(B) Collisions with Argon (v_i=1, J_i=55)

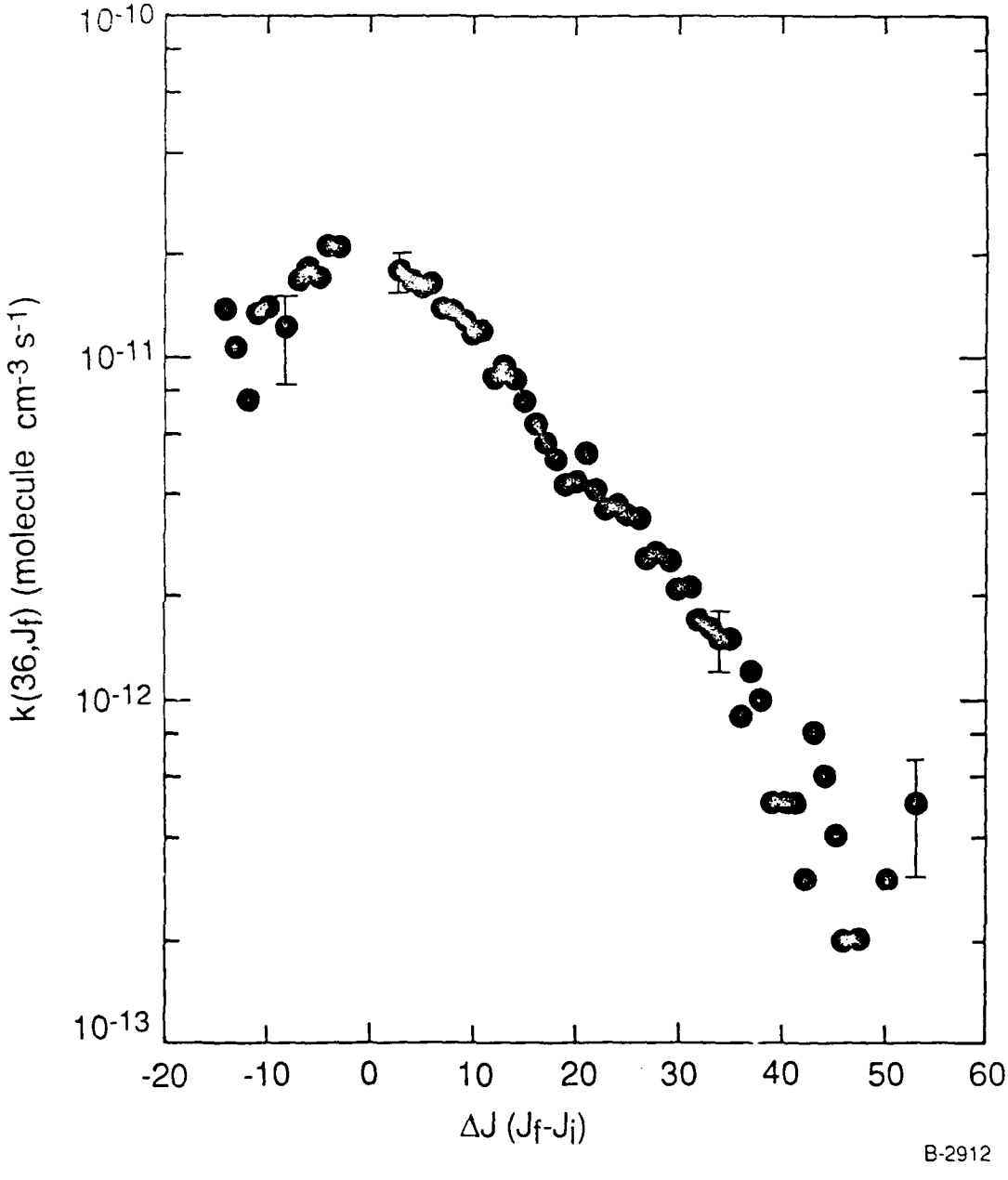

Figure 37.

R-T Rate Coefficients for ICl(B) + He (v_i=1, J_i=36)

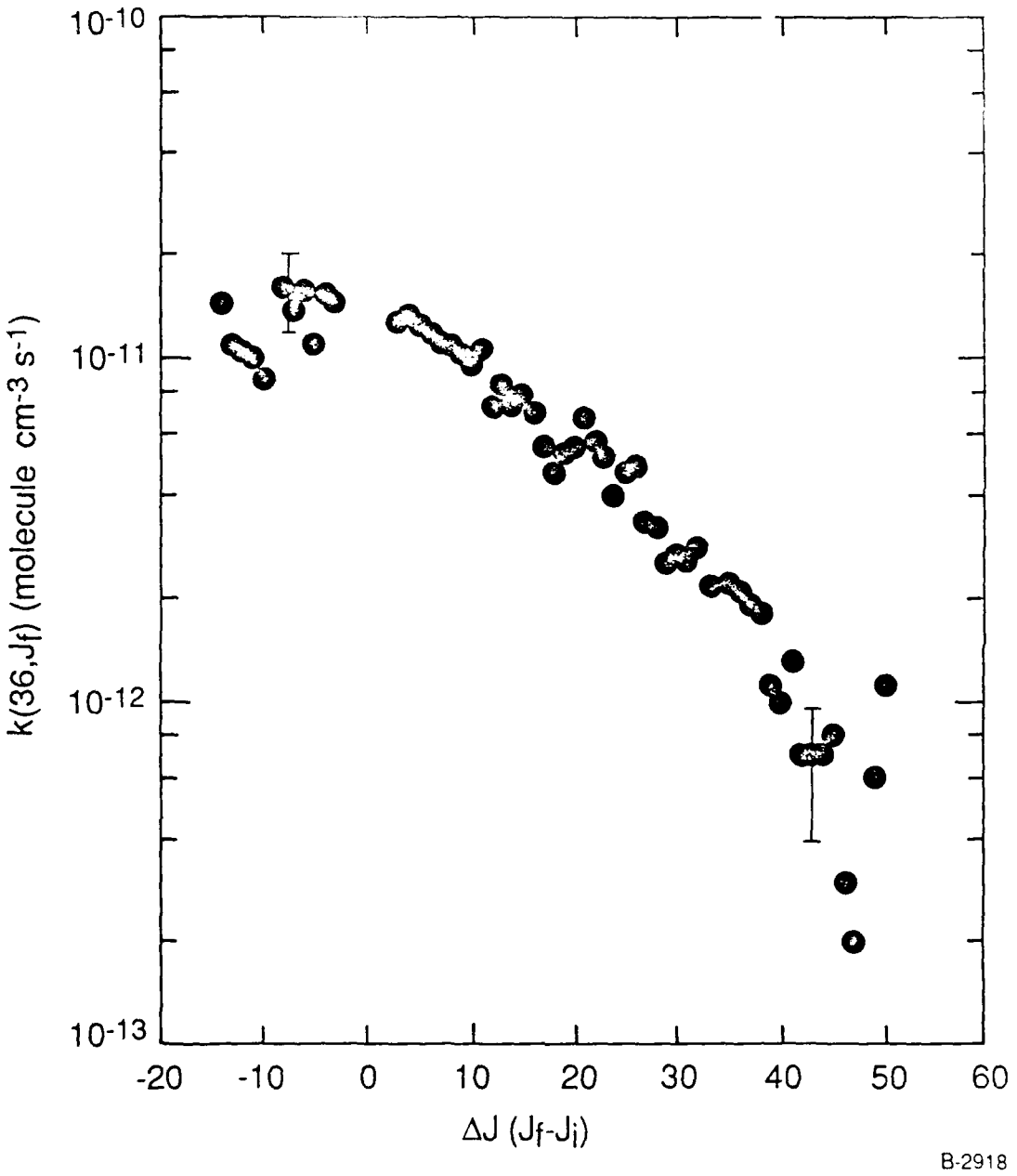

Figure 38.

R-T Rate Coefficients for ICl(B) Collisions with Argon (v_i=1, J_i=36)

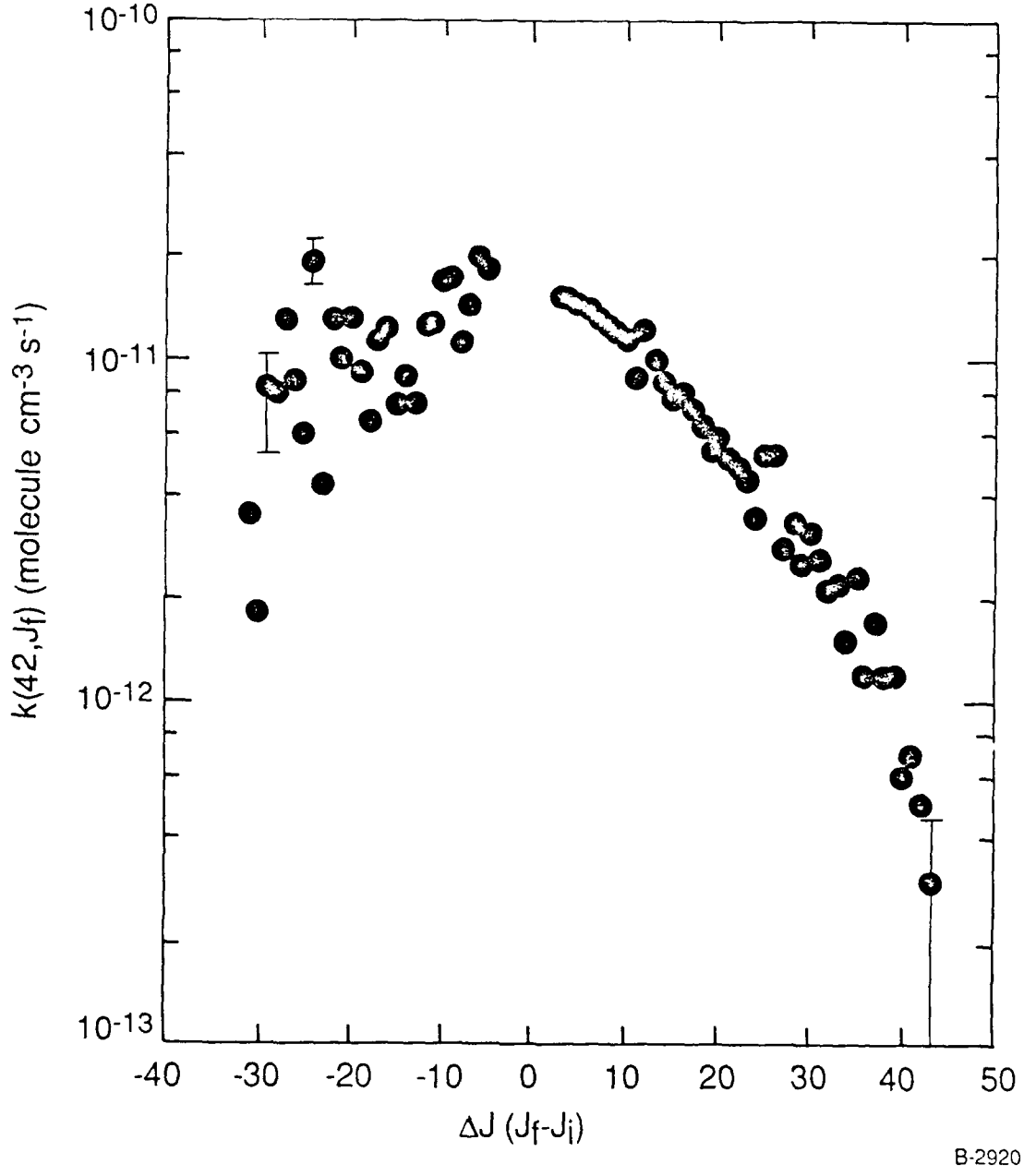

Figure 39.

R-T Rate Coefficients for ICl(B) Plus Helium (v'_i=1, J'_i=42)

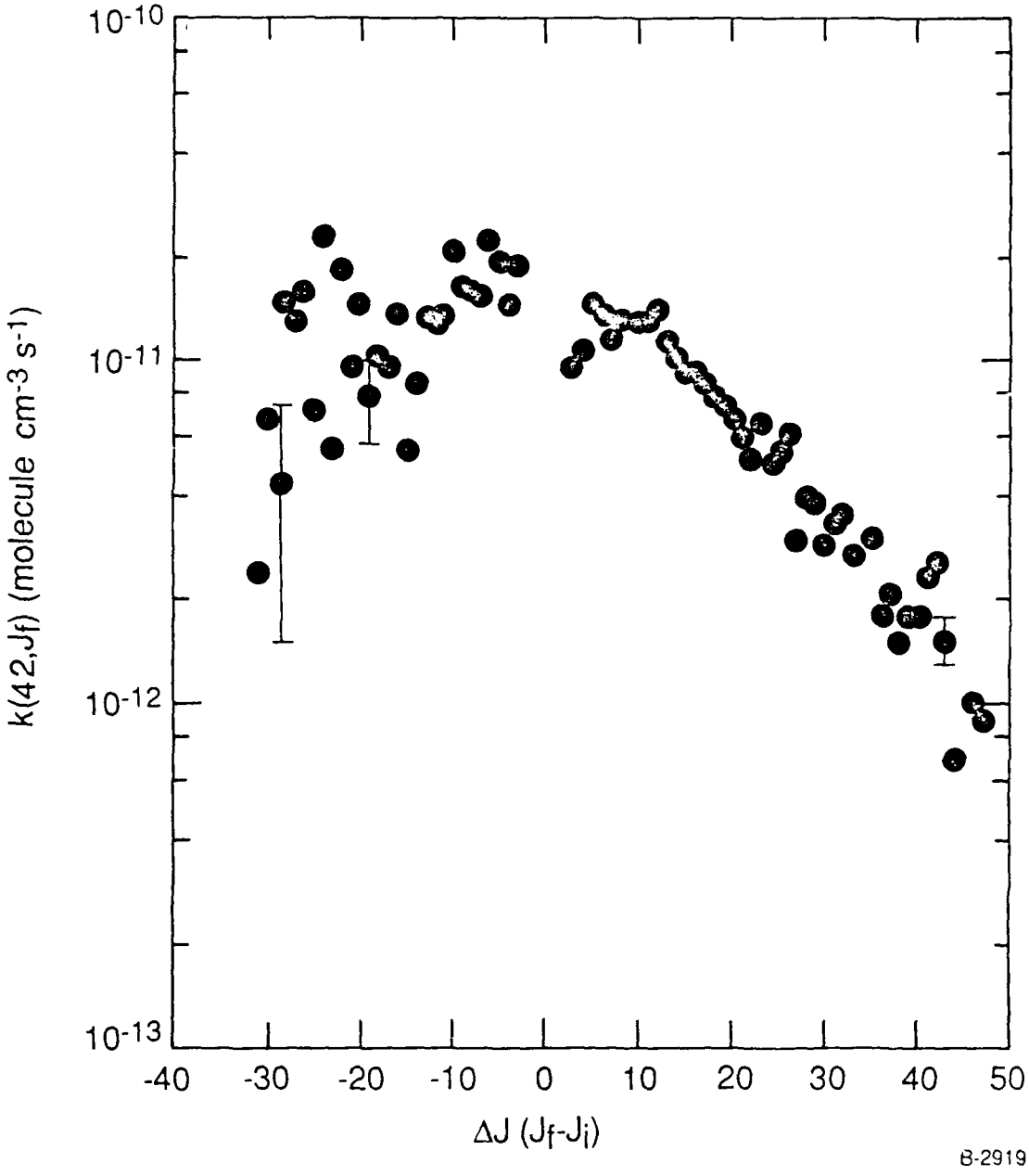

Figure 40.

R-T Rate Coefficients for ICl(B) Plus Ar (v'_i=1, J'_i=42)

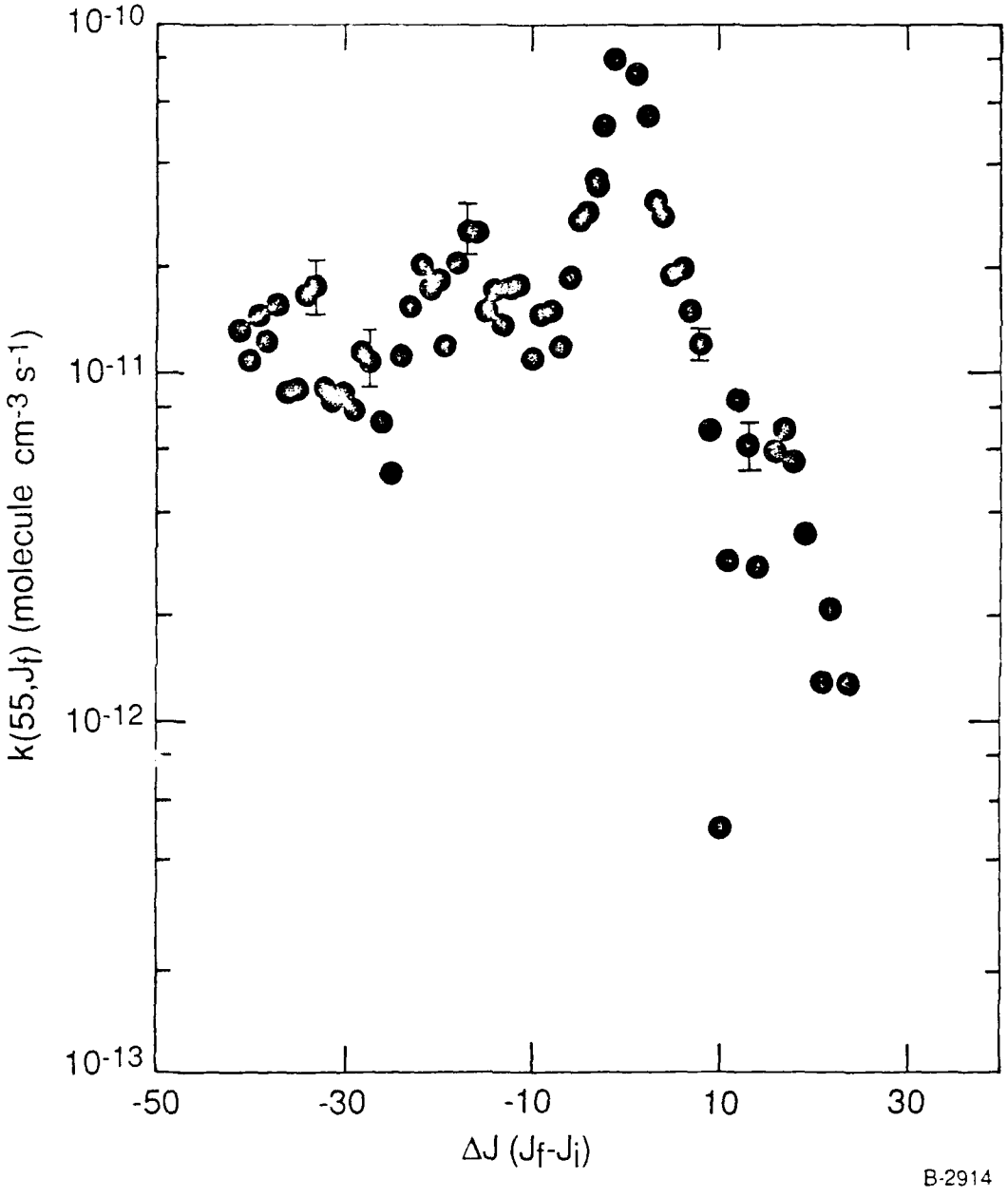

Figure 41.

Rate Coefficients for Rotational Energy Transfer from ICl(B) (v_i=1, J_i=55). Collision partner was ICl(X)

C.6 Scaling Law Tests

There are several motivations for developing and verifying scaling laws to describe R-T rate coefficients.[1,2] Perhaps the most important reason is one of practicality; it is unrealistic to tabulate rate coefficients that describe all possible R-T processes even within one electronic state. The situation is drastically simplified if all R-T rate coefficients can be scaled to a few fundamental parameters. Indeed, the goal of this approach is to obtain a closed form expression that can be used to generate R-T rate coefficients. This would be particularly valuable in kinetic codes, e.g., chemical laser codes.

From a more fundamental perspective, there are also reasons for testing scaling laws. Some of the parameters in the scaling laws that have been developed can be related to physically meaningful quantities such as the interaction potentials. Consequently one can gain fundamental insight into some of the physics of the R-T collision.

There are several scaling laws that have been developed over the past two decades in order to predict all $k(i \rightarrow f)$ given that a few can be measured. For brevity we do not discuss the derivations of these scaling laws but instead we emphasize the important features of them and compare each to our data sets. There are two basic types of these laws: 1) those based upon the amount of energy exchanged and 2) those based upon the amount of angular momentum exchanged.

C.6.1 Energy Based Fitting Laws

The oldest and simplest fitting law is the exponential gap law given by Eq. (9)

$$k(i \to f)^{EGL} = a\, e^{-(\Theta|\Delta E|)} \cdot R(\Delta E)(2J_f+1) \qquad (9)$$

where a and Θ are fitting parameters and $R(\Delta E)$ is the ratio of the final density of translational states to the initial density of translational states. This form was developed by Polanyi and Woodall[37] in their studies of HF(v) relaxation and has been applied to a number of other species.

Pritchard and co-workers[38,39] developed an alternate formalism that scaled the R-T rate coefficients to a power gap law given by Eq. (10)

$$k(i \to f)^{SPGL} = a\left|\Delta E/B_v\right|^{-\alpha} \cdot N_\lambda(J_i, J_f)(R(\Delta E)) \quad . \qquad (10)$$

In Eq. (10) a, α, and λ are fitting parameters, B_v is the rotational constant, and N_λ is a factor that allows for a restriction on ΔM or a change in orientation of the molecule during the collision.

C.6.2 Angular Momentum Based Laws

The S-matrix formalism was applied to the R-T process by DePristo and co-workers[40] and led to two scaling laws that have been successfully applied to R-T transfer in several homonuclear molecules such as I_2 and Na_2. For illustration we present the expressions for these two scaling laws in Eqs. (12) and (13). The salient point is that the rate coefficient, $k(i \to f)$, for the R-T process $J_i \to J_f$ is expressed in terms of a basis rate coefficient $k(\to 0)$. The infinite order sudden (IOS) law is given by

$$k(i \to f)^{IOS} = (2J_f+1)\exp[(E_{J_i} - E_{J>})/kT] \times \left[\sum \begin{pmatrix} J_i & & J_f \\ 0 & 0 & 0 \end{pmatrix}^2 (2\ +1)\ k(\ \to 0)\right] \qquad (12)$$

where

$j_>$ = larger of (j_i, j_f)

$\begin{pmatrix} \cdot & \cdot & \cdot \\ \cdot & \cdot & \cdot \end{pmatrix}$ = 3j symbol

and

$$k(\ell \to 0) = a[\ell(\ell+1)]^{-\gamma} \quad .$$

The sum over ℓ is taken over $|j_i - j_f| \leq \ell \leq |j_i + j_f|$ and a and γ are the fitting parameters.

The underlying principle of the IOS approximation is that the R-T collision is essentially instantaneous and consequently the molecule cannot rotate during the collision. If the perhaps more realistic assumption is made that the collision does take a finite time, then additional terms are added to the IOS expression and we have the Energy Corrected Sudden law (ECS) given by Eq. (11)

$$k^{ECS}(j_i, j_f) = (2j_f+1) \exp[(E_{j_i} - E_{j>})/kT] \times \left[\sum \begin{pmatrix} j_i & & j_f \\ 0 & 0 & 0 \end{pmatrix}^2 (2l+1) \left[A^{j>}\right]^2 k(\ell \to 0) \right] \quad . \tag{11}$$

In Eq. (4)

$$A^{j>} = \frac{1 + \tau^2/6}{1 + \tau_{j>}^2/6}$$

where $\tau_\ell = 4\pi \ell_c \, cB(j+1/2)/\bar{v}$. The parameter ℓ_c is interpreted on the collision length and $\bar{v}$ is the mean relative velocity, and τ_ℓ is an effective collision time. Since ℓ_c is a fitting parameter, we see how this law can give some physical insight into the R-T process.

C.7 Fitting Law Analysis in IF(B)

We compare the four fitting laws described previously with particular emphasis on J_i=72 and some of these results are shown in Figures 42 through 44 using He, Ne, and Xe bath gases. Figures 42(a-d) show fits using the four laws for He, Figures 43(a-d) show similar comparisons for Ne, and Figures 44(a-d) show the same comparisons for Xe as the collision partner. We note that the simplest description, the energy gap law, is inferior to the other three fitting laws. Interestingly, the power gap law compares favorably with the angular momentum based laws. This same result was also observed by Pritchard and co-workers in $I_2(B)$.[8,7]

The predictive power of the scaling laws is of critical importance to incorporation of any law into a kinetic code that includes rotational energy transfer. We have begun to test these laws and present some preliminary results below. In Figure 45 we show data for R-T rate coefficients with helium where J_i=27. The solid line is the prediction of the IOS law using the parameters obtained from the J_i=72 data in Figure 42. In Figure 45 the solid line is not a fit to the J_i=27 data. Rather it represents the R-T rate coefficient for J_i=27 predicted from the parameters determined from the J_i=72 data. This is an extremely encouraging and exciting result. A similar prediction of the J_i=13 data is shown in Figure 46.

The practical importance of the results shown in Figures 44 through 46 is that we have shown that one of the commonly used scaling laws IOS appears to give a good quantitative description of the R-T rate coefficients for IF(B) using He as a bath gas. It is likely that He would be the carrier gas in any IF chemical laser. Thus R-T relaxation can be analytically predicted.

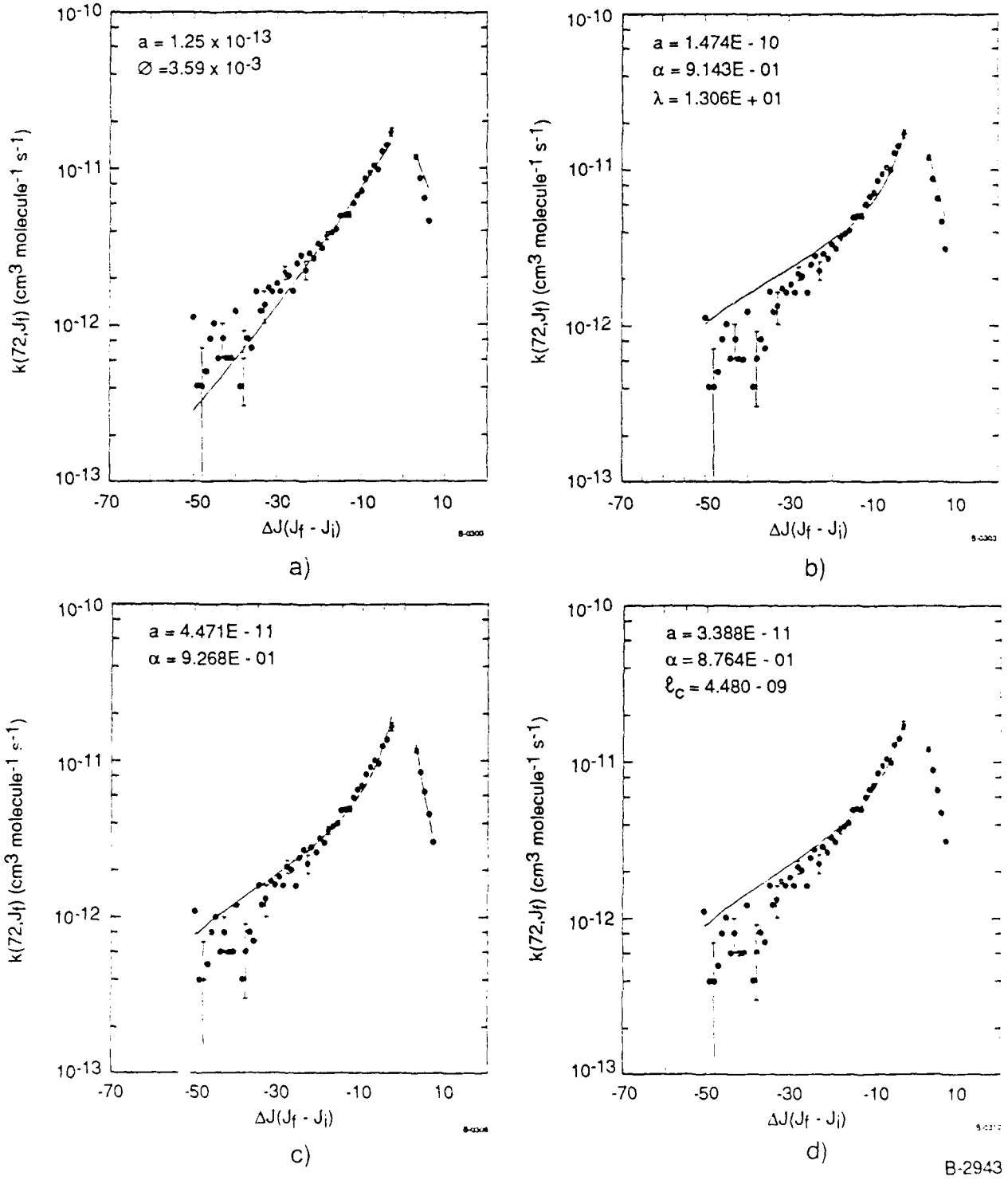

Figure 42.

Comparisons of Four Fitting Laws to IF + He Data for J_i=72
a) EG Law, b) SPG Law, c) IOS Law, d) ECS Law

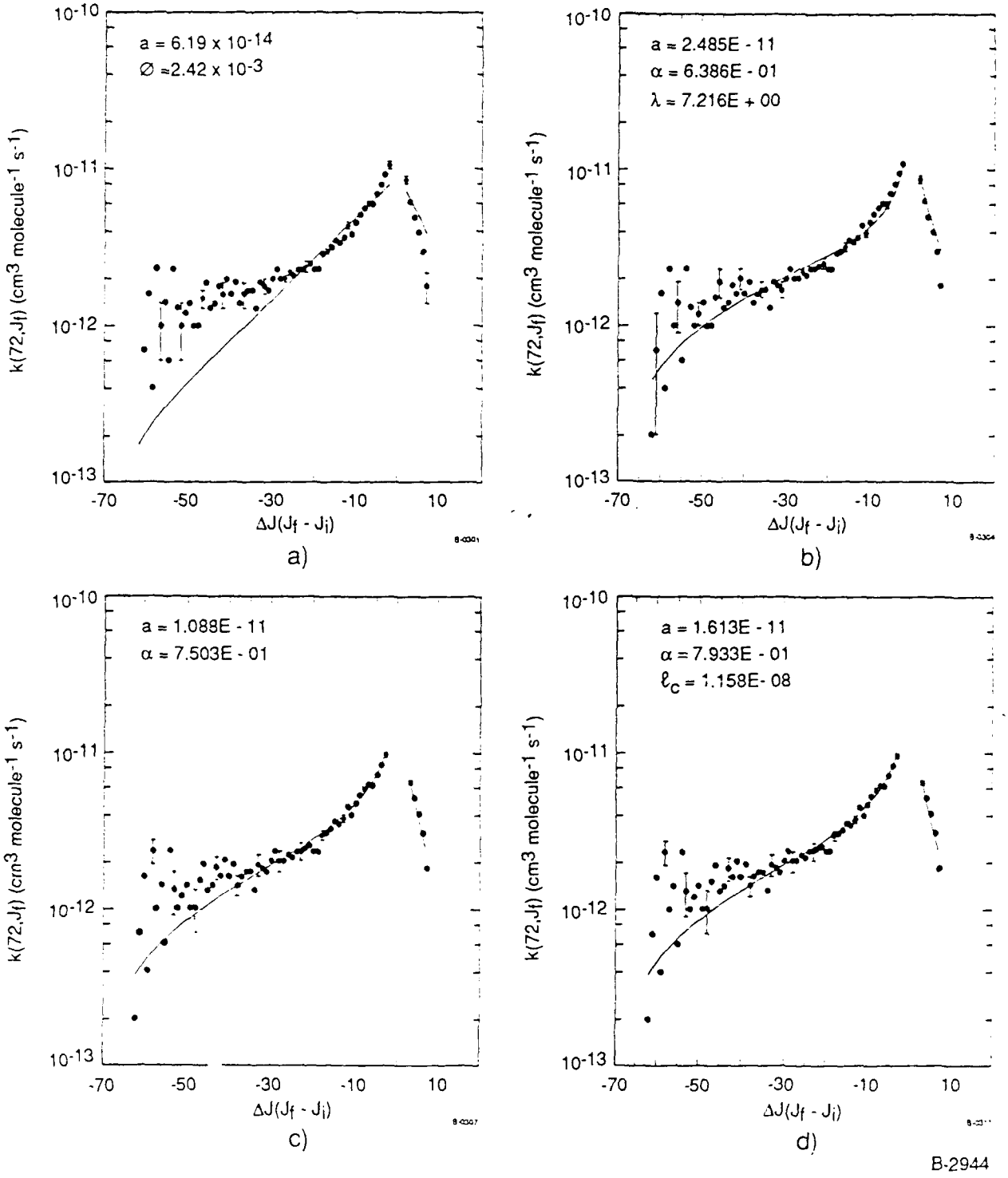

Figure 43.

Comparisons of Four Fitting Laws to IF + Ne Data for J_i=72
a) EG Law, b) SPG Law, c) IOS Law, d) ECS Law

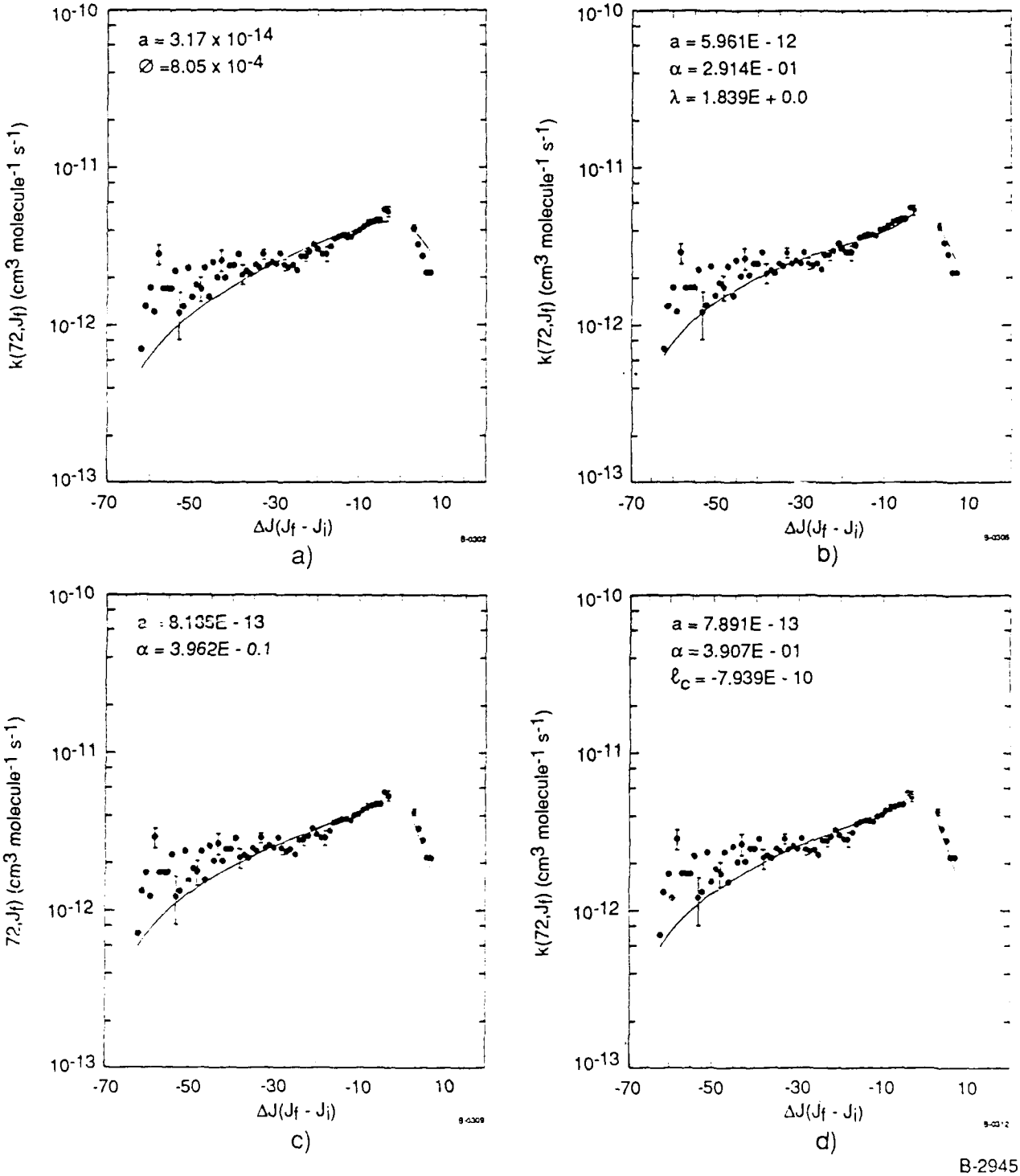

Figure 44.

Comparisons of Four Fitting Laws to IF + Xe Data for J_i=72
a) EG Law, b) SPG Law, c) IOS Law, d) ECS Law

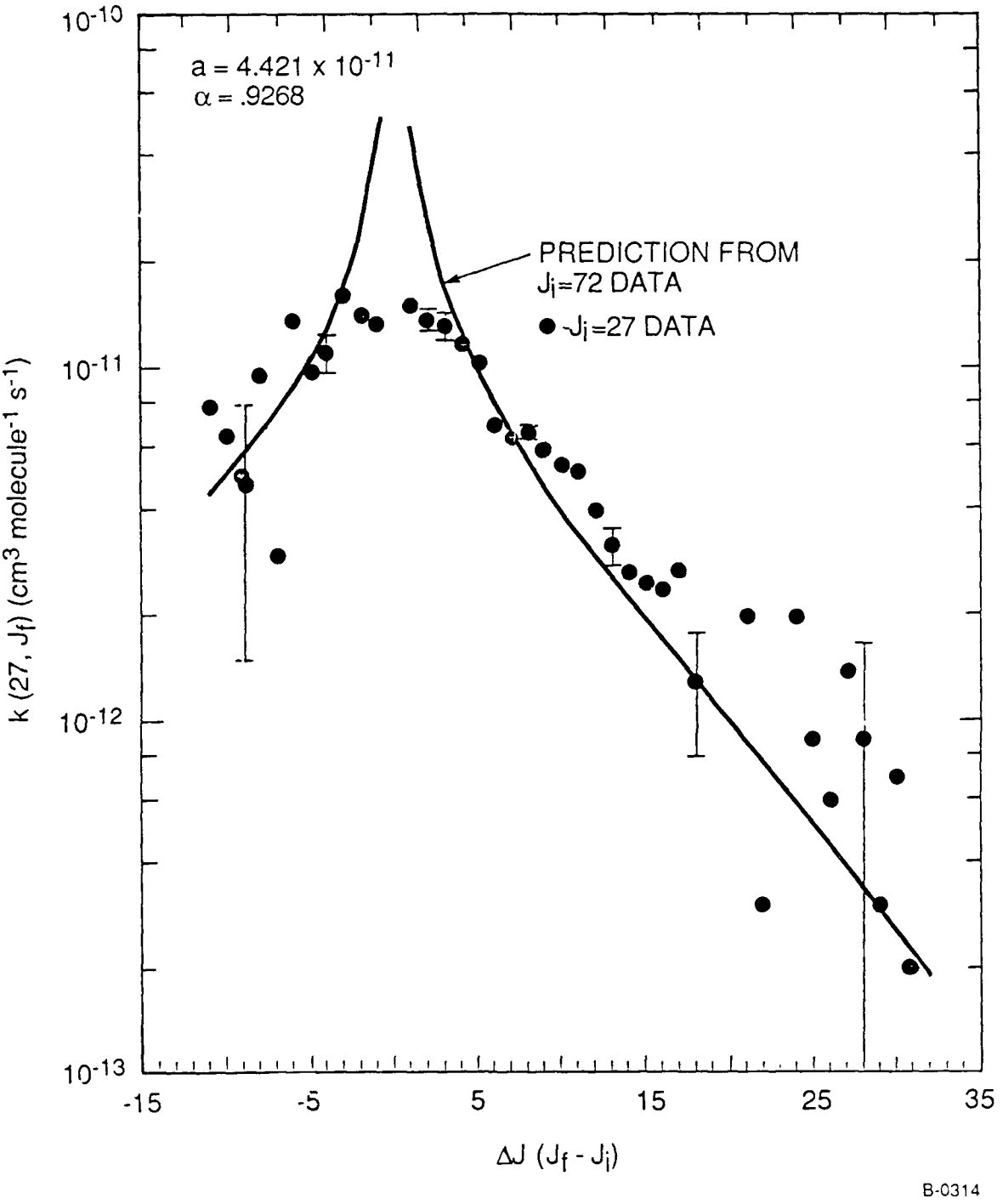

Figure 45.

Comparison of Prediction of IOS Law to Data for IF + He, J_i = 27. Solid line is the prediction for J_i=27 based upon parameters observed from J_i=72 data.

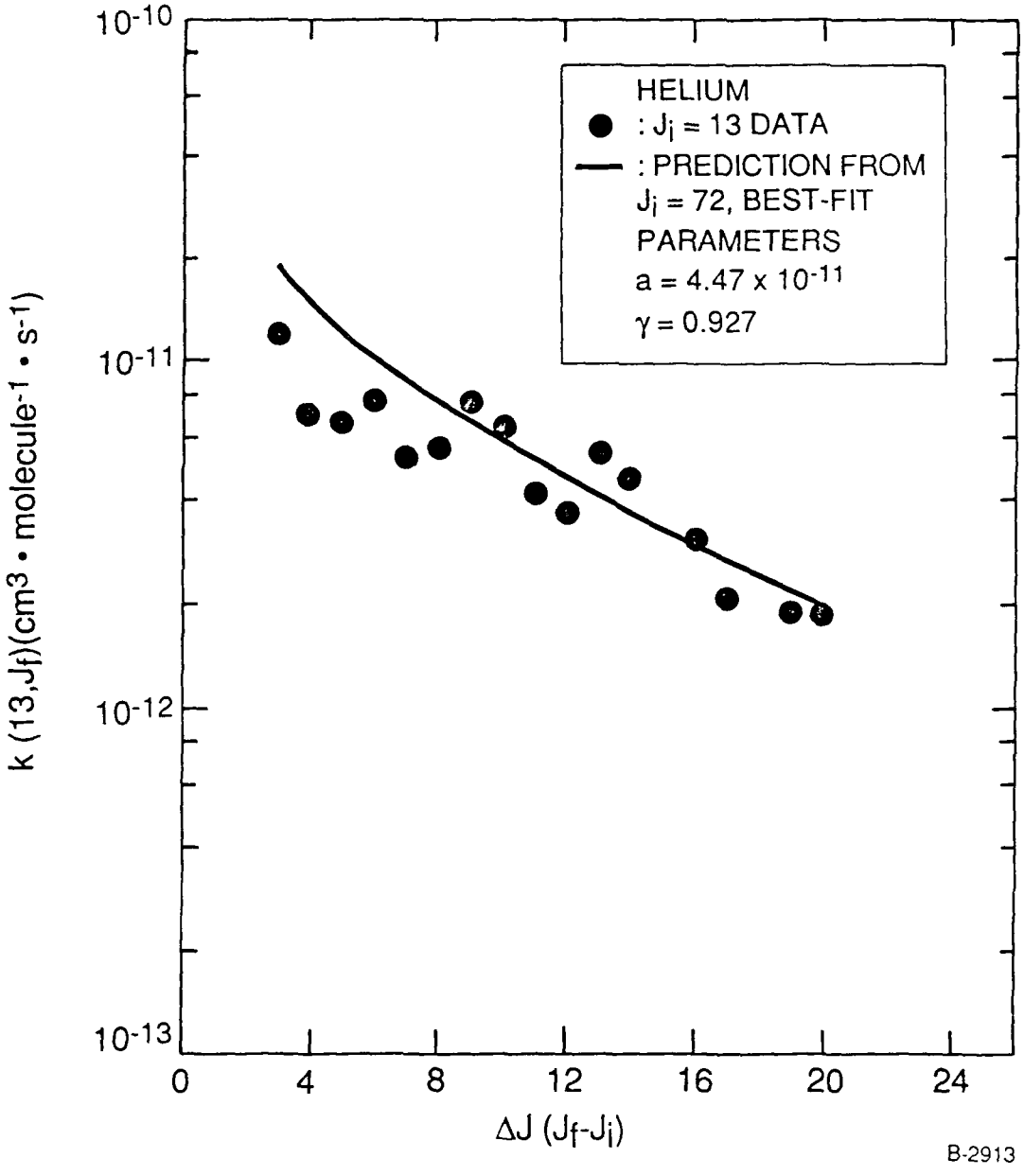

Figure 46.

Prediction of R-T Rate Coefficients for J_i=13. Prediction made using IOS Law from J_i=72 data and He bath gas

A similar comparison using Xe is shown in Figures 47(a) through 47(c). We see that the statistical Power Gap Law gives a reasonably good description.

In contrast to the above results, in Figures 48(a) through 48(c) we present results using the Energy Gap Law to predict R-T rate coefficients using Ar as a collision partner. We see that the rather simple EGL is not adequate.

We are continuing the comparisons of scaling laws to other species such as ICl. In addition we will be determining R-T transfer in IF using polar partners as part of a follow-on effort.

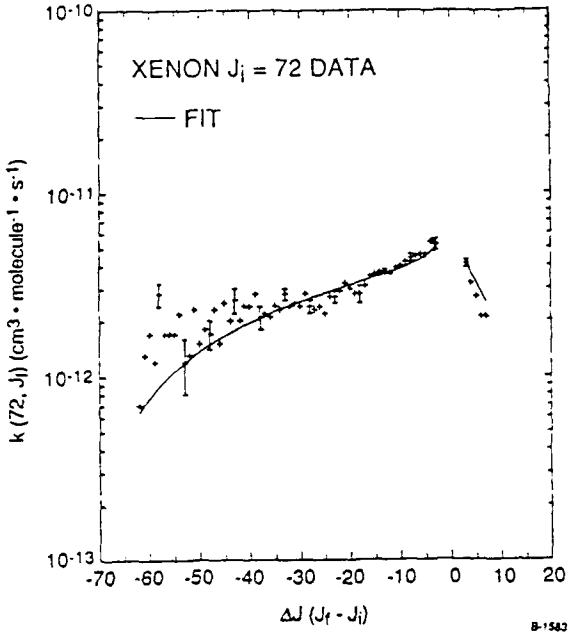

(a)

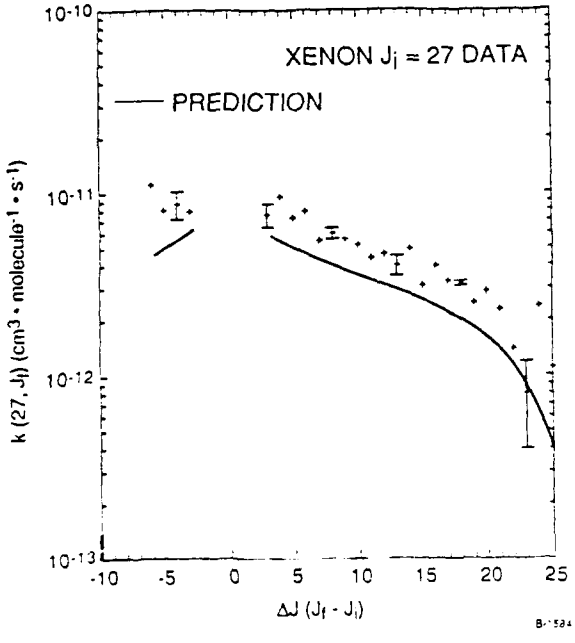

(b)

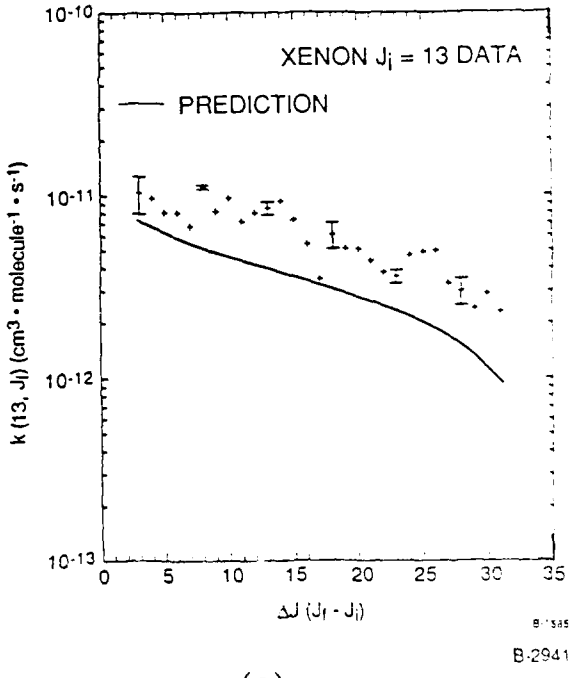

(c)

Figure 47.

(a) SPGL Fit to J_i=72 Data; (b) Prediction for J_i=27; (c) Prediction for J_i=13. Xenon was the collision partner.

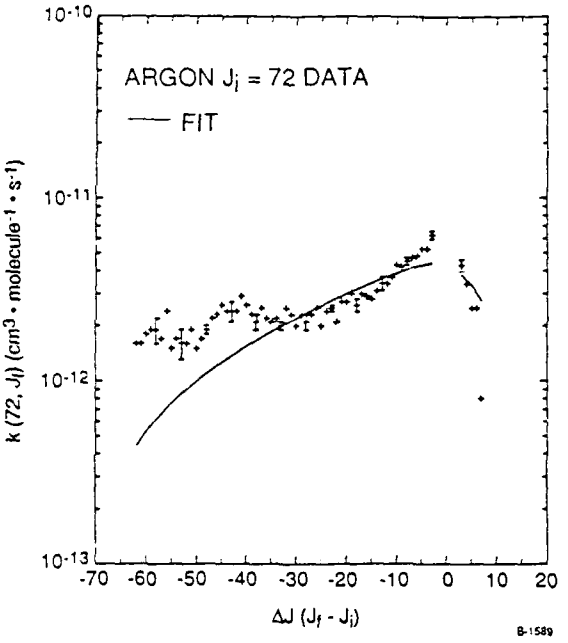

(a)

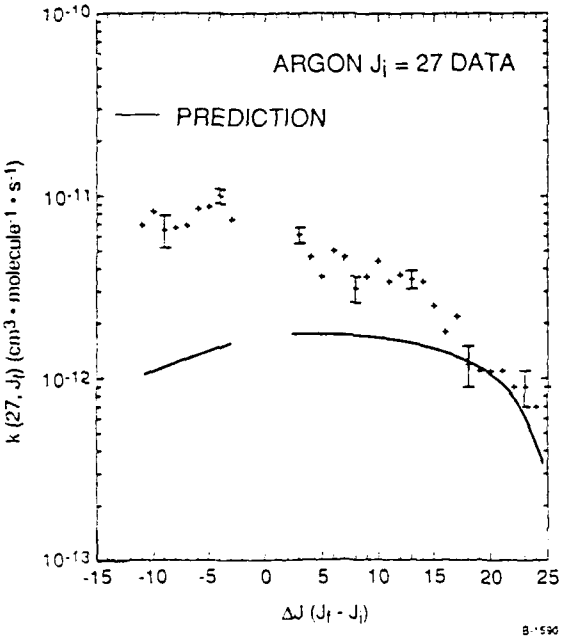

(b)

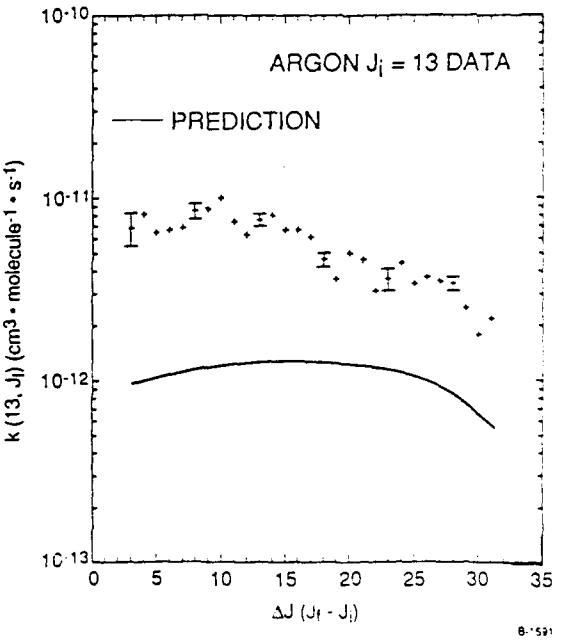

(c)

Figure 48.

(a) EGL Fit to J_i=72 Data; (b) Prediction for J_i=27; (c) Prediction for J_i=13 Bath gas was Ar.

D. References

1. J.I. Steinfeld and P. Ruttenberg, JILA Information Center Report 23, (1983).
2. J.I. Steinfeld, J. Phys. Chem. Ref. Data 13, 445 (1984); Suppl. ibid. 16, 903 (1987).
3. J.I. Steinfeld and W. Klemperer, J. Chem. Phys. 42, 3475 (1965).
4. R. Clark and A.J. McCaffery, Mole. Phys. 35, 609 (1978).
5. R. Clark and A.J. McCaffery, Mole. Phys. 35, 617 (1978).
6. T.A. Brunner, N. Smith, A.W. Karp, and D.E. Pritchard, J. Chem. Phys. 74, 3324 (1981).
7. K.L. Saenger, N. Smith, S.L. Dexheimer, C. Engelke, and D.E. Pritchard, J. Chem. Phys. 79, 4076 (1983).
8. S.L. Dexheimer, M. Durand, T.A. Brunner, and D.E. Pritchard, J. Chem. Phys. 76, 4996 (1982).
9. S.L. Dexheimer, T.A. Brunner, and D.E. Pritchard, J. Chem. Phys. 79, 5206 (1983).
10. M.A.A. Clyne, M.C. Heaven, and S.J. Davis, J. Chem. Soc. Faraday Trans. 2 76, 961 (1980).
11. P.J. Wolf and S.J. Davis, J. Chem. Phys. 87, 3492 (1987).
12. E.A. Dorko, L. Hanko, P.J. Wolf, and M. McAuliffe, Gas Flow and Chemical Lasers 6, Springer Verlag, New York (1986).
13. B.K. Clark and I.M. Littlewood, Optics Comm. 62, 91 (1987).
14. R.C. Byer, R.C. Herbst, H. Kildal, and M.D. Levenson, Appl. Phys. Lett. 20, 413 (1972).
15. B. Hartmann, B. Kleman, and O. Steinwall, Opt. Commun. 21, 33 (1977).

16. J.B. Koffend and R.W. Field, J. Appl. Phys. 48, 4468 (1977).

17. B. Wellegehausen, IEEE J. Quantum Electron. 15, 1108 (1979).

18. F.J. Wodarczyk and H.R. Schlossberg, J. Chem. Phys. 67, 4476 (1977).

19. G.P. Perram and S.J. Davis, J. Chem. Phys. 84, 2526 (1986).

20. S.J. Davis and L. Hanko, Appl. Phys. Lett. 37, 692 (1980).

21. S.J. Davis, L. Hanko, and R.F. Shea, J. Chem. Phys. 78, 172 (1983).

22. S.J. Davis and K.W. Holtzclaw, (manuscript in preparation).

23. E.H. Appleman and M.A.A. Clyne, JCS Faraday I, 71, 2072 (1975).

24. T. Trickl and J. Wanner, J. Chem. Phys. 78, 6091 (1983).

25. M.A.A. Clyne and I.S. McDermid, JCS Faraday II, 74, 1644 (1978).

26. P.J. Wolf and S.J. Davis, J. Chem. Phys. 83, 91 (1985).

27. P.D. Whitefield and M.R. Berman, "Oxygen IF Kinetics," AFWL TR-84, Air Force Weapons Laboratory, Kirtland AFB, NM 87117 (1985).

28. B. Girard, N. Billy, G. Gouédard, and J. Vigue, J. Chem. Phys. 88, 2342 (1988).

29. K. Bergmann and W. Demtröder, Z. Physik 243, 1 (1971).

30. D.R. Crosley, J. Chem. Phys. 67, 2085 (1977).

31. T. Trickl and J. Wanner, J. Mole. Spectr. 104, 174-182 (1984).

32. A. Fontijn, C.B. Meyer, and H.I. Schiff, J. Chem. Phys. 40, 64 (1964).

33. J.O. Hirschfelder, C.F. Curtiss, and R.B. Bird, Molecular Theory of Gaseous and Liquids (John Wiley and Sons, Inc., New York, New York, 1954).

34. M.A.A. Clyne and I.S. McDermid, J. Chem. Soc. Faraday Trans. 2 73, 1094 (1977).

35. R.D. Gordon and K.K. Innes, J. Chem. Phys. 71, 2824 (1979)

36. M. Kitamura, T. Kondow, K. Kuchitsu, T. Munakata, and T. Kasuya, J. Chem. Phys. 82, 4986 (1985).

37. J.C. Polanyi and K.B. Woodall, J. Chem. Phys. 56, 1563 (1972).

38. D.E. Pritchard, N. Smith, R.D. Driver, T.A. Brunner, J. Chem. Phys. 70, 2115 (1979).

39. T.A. Brunner, N. Smith, A.W. Dapr, and D.E. Pritchard, J. Chem. Phys. 74, 3324 (1981).

40. A.E. DePristo, S.D. Augustin, R. Ramaswamy, and H. Rabitz, J. Chem. Phys. 71(2), 850 (1979).

APPENDIX A

SAMPLE LIST OF R-T RATE COEFFICIENTS

DETERMINED IN THIS STUDY

IF(B) + He

(J_i=72, v'=6)

J_F	k(72,J) (10^{-12} cm^3 $molec^{-1}$ s^{-1})	(sigma)
0	—	—
1	—	—
2	—	—
3	—	—
4	—	—
5	—	—
6	0.5	(0.3)
7	-0.2	(0.3)
8	0.1	(0.6)
9	0.5	(0.6)
10	0.6	(0.7)
11	-0.6	(0.5)
12	0.8	(0.5)
13	-0.2	(0.4)
14	0.5	(0.6)
15	0.3	(0.3)
16	0.7	(0.6)
17	0.0	(0.3)
18	-0.5	(0.8)
19	0.5	(0.5)
20	0.7	(0.4)
21	0.0	(0.3)
22	1.1	(0.2)
23	0.4	(0.5)
24	0.4	(0.3)
25	0.5	(0.4)
26	0.8	(0.2)
27	1.0	(0.2)
28	0.6	(0.4)
29	0.8	(0.2)
30	0.6	(0.3)
31	0.6	(0.3)
32	1.2	(0.2)
33	0.4	(0.4)
34	0.6	(0.3)
35	0.8	(0.3)
36	0.7	(0.2)
37	1.6	(0.3)
38	1.2	(0.3)
39	1.3	(0.3)
40	1.7	(0.3)
41	1.6	(0.1)
42	1.8	(0.4)
43	1.6	(0.2)
44	2.1	(0.2)
45	2.0	(0.2)
46	1.6	(0.2)
47	2.4	(0.3)
48	2.7	(0.3)
49	2.2	(0.3)
50	2.8	(0.4)
51	2.6	(0.2)
52	3.2	(0.2)
53	3.0	(0.2)
54	3.6	(0.2)
55	3.8	(0.3)
56	4.0	(0.2)
57	4.8	(0.2)
58	4.9	(0.3)
59	4.9	(0.2)
60	5.8	(0.4)
61	6.5	(0.4)
62	6.9	(0.3)
63	8.2	(0.3)
64	9.1	(0.3)
65	10.0	(0.3)
66	9.5	(0.4)
67	12.3	(0.3)
68	13.6	(0.6)
69	16.5	(1.0)
70	21.7	(1.3)
71	18.8	(1.2)
72	—	—
73	17.0	(0.8)
74	16.2	(0.8)
75	11.5	(0.4)
76	8.4	(0.4)
77	6.3	(0.2)
78	4.5	(0.3)
79	3.0	(0.7)
80	3.2	(0.6)
81	2.6	(0.7)
82	2.0	(1.0)
83	1.9	(0.7)
84	1.2	(0.6)
85	1.9	(0.6)
86	1.5	(0.5)
87	1.2	(0.4)

Σk_F = 3.0 x 10^{-10} cm^3 $molecule^{-1}$ s^{-1}

IF(B) + Ne

(J_1=72, v'=6)

J_F	k(72,J) (sigma) (10^{-12} cm^3 $molec^{-1}$ s^{-1})	
0	—	—
1	—	—
2	0.9	(0.2)
3	—	—
4	—	—
5	0.2	(0.2)
6	0.4	(0.3)
7	—	—
8	1.3	(0.7)
9	0.0	(0.6)
10	0.2	(0.4)
11	0.7	(0.5)
12	1.6	(0.2)
13	0.4	(0.3)
14	2.3	(0.4)
15	1.0	(0.4)
16	1.4	(0.5)
17	0.6	(0.5)
18	2.3	(0.4)
19	1.3	(0.4)
20	1.0	(0.4)
21	1.2	(0.2)
22	1.4	(0.3)
23	1.0	(0.2)
24	1.0	(0.3)
25	1.5	(0.2)
26	1.9	(0.4)
27	1.3	(0.3)
28	1.4	(0.3)
29	1.8	(0.3)
30	1.6	(0.3)
31	2.0	(0.3)
32	1.6	(0.2)
33	1.9	(0.2)
34	1.4	(0.2)
35	1.6	(0.3)
36	1.7	(0.2)
37	1.7	(0.2)
38	1.3	(0.1)
39	1.9	(0.3)
40	1.8	(0.2)
41	1.7	(0.2)
42	2.0	(0.2)
43	2.3	(0.3)
44	2.0	(0.3)

J_F	k(72,J) (sigma) (10^{-12} cm^3 $molec^{-1}$ s^{-1})	
45	2.0	(0.1)
46	2.2	(0.1)
47	2.1	(0.2)
48	2.3	(0.1)
49	2.3	(0.3)
50	2.4	(0.2)
51	2.5	(0.2)
52	2.3	(0.2)
53	2.3	(0.2)
54	2.9	(0.2)
55	3.0	(0.1)
56	3.2	(0.2)
57	3.5	(0.2)
58	3.4	(0.2)
59	3.7	(0.2)
60	4.4	(0.2)
61	3.9	(0.2)
62	4.6	(0.2)
63	5.2	(0.1)
64	5.7	(0.2)
65	6.1	(0.2)
66	6.0	(0.3)
67	7.0	(0.3)
68	8.1	(0.4)
69	9.4	(0.3)
70	10.8	(0.6)
71	10.4	(0.4)
72	—	—
73	9.6	(0.4)
74	8.7	(0.5)
75	6.3	(0.2)
76	5.0	(0.3)
77	4.0	(0.2)
78	3.0	(0.2)
79	1.8	(0.4)
80	2.3	(0.3)
81	2.2	(0.3)
82	2.4	(0.3)
83	1.8	(0.4)
84	1.3	(0.3)
85	1.5	(0.3)
86	1.0	(0.3)
87	1.1	(0.2)

$\Sigma k = 2.3 \times 10^{-10}$ cm^3 $molecule^{-1}$ s^{-1}

IF(B) + Ar

(J_i=72, v'=6)

J_F	k(72,J) (10^{-12} cm^3 $molec^{-1}$ s^{-1})	(sigma)
0	[illegible]	[illegible]
1	[illegible]	[illegible]
2	[illegible]	[illegible]
3	[illegible]	[illegible]
4	[illegible]	[illegible]
5	0.5	(0.4)
6	[illegible]	[illegible]
7	0.6	(0.8)
8	1.1	(0.8)
9	1.6	(0.7)
10	1.6	(0.9)
11	1.6	(0.5)
12	1.8	(0.5)
13	1.9	(0.4)
14	1.9	(0.3)
15	[illegible]	(0.3)
16	2.4	(0.4)
17	1.5	(0.6)
18	1.7	(0.6)
19	1.6	(0.3)
20	1.6	(0.2)
21	1.9	(0.3)
22	1.5	(0.3)
23	[illegible]	(0.4)
24	1.9	(0.1)
25	2.2	(0.3)
26	2.3	(0.5)
27	2.6	(0.4)
28	2.4	(0.4)
29	2.4	(0.3)
30	2.4	(0.3)
31	2.9	(0.2)
32	2.6	(0.2)
33	2.3	(0.3)
34	2.1	(0.2)
35	2.5	(0.3)
36	2.2	(0.2)
37	2.1	(0.1)
38	2.2	(0.2)
39	2.0	(0.1)
40	2.5	(0.1)
41	2.3	(0.3)
42	2.0	(0.2)
43	2.3	(0.3)
44	2.1	(0.2)
45	2.3	(0.2)
46	2.5	(0.2)
47	2.0	(0.1)
48	2.4	(0.2)
49	2.5	(0.1)
50	2.1	(0.1)
51	2.7	(0.2)
52	2.7	(0.3)
53	3.0	(0.2)
54	2.6	(0.2)
55	3.0	(0.3)
56	2.9	(0.1)
57	2.8	(0.3)
58	3.1	(0.1)
59	3.4	(0.3)
60	3.4	(0.3)
61	3.7	(0.2)
62	4.3	(0.3)
63	4.2	(0.2)
64	4.5	(0.2)
65	4.7	(0.3)
66	4.8	(0.3)
67	5.3	(0.3)
68	5.3	(0.4)
69	6.3	(0.3)
70	6.6	(0.2)
71	6.9	(0.6)
72	[illegible]	[illegible]
73	5.8	(0.5)
74	5.1	(0.4)
75	4.3	(0.3)
76	3.4	(0.3)
77	2.5	(0.2)
78	2.5	(0.2)
79	0.8	(0.3)
80	[illegible]	(0.2)
81	[illegible]	(0.2)
[illegible]	1.5	(0.4)
83	0.7	(0.3)
84	1.4	(0.4)
85	0.8	(0.2)
86	0.5	(0.2)
87	1.1	(0.2)

$\Sigma k = 2.1 \times 10^{-10}$ cm^3 $molecule^{-1}$ s^{-1}

IF(B) + Xe

(J_i=72, v'=6)

J_F	k(72,J) (10^{-12} cm^3 $molec^{-1}$ s^{-1})	(sigma)
0	--	--
1	--	--
2	0.8	(0.4)
3	--	--
4	--	--
5	0.3	(0.2)
6	--	--
7	0.7	(0.5)
8	0.4	(0.8)
9	1.7	(0.6)
10	0.7	(0.5)
11	1.3	(0.6)
12	1.7	(0.5)
13	1.2	(0.4)
14	2.8	(0.4)
15	1.7	(0.4)
16	1.7	(0.4)
17	1.7	(0.4)
18	2.2	(0.4)
19	1.2	(0.4)
20	1.3	(0.5)
21	2.3	(0.3)
22	1.5	(0.5)
23	1.8	(0.4)
24	1.7	(0.3)
25	2.3	(0.4)
26	1.5	(0.3)
27	2.5	(0.3)
28	2.0	(0.1)
29	2.6	(0.4)
30	2.0	(0.3)
31	2.4	(0.3)
32	2.4	(0.4)
33	2.8	(0.4)
34	2.1	(0.3)
35	2.2	(0.3)
36	2.1	(0.3)
37	2.4	(0.3)
38	2.3	(0.3)
39	2.8	(0.2)
40	2.4	(0.3)
41	2.5	(0.3)
42	2.4	(0.3)
43	2.8	(0.2)
44	2.4	(0.2)
45	2.3	(0.3)
46	2.4	(0.5)
47	2.2	(0.2)
48	2.7	(0.2)
49	2.7	(0.2)
50	2.9	(0.1)
51	3.2	(0.2)
52	3.0	(0.4)
53	2.8	(0.3)
54	2.8	(0.3)
55	3.1	(0.3)
56	3.5	(0.3)
57	3.6	(0.2)
58	3.7	(0.5)
59	3.7	(0.1)
60	3.6	(0.2)
61	3.9	(0.2)
62	4.0	(0.4)
63	4.2	(0.2)
64	4.4	(0.2)
65	4.5	(0.3)
66	4.6	(0.4)
67	4.6	(0.4)
68	5.4	(0.4)
69	5.2	(0.4)
70	4.7	(0.4)
71	2.9	(0.7)
72	--	--
73	3.0	(0.4)
74	3.3	(0.3)
75	4.1	(0.2)
76	3.2	(0.3)
77	2.7	(0.3)
78	2.1	(0.3)
79	2.1	(0.3)
80	2.0	(0.2)
81	1.8	(0.3)
82	1.8	(0.5)
83	1.5	(0.4)
84	0.9	(0.3)
85	1.5	(0.4)
86	0.4	(0.3)
87	0.6	(0.3)

Σk = 2.01 x 10^{-10} cm^3 $molecule^{-1}$ s^{-1}

IF(B) + CF_4

(J_i=72, v'=6)

J_P	k(72,J) (10^{-12} cm^3 $molec^{-1}$ s^{-1})	(sigma)
0	—	—
1	—	—
2	2.0	(0.7)
3	1.1	(0.7)
4	—	—
5	1.0	(1.1)
6	—	—
7	—	—
8	0.8	(0.6)
9	—	—
10	3.0	(1.1)
11	0.5	(1.1)
12	3.4	(1.0)
13	2.2	(0.6)
14	3.4	(0.6)
15	2.4	(0.5)
16	3.7	(0.7)
17	3.8	(0.2)
18	3.7	(0.4)
19	2.7	(0.5)
20	2.8	(0.5)
21	3.4	(0.4)
22	3.0	(0.3)
23	2.6	(0.3)
24	3.1	(0.3)
25	2.8	(0.2)
26	2.1	(0.7)
27	3.6	(0.2)
28	3.5	(0.3)
29	3.7	(0.4)
30	3.6	(0.3)
31	4.2	(0.2)
32	3.7	(0.2)
33	3.8	(0.4)
34	4.0	(0.4)
35	3.9	(0.4)
36	3.1	(0.2)
37	2.9	(0.2)
38	2.9	(0.2)
39	2.7	(0.3)
40	2.3	(0.2)
41	2.8	(0.4)
42	2.8	(0.3)
43	3.1	(0.3)
44	3.0	(0.3)
45	3.2	(0.2)
46	3.1	(0.3)
47	3.3	(0.2)
48	3.4	(0.3)
49	3.4	(0.2)
50	3.0	(0.4)
51	3.3	(0.1)
52	2.8	(0.3)
53	3.1	(0.2)
54	3.1	(0.2)
55	3.3	(0.3)
56	3.0	(0.2)
57	3.6	(0.2)
58	3.2	(0.2)
59	3.7	(0.3)
60	3.5	(0.3)
61	3.7	(0.2)
62	3.3	(0.4)
63	3.7	(0.2)
64	3.7	(0.2)
65	3.8	(0.2)
66	3.8	(0.2)
67	4.0	(0.4)
68	4.0	(0.4)
69	4.0	(0.3)
70	4.0	(0.4)
71	5.4	(0.6)
72	—	—
73	5.4	(0.3)
74	3.6	(0.4)
75	3.2	(0.2)
76	2.7	(0.2)
77	2.4	(0.3)
78	2.2	(0.2)
79	0.7	(0.3)
80	1.6	(0.1)
81	1.7	(0.2)
82	1.9	(0.2)
83	1.9	(0.3)
84	1.9	(0.5)
85	1.7	(0.4)
86	1.7	(0.3)
87	1.6	(0.3)

$\Sigma k = 2.5 \times 10^{-10}$ cm^3 $molecule^{-1}$ s^{-1}

IF(B) + He

(J_i=27, v'=6)

J_F	k(27,J) (10^{-12} cm^3 $molec^{-1}$ s^{-1})	(sigma)
0	—	—
1	2.3	(1.9)
2	—	—
3	2.9	(2.6)
4	—	—
5	-0.5	(1.7)
6	3.2	(3.2)
7	—	—
8	-0.3	(4.4)
9	2.6	(4.5)
10	3.2	(3.1)
11	3.8	(3.7)
12	2.7	(3.2)
13	2.1	(3.2)
14	8.7	(2.2)
15	-0.3	(3.4)
16	8.0	(1.3)
17	6.6	(2.0)
18	4.8	(3.3)
19	9.9	(3.6)
20	3.0	(1.6)
21	13.9	(1.6)
22	10.1	(1.7)
23	11.4	(1.4)
24	16.5	(1.9)
25	14.7	(1.4)
26	13.8	(2.5)
27	—	—
28	15.5	(1.2)
29	14.2	(1.0)
30	13.6	(1.2)
31	12.2	(1.3)
32	10.6	(1.3)
33	7.1	(0.8)
34	6.5	(0.4)
35	6.8	(0.3)
36	6.1	(0.2)
37	5.5	(0.2)
38	5.3	(0.7)
39	4.1	(0.7)
40	3.2	(0.4)
41	2.7	(0.7)
42	2.5	(0.3)
43	2.4	(0.8)
44	2.7	(1.0)
45	1.3	(0.5)
46	0.0	(0.8)
47	0.1	(0.9)
48	2.0	(0.5)
49	0.3	(0.7)
50	0.7	(0.8)
51	2.0	(0.4)
52	0.9	(0.5)
53	0.6	(0.6)
54	1.4	(0.8)
55	0.9	(0.8)
56	0.3	(0.5)
57	0.7	(0.3)
58	0.2	(0.5)
59	0.0	(0.0)
60	-0.1	(0.5)
61	0.9	(0.4)
62	0.4	(0.6)
63	-0.2	(0.5)
64	0.3	(0.3)
65	0.6	(0.6)
66	0.7	(0.4)
67	-0.1	(0.6)
68	0.1	(0.7)

$\Sigma k = 2.8 \times 10^{-10}$ cm^3 $molecule^{-1}$ s^{-1}

IF(B) + Ar

(J_i=27, v'=6)

J_F	k(27,J) (10^{-12} cm^3 $molec^{-1}$ s^{-1})	(sigma)
0	—	—
1	—	—
2	—	—
3	—	—
4	3.0	(3.7)
5	4.9	(3.9)
6	3.0	(5.5)
7	—	—
8	4.7	(1.9)
9	—	—
10	10.1	(3.3)
11	—	—
12	2.6	(3.2)
13	9.4	(2.4)
14	1.7	(1.5)
15	7.7	(1.3)
16	4.9	(2.6)
17	—	—
18	7.0	(0.7)
19	7.2	(0.6)
20	7.3	(0.5)
21	8.5	(1.4)
22	6.7	(0.6)
23	7.7	(0.7)
24	9.0	(1.1)
25	7.5	(1.5)
26	6.3	(1.3)
27	—	—
28	2.1	(2.2)
29	4.6	(1.3)
30	5.9	(0.6)

J_F	k(27,J) (10^{-12} cm^3 $molec^{-1}$ s^{-1})	(sigma)
31	6.7	(0.8)
32	5.7	(0.8)
33	5.3	(1.1)
34	4.7	(1.2)
35	4.6	(0.6)
36	4.4	(0.5)
37	4.1	(0.4)
38	4.9	(0.6)
39	3.8	(0.4)
40	2.3	(0.8)
41	3.9	(1.0)
42	2.6	(1.0)
43	1.3	(1.6)
44	1.5	(0.8)
45	3.8	(0.8)
46	0.4	(0.5)
47	1.2	(0.3)
48	0.5	(0.7)
49	2.3	(0.6)
50	0.3	(0.5)
51	1.6	(0.8)
52	0.1	(0.9)
53	1.0	(0.9)
54	-0.4	(0.9)
55	0.9	(0.6)
56	0.7	(0.9)
57	0.0	(0.6)
58	-0.2	(0.6)
59	0.4	(0.3)
60	-0.7	(0.7)

$\Sigma k = 2.0 \times 10^{-10}$ cm^3 $molecule^{-1}$ s^{-1}

IF(B) + Xe

(J_i=27, v'=6)

J_F	k(27,J) (10^{-12} cm^3 $molec^{-1}$ s^{-1})	(sigma)
0	0.7	(1.1)
1	—	—
2	-1.4	(2.5)
3	6.1	(2.5)
4	0.6	(2.2)
5	6.8	(3.7)
6	2.9	(2.7)
7	—	—
8	15.5	(2.2)
9	—	—
10	13.3	(1.7)
11	—	—
12	10.6	(1.5)
13	2.9	(2.4)
14	7.9	(3.0)
15	5.4	(2.0)
16	8.8	(1.2)
17	5.0	(1.5)
18	9.2	(2.9)
19	5.4	(2.9)
20	9.4	(2.7)
21	9.6	(1.4)
22	9.9	(0.8)
23	10.0	(1.3)
24	8.2	(0.7)
25	8.7	(0.7)
26	6.7	(1.4)
27	0.0	(0.0)
28	2.4	(1.6)
29	5.9	(1.6)
30	5.8	(1.0)
31	7.3	(0.9)
32	5.6	(0.9)
33	5.1	(0.8)
34	3.5	(1.0)

J_F	k(27,J) (10^{-12} cm^3 $molec^{-1}$ s^{-1})	(sigma)
35	5.0	(0.2)
36	5.1	(0.2)
37	5.2	(0.3)
38	6.1	(1.5)
39	5.9	(0.7)
40	4.5	(0.7)
41	5.3	(0.5)
42	4.1	(0.6)
43	3.8	(0.4)
44	2.9	(0.7)
45	2.5	(0.2
46	1.0	(0.5)
47	2.2	(0.3)
48	1.1	(0.8)
49	0.9	(0.6)
50	0.4	(0.7)
51	1.8	(0.3)
52	1.3	(0.5)
53	1.7	(0.5)
54	1.4	(0.3)
55	1.3	(0.3)
56	-0.1	(0.4)
57	0.4	(0.4)
58	1.0	(0.2)
59	1.1	(0.4)
60	-0.2	(0.4)
61	0.3	(0.4)
62	0.6	(0.2)
63	0.3	(0.4)
64	0.5	(0.3)
65	-0.2	(0.3)
66	0.2	(0.5)
67	-0.4	(0.4)
68	-0.8	(0.5)

$\Sigma k = 2.6 \times 10^{-10}$ cm^3 $molecule^{-1}$ s^{-1}

IF(B) + He

(J_i=13, v'=6)

J_F	k(13,J)	(sigma)
	(10^{-12} cm^3 $molec^{-1}$ s^{-1})	
0	—	—
1	—	—
2	—	—
3	—	—
4	-8.3	(6.6)
5	25.9	(7.4)
6	—	—
7	—	—
8	17.8	(3.9)
9	11.8	(7.5)
10	8.2	(7.0)
11	17.5	(4.8)
12	7.1	(4.4)
13	—	—
14	—	—
15	16.1	(2.3)
16	12.1	(1.5)
17	7.1	(0.7)
18	6.7	(1.1)
19	7.7	(1.2)
20	5.3	(0.9)
21	5.9	(1.4)
22	7.0	(0.9)
23	6.4	(1.6)
24	4.2	(1.6)
25	3.7	(0.7)
26	5.0	(0.6)
27	4.7	(0.8)
28	—	—
29	3.1	(0.1)
30	2.1	(0.9)
31	0.1	(0.4)
32	1.9	(0.8)
33	1.9	(1.1)
34	0.7	(0.4)
35	-1.0	(0.4)
36	0.0	(0.4)
37	0.4	(0.3)
38	0.6	(0.5)
39	1.7	(0.5)
40	1.1	(1.0)
41	-0.2	(0.9)
42	0.3	(0.7)
43	—	—
44	1.1	(0.3)

Σk = 1.9 x 10^{-10} cm^3 $molecule^{-1}$ s^{-1}

IF(B) + Ar

(J_i=13, v'=6)

J_F	k(13,J)	(sigma)
	(10^{-12} cm^3 $molec^{-1}$ s^{-1})	
0	--	--
1	--	--
2	--	--
3	[illegible]	(4.1)
4	[illegible]	(5.6)
5	[illegible]	(2.6)
6	--	--
7	--	--
8	17.6	(1.2)
9	--	--
10	14.9	(1.3)
11	4.8	(1.8)
12	[illegible]	(2.2)
13	--	--
14	--	--
15	[illegible]	(0.8)
16	[illegible]	(1.4)
17	[illegible]	(1.1)
18	8.5	(1.3)
19	8.7	(1.6)
20	8.9	(1.1)
21	8.5	(0.8)
22	8.7	(0.4)
23	[illegible]	(0.9)
24	7.4	(0.8)
25	6.3	(0.6)
26	7.6	(0.6)
27	[illegible]	(0.6)
28	6.7	(0.4)
29	6.7	(0.5)
30	[illegible]	(0.6)
31	4.6	(0.4)
32	3.6	(0.5)
33	5.0	(0.6)
34	4.6	(0.4)

J_F	k(13,J)	(sigma)
	(10^{-12} cm^3 $molec^{-1}$ s^{-1})	
35	3.1	(0.5)
36	3.6	(0.5)
37	4.4	(0.2)
38	3.4	(0.5)
39	3.7	(0.4)
40	3.5	(0.4)
41	3.4	(0.3)
42	2.5	(0.3)
43	1.8	(0.3)
44	2.2	(0.3)
45	1.2	(0.3)
46	1.1	(0.2)
47	1.1	(0.2)
48	1.1	(0.1)
49	0.9	(0.2)
50	0.9	(0.2)
51	0.7	(0.4)
52	0.9	(0.2)
53	0.7	(0.4)
54	0.9	(0.2)
55	0.7	(0.3)
56	0.7	(0.3)
57	0.7	(0.3)
58	0.6	(0.1)
59	0.4	(0.2)
60	0.3	(0.2)
61	-0.2	(0.2)
62	0.1	(0.2)
63	0.3	(0.2)
64	0.1	(0.1)
65	0.0	(0.2)
66	0.3	(0.2)
67	0.2	(0.2)
68	-0.4	(0.3)

$\Sigma k = 2.4 \times 10^{-10}$ cm^3 $molecule^{-1}$ s^{-1}

IF(B) + Xe

(J_i=13, v'=6)

J_F	k(13,J) (10^{-12} cm^3 $molec^{-1}$ s^{-1})	(sigma)
0	—	—
1	—	—
2	—	—
3	—	—
4	—	—
5	—	—
6	10.0	(1.5)
7	—	—
8	4.7	(1.4)
9	14.5	(2.0)
10	—	—
11	15.9	(1.0)
12	—	—
13	—	—
14	6.0	(5.2)
15	9.2	(2.2)
16	10.4	(2.4)
17	9.7	(0.9)
18	8.1	(1.0)
19	8.1	(1.0)
20	6.8	(1.2)
21	11.2	(0.3)
22	8.2	(2.6)
23	9.7	(1.1)
24	7.9	(1.1)
25	8.0	(1.1)
26	8.5	(0.7)
27	9.3	(0.8)

J_F	k(13,J) (10^{-12} cm^3 $molec^{-1}$ s^{-1})	(sigma)
28	7.2	(0.9)
29	5.4	(0.9)
30	3.5	(0.7)
31	6.1	(1.0)
32	5.1	(0.6)
33	3.1	(0.8)
34	4.4	(0.5)
35	3.8	(0.7)
36	3.6	(0.3)
37	4.7	(0.9)
38	4.9	(0.5)
39	5.0	(0.5)
40	3.3	(0.3)
41	3.0	(0.5)
42	2.4	(0.5)
43	2.9	(0.3)
44	2.3	(0.2)
45	1.9	(0.3)
46	—	—
47	—	—
48	0.2	(0.2)
49	0.4	(0.1)
50	1.0	(0.3)
51	1.0	(0.3)
52	0.8	(0.3)
53	1.2	(0.2)
54	1.0	(0.2)

$\Sigma k = 1.9 \times 10^{-10}$ cm^3 $molecule^{-1}$ s^{-1}

ICl(B) + He

(J_i=55, v'=1)

J_F	k(55,J)	(sigma)
	(10^{-12} cm^3 molec^{-1} s-1)	
0	—	—
1	—	—
2	—	—
3	—	—
4	—	—
5	—	—
6	—	—
7	0.9	(0.5)
8	—	—
9	1.0	(0.6)
10	-0.6	(0.3)
11	-0.5	(0.3)
12	—	—
13	2.2	(0.8)
14	0.3	(1.5)
15	4.3	(2.0)
16	4.1	(1.4)
17	3.6	(1.9)
18	6.2	(2.3)
19	4.0	(1.9)
20	4.3	(1.5)
21	7.1	(0.6)
22	4.5	(0.8)
23	5.4	(1.2)
24	3.7	(1.0)
25	4.1	(0.7)
26	4.0	(0.9)
27	3.2	(1.3)
28	3.9	(1.0)
29	3.4	(1.0)
30	3.7	(0.7)
31	6.1	(0.5)
32	7.0	(0.6)
33	6.7	(0.6)
34	7.8	(0.4)
35	7.4	(1.1)
36	9.2	(1.1)
37	9.0	(0.9)
38	10.9	(1.0)
39	10.7	(0.7)
40	9.3	(0.4)
41	9.0	(0.6)
42	8.9	(0.9)
43	10.5	(1.0)
44	9.8	(0.8)
45	10.7	(1.1)

J_F	k(55,J)	(sigma)
	(10^{-12} cm^3 molec^{-1} s-1)	
46	11.4	(0.6)
47	12.6	(0.6)
48	12.4	(1.0)
49	14.8	(0.9)
50	16.7	(0.6)
51	16.3	(0.5)
52	16.3	(0.9)
53	16.9	(1.3)
54	10.7	(1.0)
55	—	—
56	12.0	(1.0)
57	17.1	(0.9)
58	14.0	(0.9)
59	14.4	(0.6)
60	11.9	(1.0)
61	12.3	(0.4)
62	9.9	(0.5)
63	9.8	(0.2)
64	8.4	(0.1)
65	7.4	(0.3)
66	6.8	(0.3)
67	5.8	(0.4)
68	5.6	(0.3)
69	5.3	(0.5)
70	4.7	(0.3)
71	3.9	(0.5)
72	5.1	(0.5)
73	3.4	(0.4)
74	2.8	(0.2)
75	3.3	(0.6)
76	2.7	(0.3)
77	2.4	(0.6)
78	1.9	(0.2)
79	2.7	(0.3)
80	2.3	(0.5)
81	1.8	(0.3)
82	2.1	(0.5)
83	1.3	(0.3)
84	1.6	(0.4)
85	2.0	(0.4)
86	2.2	(0.4)
87	1.3	(0.5)
88	1.6	(0.6)
89	2.4	(0.6)
90	2.7	(0.5)

$\Sigma k = 5.3 \times 10^{-10}$ cm^3 molecule^{-1} s^{-1}

ICl(B) + Ar

(J_i=55, v'=1)

J_F	k(55,J) (10^{-12} cm^3 $molec^{-1}$ s^{-1})	(sigma)
0	—	—
1	—	—
2	—	—
3	—	—
4	—	—
5	—	—
6	3.5	(0.6)
7	—	—
8	—	—
9	-0.4	(0.5)
10	1.6	(0.8)
11	—	—
12	—	—
13	—	—
14	9.7	(0.8)
15	3.3	(1.9)
16	14.8	(2.1)
17	4.9	(1.2)
18	15.3	(1.4)
19	1.9	(1.7)
20	12.5	(2.0)
21	13.6	(1.0)
22	12.0	(1.1)
23	7.4	(0.7)
24	5.9	(1.3)
25	5.7	(1.3)
26	5.8	(0.6)
27	7.5	(0.6)
28	8.0	(1.0)
29	4.3	(1.1)
30	4.7	(0.9)
31	8.9	(0.8)
32	12.5	(0.6)
33	11.9	(0.8)
34	12.2	(0.8)
35	12.2	(0.6)
36	11.9	(0.8)
37	11.7	(1.0)
38	10.6	(0.7)
39	10.4	(0.4)
40	10.5	(0.9)
41	11.6	(0.9)
42	10.9	(0.6)
43	10.4	(0.8)
44	10.7	(0.4)
45	10.3	(0.6)

J_F	k(55,J) (10^{-12} cm^3 $molec^{-1}$ s^{-1})	(sigma)
46	10.9	(0.3)
47	11.3	(0.4)
48	11.2	(0.8)
49	12.2	(0.6)
50	12.2	(0.9)
51	11.9	(0.8)
52	11.6	(0.7)
53	11.2	(0.8)
54	8.9	(1.4)
55	—	—
56	9.9	(1.0)
57	10.6	(0.5)
58	10.0	(0.6)
59	10.9	(0.5)
60	10.0	(0.5)
61	8.4	(0.5)
62	7.9	(0.6)
63	7.6	(0.4)
64	6.7	(0.3)
65	5.9	(0.3)
66	6.9	(0.5)
67	6.0	(0.3)
68	4.9	(0.3)
69	5.5	(0.6)
70	4.2	(0.4)
71	3.7	(0.2)
72	4.6	(0.3)
73	3.5	(0.3)
74	2.9	(0.3)
75	3.0	(0.4)
76	2.7	(0.3)
77	2.2	(0.4)
78	2.6	(0.5)
79	1.9	(0.3)
80	1.1	(0.1)
81	1.9	(0.4)
82	1.4	(0.4)
83	1.6	(0.3)
84	1.9	(0.3)
85	1.6	(0.3)
86	0.9	(0.4)
87	1.1	(0.4)
88	0.8	(0.1)
89	0.9	(0.3)
90	0.3	(0.2)

Σk = 5.7 x 10^{-10} cm^3 $molecule^{-1}$ s^{-1}

ICl + He

(J_i=42, v'=1)

J_F	k(42,J) (10^{-12} cm^3 $molec^{-1}$ s^{-1})	(sigma)
0	-.-	-.-
1	-.-	-.-
2	-.-	-.-
3	-.-	-.-
4	-.-	-.-
5	-.-	-.-
6	0.6	(1.2)
7	-.-	-.-
8	-.-	-.-
9	-.-	-.-
10	-.-	-.-
11	3.5	(1.5)
12	1.8	(2.8)
13	8.3	(2.6)
14	7.9	(1.3)
15	13.1	(3.0)
16	8.6	(3.0)
17	6.0	(1.6)
18	19.4	(2.4)
19	4.3	(3.4)
20	13.2	(3.6)
21	10.0	(2.1)
22	13.1	(2.2)
23	9.1	(1.1)
24	6.6	(2.4)
25	11.4	(1.7)
26	12.4	(1.8)
27	7.3	(1.8)
28	8.9	(1.6)
29	7.4	(1.6)
30	12.5	(1.5)
31	12.7	(1.7)
32	16.9	(1.5)
33	17.6	(3.0)
34	11.1	(1.4)
35	14.5	(1.9)
36	20.0	(0.7)
37	18.6	(1.2)
38	18.3	(1.1)
39	17.6	(1.6)
40	16.2	(1.6)
41	9.3	(1.7)
42	-.-	-.-
43	12.8	(1.8)
44	17.7	(0.9)
45	15.4	(1.8)
46	15.1	(0.9)
47	14.7	(1.4)
48	14.0	(0.3)
49	13.0	(0.9)
50	12.7	(0.4)
51	12.1	(0.3)
52	11.5	(0.2)
53	8.8	(0.8)
54	12.2	(0.6)
55	10.0	(1.0)
56	8.6	(0.6)
57	7.7	(0.3)
58	8.0	(0.4)
59	7.1	(0.2)
60	6.4	(0.2)
61	5.5	(0.5)
62	5.9	(0.4)
63	5.1	(0.7)
64	4.9	(0.3)
65	4.4	(0.3)
66	3.5	(0.1)
67	5.2	(0.3)
68	5.3	(0.3)
69	2.8	(0.2)
70	3.3	(0.2)
71	2.5	(0.4)
72	3.1	(0.4)
73	2.6	(0.5)
74	2.1	(0.3)
75	2.2	(0.2)
76	1.5	(0.3)
77	2.3	(0.2)
78	1.2	(0.3)
79	1.7	(0.2)
80	1.2	(0.2)
81	1.2	(0.2)
82	0.6	(0.2)
83	0.7	(0.3)
84	0.5	(0.2)
85	0.3	(0.2)
86	-0.1	(0.3)
87	0.0	(0.1)
88	-0.1	(0.2)
89	1.0	(0.3)

$\Sigma k = 6.4 \times 10^{-10}$ cm^3 $molecule^{-1}$ s^{-1}

ICl + Ar

(J_i=42, v'=1)

J_F	k(42,J) (10^{-12} cm^3 $molec^{-1}$ s^{-1})	(sigma)
0	—	—
1	—	—
2	—	—
3	—	—
4	—	—
5	6.5	(1.8)
6	—	—
7	—	—
8	—	—
9	—	—
10	—	—
11	2.4	(0.9)
12	6.7	(2.5)
13	4.6	(3.1)
14	14.7	(0.9)
15	12.7	(2.6)
16	15.7	(1.8)
17	7.1	(1.6)
18	23.1	(1.7)
19	5.5	(1.9)
20	18.2	(2.8)
21	9.5	(1.2)
22	14.5	(1.4)
23	7.8	(2.0)
24	10.3	(1.5)
25	9.5	(1.9)
26	13.5	(1.9)
27	5.5	(0.9)
28	8.6	(0.5)
29	13.0	(0.6)
30	12.9	(1.1)
31	13.5	(1.0)
32	20.8	(1.2)
33	16.4	(1.9)
34	15.8	(1.3)
35	15.2	(2.0)
36	22.4	(1.5)
37	19.1	(1.0)
38	14.7	(0.7)
39	19.0	(0.7)
40	13.3	(0.7)
41	4.5	(1.2)
42	—	—
43	11.2	(1.0)
44	13.3	(1.5)
45	9.4	(2.0)

J_F	k(42,J) (10^{-12} cm^3 $molec^{-1}$ s^{-1})	(sigma)
46	10.6	(0.7)
47	14.5	(0.6)
48	13.4	(0.6)
49	11.6	(0.8)
50	13.1	(0.3)
51	13.0	(0.3)
52	13.0	(0.3)
53	13.0	(0.7)
54	14.0	(1.0)
55	11.5	(0.5)
56	10.2	(0.3)
57	9.1	(0.6)
58	9.2	(0.8)
59	8.5	(0.2)
60	7.8	(0.2)
61	7.4	(0.2)
62	6.8	(0.4)
63	6.0	(0.3)
64	5.1	(0.2)
65	6.6	(0.3)
66	5.0	(0.2)
67	5.4	(0.4)
68	6.2	(0.6)
69	3.0	(0.2)
70	4.0	(0.4)
71	3.8	(0.3)
72	2.9	(0.1)
73	3.3	(0.2)
74	3.6	(0.4)
75	2.7	(0.2)
76	0.4	(0.4)
77	3.0	(0.4)
78	1.8	(0.2)
79	2.1	(0.4)
80	1.5	(0.3)
81	1.8	(0.2)
82	1.8	(0.3)
83	2.3	(0.6)
84	2.6	(0.5)
85	1.5	(0.2)
86	0.7	(0.3)
87	0.0	(0.3)
88	1.0	(0.2)
89	0.9	(0.2)
90	0.3	(0.5)
91	0.4	(0.5)

$\Sigma k = 7.0 \times 10^{-10}$ cm^3 $molecule^{-1}$ s^{-1}

ICl + He

(J_i=36, v'=1)

J_F	k(36,J) (10^{-12} cm^3 $molec^{-1}$ s^{-1})	(sigma)
22	13.9	(1.2)
23	10.6	(1.1)
24	7.5	(1.2)
25	13.4	(1.0)
26	14.1	(2.1)
27	—	—
28	12.3	(4.4)
29	16.8	(1.2)
30	18.3	(0.8)
31	17.1	(1.3)
32	21.4	(0.5)
33	21.2	(1.0)
34	18.1	(1.3)
35	16.9	(2.1)
36	—	—
37	14.5	(1.9)
38	17.0	(1.5)
39	18.0	(1.3)
40	16.7	(0.8)
41	16.0	(0.6)
42	16.2	(1.0)
43	13.9	(0.9)
44	13.6	(0.5)
45	12.7	(0.5)
46	11.8	(0.5)
47	11.8	(0.8)
48	8.7	(0.4)
49	9.5	(0.5)
50	8.6	(0.4)
51	7.4	(0.4)
52	6.4	(0.6)
53	5.7	(1.0)
54	5.0	(0.8)
55	4.3	(0.4)
56	4.4	(0.2)
57	5.3	(0.3)
58	4.1	(0.4)
59	3.6	(0.2)
60	3.7	(0.2)
61	3.5	(0.2)
62	3.4	(0.3)
63	2.6	(0.2)
64	2.7	(0.3)
65	2.6	(0.4)
66	2.1	(0.3)
67	2.1	(0.2)
68	1.7	(0.3)
69	1.6	(0.3)
70	1.5	(0.2)
71	1.5	(0.2)
72	0.9	(0.2)
73	1.2	(0.1)
74	1.0	(0.1)
75	0.5	(0.1)
76	0.5	(0.1)
77	0.5	(0.2)
78	0.3	(0.1)
79	0.8	(0.1)
80	0.6	(0.1)
81	0.4	(0.2)
82	0.2	(0.1)
83	—	—
84	0.2	(0.1)
85	0.0	(0.2)
86	0.3	(0.2)
87	—	—
88	—	—
89	0.5	(0.2)
90	0.8	(0.2)

$\Sigma k = 4.8 \times 10^{-10}$ cm^3 $molecule^{-1}$ s^{-1}

ICl + Ar

(J_i=36, v'=1)

J_F	k(36,J) (10^{-12} cm^3 $molec^{-1}$ s^{-1})	(sigma)
22	14.5	(1.1)
23	11.0	(1.9)
24	10.5	(1.6)
25	10.0	(1.6)
26	8.7	(2.2)
27	—	—
28	16.2	(4.5)
29	14.0	(1.7)
30	15.8	(0.8)
31	11.1	(1.3)
32	15.4	(1.3)
33	14.7	(1.8)
34	16.6	(0.9)
35	16.7	(1.5)
36	—	—
37	10.9	(1.9)
38	12.4	(1.2)
39	12.8	(1.2)
40	13.4	(1.4)
41	12.6	(1.0)
42	11.8	(1.0)
43	11.3	(1.2)
44	10.9	(0.7)
45	10.4	(0.7)
46	9.8	(0.6)
47	10.7	(0.7)
48	7.2	(0.7)
49	8.5	(0.8)
50	7.3	(0.7)
51	7.8	(0.6)
52	7.0	(0.4)
53	5.6	(0.9)
54	4.6	(1.0)
55	5.3	(0.6)
56	5.6	(0.7)
57	6.8	(0.5)
58	5.7	(0.4)
59	5.2	(0.2)
60	4.0	(0.6)
61	4.7	(0.4)
62	4.8	(0.5)
63	3.4	(0.5)
64	3.2	(0.4)
65	2.5	(0.4)
66	2.7	(0.2)
67	2.6	(0.4)
68	2.8	(0.2)
69	2.2	(0.4)
70	2.2	(0.3)
71	2.2	(0.4)
72	2.1	(0.3)
73	1.9	(0.2)
74	1.8	(0.4)
75	1.1	(0.5)
76	1.0	(0.3)
77	1.3	(0.2)
78	0.7	(0.3)
79	0.7	(0.3)
80	0.7	(0.3)
81	0.8	(0.3)
82	0.3	(0.3)
83	0.2	(0.3)
84	0.1	(0.3)
85	0.6	(0.3)
86	1.1	(0.4)
87	—	—
88	-0.1	(0.1)
89	—	—
90	0.4	(0.2)

$\Sigma k = 4.3 \times 10^{-10}$ cm^3 $molecule^{-1}$ s^{-1}

ICl(B) + ICl(X)

(J_i=55, v'=1)

J_F	k(55,J)	(sigma)
	(10^{-12} cm^3 $molec^{-1}$ s^{-1})	
0	—	—
1	—	—
2	—	—
3	—	—
4	—	—
5	—	—
6	—	—
7	—	—
8	-0.7	(1.4)
9	—	—
10	1.2	(1.7)
11	—	—
12	—	—
13	—	—
14	13.2	(2.5)
15	10.7	(3.5)
16	14.6	(3.6)
17	12.3	(4.0)
18	15.7	(2.7)
19	8.7	(2.0)
20	8.9	(4.8)
21	16.5	(1.2)
22	17.8	(3.3)
23	8.9	(2.1)
24	8.2	(1.9)
25	8.7	(2.0)
26	7.8	(1.7)
27	11.4	(1.8)
28	10.6	(1.9)
29	7.3	(2.2)
30	5.2	(1.5)
31	11.3	(1.0)
32	15.3	(2.2)
33	20.3	(2.3)
34	17.4	(1.6)
35	18.3	(1.6)
36	11.9	(4.4)
37	20.5	(2.8)
38	25.6	(1.8)
39	25.3	(1.3)
40	15.1	(3.3)
41	17.3	(1.7)
42	13.8	(2.0)
43	17.5	(1.4)
44	17.7	(1.3)
45	11.1	(2.2)

J_F	k(55,J)	(sigma)
	(10^{-12} cm^3 $molec^{-1}$ s^{-1})	
46	14.7	(1.7)
47	15.0	(2.0)
48	12.0	(2.4)
49	18.7	(3.2)
50	27.0	(0.6)
51	28.8	(1.6)
52	35.0	(1.0)
53	50.3	(2.4)
54	80.5	(5.6)
55	—	—
56	74.1	(4.6)
57	53.7	(2.9)
58	31.2	(1.8)
59	27.9	(1.1)
60	19.0	(1.2)
61	19.8	(0.8)
62	14.9	(1.5)
63	12.1	(1.0)
64	6.9	(1.6)
65	0.5	(3.1)
66	2.9	(2.1)
67	8.4	(0.9)
68	6.3	(1.0)
69	2.8	(2.0)
70	-0.2	(2.8)
71	6.0	(1.0)
72	7.0	(1.1)
73	5.6	(0.8)
74	3.5	(1.5)
75	-3.6	(3.0)

$\Sigma k = 9.9 \times 10^{-10}$ cm^3 $molecule^{-1}$ s^{-1}